Chiral Resolution Control in Batch and Continuous Crystallization Processes for a Conglomerate Forming Compound

Andrew Steven Dunn

Supervisor: Prof. Joop H. ter Horst

EPSRC Future Manufacturing Research Hub in Continuous Manufacture and Crystallisation

Thesis submitted in satisfaction with the requirements of the Strathclyde Institute of Pharmacy and Biomedical Sciences at the University of Strathclyde for the Degree of Doctor of Philosophy.

September 2019

DECLARATION

I declare that this thesis is entirely my own work and has not been submitted previously to this or any other university. Where the work of others is utilized this is acknowledged and cited in the proper manner.

Andrew Steven Dunn Date

DEDICATION

To Mum, Dad, Christopher and Kayleigh.

Mullac abú.

ACKNOWLEDGEMENTS

First and foremost I'd like to thank Prof. Joop H. ter Horst for being a fantastic supervisor. He encouraged me to be creative in the lab and to come up with my own weird and wonderful (maybe??) ideas and encouraging me to travel on placement and attend conferences to present my work at every opportunity. I'd also like to thank him for the excellent recommendation he gave me for my post-doc application, and because of this I am now living in Brussels having another amazing experience and creating some new memories.

I would to extend a special thank you to Dr. René Steendam, who helped me extensively during the first 2 years of my PhD, and who continues who give me guidance and advice today.

I'd like to thank all the people I've collaborated with on the work in this thesis; Dr. Vaclav Svoboda and Prof. Jan Sefcik, who co-authored the resolution control paper, Dr. Cameron Brown and Dr. Ali Anwar, who help design the setup and experiments for our coupled batch process in the OBC. To Prof. Zoltan Nagy and Dr. Botond Szilagyi; thank you for hosting me for 3 month at Purdue, it was a great experience and we came up with an awesome idea. Also to Dr. Alex Cousen, who I collaborated with on a chiral co-crystallization project of his. That didn't complicate life at all!

There are far too many other people to name but I like to thank everyone else at CMAC over the last 4 years. For all the lectures, lessons and ideas discussed in the lab. It would be great if we could have done all the work we wanted to… if only there was 100 hours in a day.

Finally I'd like to thank my family. To mum, dad, Christopher and Kayleigh, I'll never be able to repay you for the support, guidance and advice you've given me over the years to get to where I am today, and for encouraging me to get out and experience everything and anything I can to improve myself both professionally and personally.

LIST OF PUBLICATIONS

1. **Andrew S. Dunn**, Vaclav Svoboda, Jan Sefcik, Joop H. ter Horst; Resolution Control in a Continuous Preferential Crystallization Process, *Org. Process Res. Dev*, **2019**, 23 (9), 2031-2041.

2. **Andrew S. Dunn**, Ali Anwar, Cameron J. Brown, Alistair J. Florence, Joop H. ter Horst; Coupled Batch-wise Preferential Crystallization Process in a Single Moving-Fluid Oscillatory Baffled Crystallizer, ***In preparation***.

3. **Andrew S. Dunn**, Botond Szilagyi, Zoltan K. Nagy, Joop H. ter Horst; Enabling Mechanical Separation of Enantiomers through Batch Controlled Concomitant Crystallization, ***In preparation***.

4. **Andrew S. Dunn**, René R. E. Steendam, Joop H. ter Horst; Start-up and Steady State of a Continuous Preferential Crystallization in a Continuous Stirred Tank Reactor. ***In preparation***

5. Alexander J. P. Cousen, **Andrew S. Dunn**, Joop H. ter Horst, Chick C. Wilson; Chiral Multi-Component Materials of Naproxen and 2-Aminopyridine. ***In preparation***

ABSTRACT

Chiral molecules are molecules that have a non-superimposable mirror image. Each of these mirror image forms is known as an enantiomer. Such molecules exist throughout nature, from amino acid and sugar molecules, to the complex helical structure of our own DNA. However, the separation of enantiomers (resolution) is extremely important in the pharmaceutical industry due to the potentially different physiochemical response that each enantiomer can induce. Where one enantiomer binds to the target receptor in the body causing the desired therapeutic response, the other enantiomer may bind to a different receptor site causing a potentially hazardous response. One of the most common resolution methods in the pharmaceutical industry is preferential crystallization. In a preferential crystallization process, supersaturated racemic (equal mixture of both enantiomers) solution is seeded with pure crystals of the preferred enantiomer. Over time these crystals grow, removing the preferred enantiomer from solution whilst the unwanted enantiomer remains in solution. Given enough time, however, nucleation of the unwanted enantiomer in the supersaturated solution is inevitable in any preferential crystallization process, batch or continuous.

The work outlined in this thesis focuses on the control in both batch and continuous preferential crystallization processes by improving product enantiopurity and increasing the overall process yield and productivity compared to a conventional batch-wise preferential crystallization process.

Chapter 3 addresses the issue of inevitable unwanted counter enantiomer nucleation in a batch preferential crystallization process and demonstrates a novel seeding method in which this can be avoided. A controlled concomitant preferential crystallization of both enantiomers in a single vessel is demonstrated, where a bias in the crystal size distributions of each enantiomer is exploited in order to mechanically separate pure enantiomer crystals after the crystallization process. Using this strategy any unwanted primary nucleation is avoided in the process.

In Chapter 4, the simultaneous crystallization of both enantiomers in a single oscillatory baffled crystallizer is achieved whilst localizing the crystallization of each enantiomer in different sections of the crystallizer. This internally coupled system adopts the principles of a coupled batch preferential crystallization and applies it to a single reactor. The system allows the movement of solution between sections of the

setup but keeps enantiomer crystals separated. The internal setup negates the need for additional tanks, pump and heating to the system.

The start-up period of a continuous process before it reaches steady state generates a lot of unusable off-spec product. The aim of Chapter 5 is to identify the initial process parameters that influence the start-up time and also the robustness of the steady state that is achieved. A design of experiments approach is used to determine which initial process parameters are important such that they can be further optimized. This leads to shorter start-up times to steady state and less waste of valuable material by developing a robust steady state for the continuous process.

Even in continuous operation, preferential crystallization processes are inherently unstable since nucleation of the counter enantiomer will occur in time. Therefore, in Chapter 6, a novel control strategy is demonstrated that takes back control of the continuous preferential crystallization process and allows the process to continue after nucleation of the counter enantiomer has occurred. This avoids the need to stop and restarted the process whenever the counter enantiomer crystallizes.

The work in this thesis has achieved its aim in demonstrating control of preferential crystallization process in both batch and continuous platforms. The scientific progress made using new setups and strategies demonstrated have proved to be effective for chiral separation processes and have the potential to be applied on an industrial scale for the manufacture of pure chiral medicines.

The observable universe in crystalline form.

Crystals of DL*-Asparagine Monohydrate formed by evaporative crystallization*

CONTENTS

LIST OF FIGURES

LIST OF TABLES

Chapter 1

1 Introduction

1.1 Crystallization in Industry

Crystallization in the pharmaceutical industry is one of the most important unit operations in the manufacturing process for active pharmaceutical ingredients (APIs). It is used not only as a purification and separation technique to obtain pure product, but also to obtain product of the desired specification with respect to the crystal size distribution (CSD), shape, purity, polymorphic form and/or chiral form. These crystal attributes can have a significant effect on downstream processes such as filtration and drying, or formulation of the final pharmaceutical product. Furthermore, they can affect the product properties such as solubility, rate of dissolution and permeability and, in the case of chirality, the therapeutic response. Therefore, it is of paramount importance that such processes are accurately monitored and controlled so that products are produced within the desired specifications.

Crystallization processes are complex multi-mechanism processes involving nucleation, growth, agglomeration and breakage. Controlling each of these mechanisms is essential for controlling the desired crystal attributes. Therefore, it's important to be able to understand these mechanisms, since, by understanding them, we can better control them.

The CSD obtained from a crystallization process can give valuable insight into the nucleation and growth processes occurring for example, a narrow distribution of small or large particles indicates that nucleation and growth are dominant, respectively. Whereas a broad distribution can indicate that both mechanisms are occurring. Controlling the CSD in a crystallization process is important since the size of the product particles can directly affect the patient, since the product size will affect the dissolution rate and hence the bioavailability of the drug. Ultimately, however, the CSD required depends on the route of entry of the product i.e. the CSD of tableted drugs can be much larger than drug for inhalation (which are around 2-5 μm) since these particles must reach far into the lungs.

Even if the correct CSD has been obtained from a crystallization process, it is important to consider if the correct polymorph of a compound has been crystallized. A single compound can orientate itself differently within a crystal lattice in order to achieve a different crystal structure. Each of these structures i.e. polymorphs, can have different chemical (e.g. solubility or melting point) and physical (e.g. shape or colour) properties. It is important to identify early on in the development process if any polymorphs exist since the stability of each can vary greatly. It should also be noted whether or not transformation from one polymorph to another (usually metastable to stable form) will occur over time e.g. during storage. However, it is possible that transformation can occur during other stages of the manufacturing process.

Additionally, the crystal morphology of a compound can have direct effects to downstream processes. Powder flowability for example can be greatly affected by the crystal morphology. Needle like crystals for example exhibit poor flowability whereas crystals which are equant have very good flowability. It is important to note that morphology is not the same as polymorphism, since one polymorph of a compound can have several morphologies.

For crystallization processes to be efficient, sufficient yield and productivity specifications must be met. It is desired that as much material as possible is recovered from solution and crystallized. Inherently some material will remain in solution due to the solubility of the compound. However, reducing the crystallization temperature as low as possible or using processes such as evaporative or anti-solvent crystallization can be useful in increasing the yield of highly soluble compounds.

However, care should be taken when trying to increase process yield/productivity since this can also lead to increasing concentrations of impurities in the final product. Impurities in the product can be produced during various stages of the manufacturing process e.g. during synthesis, purification by crystallization or during storage. Impurities can be the result of by-products, reagents or catalysts during synthesis, solvents or anti-solvents during crystallization, or as the result of degradation during drying or storage at high temperatures for long periods of time. It is important therefore that any impurities generated during any stage of the manufacturing process are identified, quantified and recorded in the specification of the product since they can affect the solubility of the API, the crystallization behaviour

(e.g. nucleation and growth rates) and the polymorph, morphology or chirality of the drug substance obtained.

Additional complexity also arises in a crystallization process if the API of interest is chiral. Such compounds have a non-superimposable mirror image and are extremely important in the pharmaceutical industry due to their potentially different therapeutic effects. Where one chiral form (enantiomer) induces the desired response, the opposite form can either induce no response or, by binding to another receptor in the body, it can induce a potentially harmful response. Therefore, it is important in industry to ensure that the correct chiral form is produced in order for the health and safety of the patient. The complexity arises since both enantiomers of a chiral compound have identical physical and chemical properties.[1] However, as will be discussed in this thesis, there are processes and strategies that can be employed in order to separate chiral compounds to achieve enantiopure product which can then be used for treatment in patients.

1.2 Fundamentals of Crystallization

1.2.1 Supersaturation

Crystallization is driven by a change in Gibbs free energy; by minimizing this free energy there is an increase in stability. In a saturated solution, the chemical potentials of both the solute in liquid phase, $\mu_{solute,l}$, and the solute in the solid phase, $\mu_{solute,s}$, are equal to one another, therefore, the difference in chemical potential, $\Delta\mu$, is zero,

$$\Delta\mu = \mu_{solute,l} - \mu_{solute,s} = 0 \tag{1.1}$$

Hence, the solution is in thermodynamic equilibrium with the solid phase. If there is a positive difference in chemical potentials, the solution becomes *supersaturated*, where as a negative difference in the chemical potentials indicates an *undersaturated* solution. This chemical potential can be related to the fundamental supersaturation of the system via standard potential (μ_0) and the standard activity of the solution (a) and solute (a*),

$$\mu_{solute,l} = \mu_0 + RT \ln a \tag{1.2}$$

$$\mu_{solute,s} = \mu_0 + RT \ln a^* \tag{1.3}$$

Eq. 1.2 and 1.3 can then be combined to give Eq. 1.4,

$$\frac{\Delta\mu}{RT} = \ln\left(\frac{a}{a^*}\right) = \ln S \tag{1.4}$$

However, since activities are not often known, one common way to express supersaturation is as a supersaturation ratio (*S*) of concentrations,

$$S = \frac{C}{C^*} \tag{1.5}$$

Where *C* is the actual concentration of the solution and *C** is the equilibrium concentration of solution at a given temperature i.e. the solubility of the compound.

Figure 1.1 shows a typical solubility curve for a binary solvent-solute system in terms of solute concentration in solution as a function of temperature. The diagram consists of three distinct regions termed, stable, metastable and labile. The stable region lies underneath the solubility curve. In this region, the solution is undersaturated and crystallization cannot occur. Any additional solids that are added to the system will dissolve until the concentration reaches the saturation concentration at temperature *T*. The solubility curve shows how the saturation concentration changes with temperature. For a given concentration, there is a saturation temperature T_s. On crossing the solubility curve into the metastable zone, the solution becomes supersaturated. Crystallization can occur in this region; however, crystal nucleation is not instantaneous. Crystallization can be induced in the metastable region by adding seed crystals in order to lower the energy required for crystallization to occur or an anti-solvent in order to lower the solubility. The labile region is reached on crossing the metastable limit at T_n for a given concentration either by further cooling of the system or evaporation of the solvent. In this region crystallization occurs

instantaneouslyly without the need for the presence of seed crystals. The difference between T_s and T_n is known as the metastable zone width (MSZW).

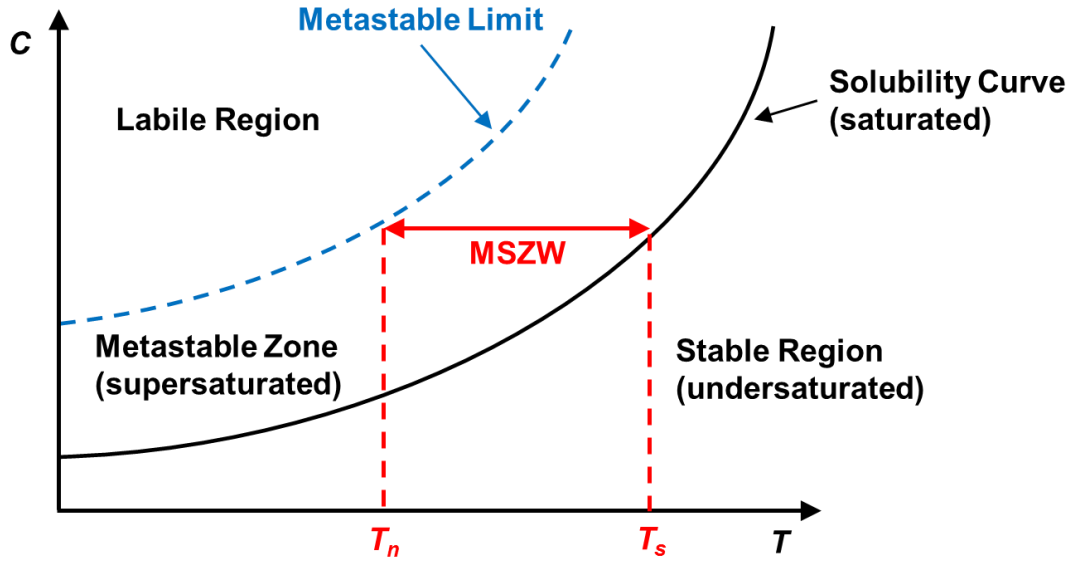

Figure 1.1. Binary phase diagram of a typical solvent-solute system showing solute solubility and metastable limit as a function of temperature.

1.2.2 Crystal Nucleation

Crystal nucleation can be divided into two main categories: primary and secondary nucleation. Primary nucleation refers to the generation of new nuclei which occurs spontaneously on crossing the metastable limit (see Section 1.2.1). Primary nucleation can be sub-categorized into homogenous and heterogeneous nucleation. Homogeneous nucleation occurs in the absence of any foreign bodies in the system (such as dust for example). Heterogeneous nucleation occurs in the presence of such bodies. Secondary nucleation occurs in the presence of parent crystals, called *seeds*, which generate secondary nuclei by either shear (contact nucleation and fluid shear) or mechanical (initial breeding, dendritic or attrition) forces. Figure 1.2 illustrates the classification of each of these nucleation processes.

1.2.2.1 Primary Nucleation

There are two main theories on mechanism of crystal nucleation: classical nucleation theory (CNT) and two-step nucleation theory (TSN).[2] Figure 1.3 illustrates the mechanism of each of these theories.[2] CNT suggests that solute molecules form

clusters with the same ordered arrangement i.e. structure, as the crystal that eventually forms. In contrast, TSN theory suggest that the initial clusters of solute molecules that form are initially disordered liquid-like cluster before forming an ordered crystalline cluster later in time.

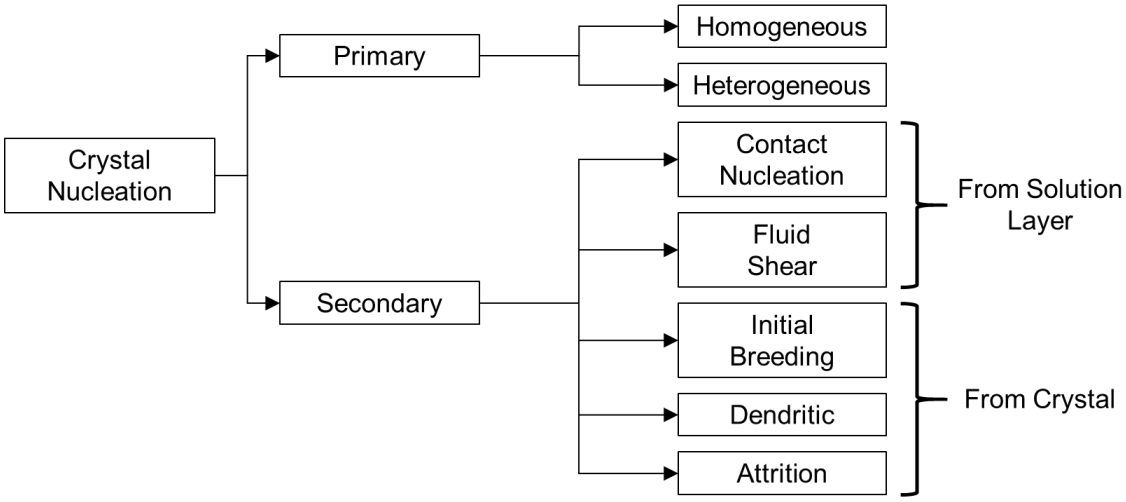

Figure 1.2. Classification of crystal nucleation phenomena. Primary nucleation can be described as homogeneous or heterogeneous. Secondary nucleation can be described at contact nucleation, fluid shear, initial breeding, attrition, dendritic breeding and fragmentation.

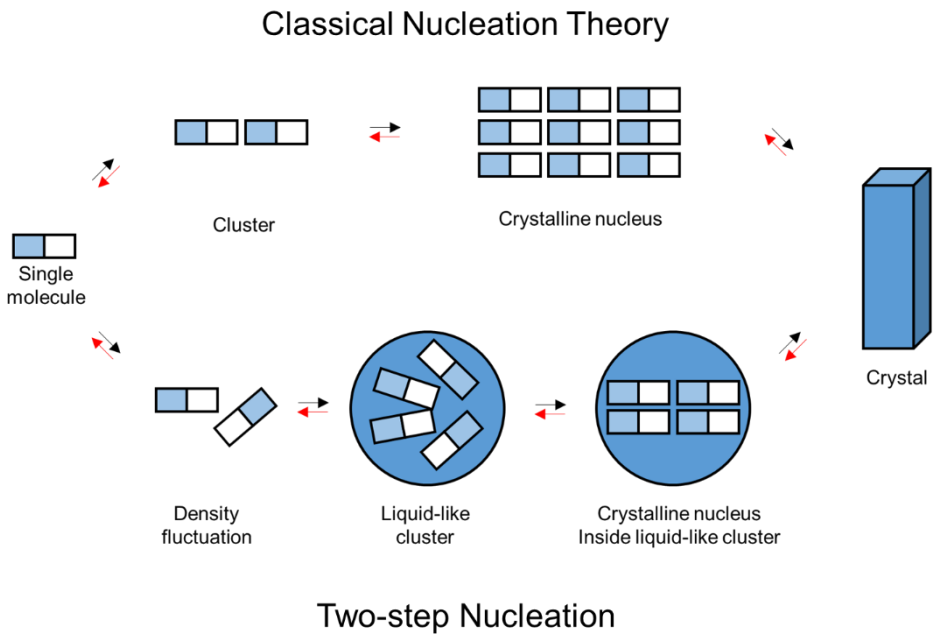

Figure 1.3. Two theorized routes of crystal nucleation at a given supersaturation; classical nucleation theory (top) and two-step nucleation theory (bottom).[2]

For either mechanism to occur, a certain energy barrier must be overcome in order for a crystal to nucleate and grow. The presence of foreign bodies (e.g. dust) in the system can provide a surface for nucleation to occur. Therefore, the energy required for heterogeneous nucleation to occur is less than the energy required for homogeneous nucleation. In either case, clusters must reach a critical radius size in order for the free energy required for nucleation to reach a maximum value at which nucleation of a crystal becomes favourable. If the critical size is not reached, then solute molecules will dissolve back into solution again. The energy require to reach the critical radius decreases with increasing supersaturation, meaning the probability of nucleation occurring increases with increasing supersaturation.[3]

1.2.2.2 Secondary Nucleation

As aforementioned, secondary nucleation occurs in the presence of seed crystals in the system. As the number of crystals in the system increases and supersaturation decreases, secondary nucleation becomes the dominant mechanism over primary nucleation. However, there are several mechanisms from which secondary nuclei are produced, as illustrated in Figure 1.2: contact nucleation, fluid shear, initial breeding, dendritic and attrition.

Contact nucleation and fluid shear occur from the displacement of the solute layer of material loosely adsorbed at the crystal surface by mechanical forces (e.g. collisions).[4] Agrawal and Paterson[5] provided a review of contact nucleation studies which found no evidence of mechanical attrition on the parent seed crystals, supporting the theory that removal of an order solute layer on the crystal surface was the source of the secondary nuclei. The number of secondary nuclei generated increases with supersaturation[6] since at higher supersaturations the thickness of the adsorption layer on the crystal surface increases leading to an increased number of solute material available for contact nucleation. For the fluid shear mechanism of secondary nucleation to occur, high supersaturation levels as well as a high shear rate (rpm) are required for extended periods of time. High levels of fluid shear are typically found in industrial crystallizers.[5,6]

Initial breeding, dendritic and attrition mechanisms all occur directly from the parent crystal, rather than an adsorption layer. Initial breeding occurs when crystalline fines of the surface of the crystal become dislodged and, if they are bigger than the

critical radius, they will act as secondary nuclei. However, since the number of fines on the crystal surface is finite, initial breeding cannot act as a sustainable source of secondary nuclei.[5] Dendritic growth on the crystal surface occurs at high supersaturations. These needle-like crystals can then be detached from the crystal surface due to mechanical forces and act as secondary nuclei. However, such growth requires highly supersaturated conditions and is therefore unlikely to occur in industrial crystallization processes. Attrition is similar to contact nucleation, where fragments of the parent crystal are removed. However, unlike contact nucleation, attrition is a purely mechanical process and occurs due to crystal-crystal, crystal-impeller or crystal-wall collisions (fragments can also be removed by fluid shear). Attrition is not dependent on supersaturation (unlike contact nucleation, which is highly dependent on supersaturation) and is only affected by experimental factors such as agitation rate and suspension density. Both mechanisms do depend on collision energy, however the energy required for attrition is much greater than the energy required for contact nucleation. Furthermore, the effect on attrition can be detected immediately, since fragments are of a larger size. In comparison, in contact nucleation there is initially no apparent damage to the parent crystal. Therefore, there is a time delay in the appearance of secondary nuclei since the nuclei require time to grow to a detectable size.

1.2.3 Crystal Growth

Once particles exceed the critical cluster size required for nucleation to occur, the particles can now start to grow. The growth of a crystal can be defined as a change in a particular dimension of the crystal over time, namely, the *linear growth rate*.[7] Since crystals can have many faces, which can grow at different rates, the linear growth rate therefore is an expression of the growth rate of one particular face i.e. the rate of displacement of the crystal surface in the perpendicular direction to that face.[8] However, where the linear growth rate is used to describe the growth rate of an overall crystal, it is used to describe the growth rate of a particular dimension of the crystal e.g. the growth rate of the equivalent spherical diameter of a crystal.[9] Crystal growth rates can also be measured by the change in mass of the crystal over time. However, surface shape and crystal volume must be known in order to calculate the growth rate this way.

Noyes and Whitney[10] first considered the theory of crystal growth via a diffusion model. In this theory, solute molecules diffused through solution towards the crystal surface. As solute molecules leave solution, the solute concentration in solution decreases, such that the concentration is higher at further distances from the crystal surface.[3,7] Hence, the solute will diffuse towards the crystal surface.[11] At the crystal surface, the molecules become ordered into the crystal lattice through an absorbed layer.[12] The idea that crystal growth is due to the presence of an adsorption layer on the crystal surface was first proposed by Volmer.[12] When solute particles arrive at the crystal surface, they do not immediately become part of the crystal lattice. They become a loosely adsorbed layer on the surface, establishing an equilibrium between the surface and the bulk solution.[3] Molecules will link into this lattice layer at 'active centres' i.e. where attractive forces will be greatest. A stepwise buildup of the crystal surface then occurs until the surface layer is complete. Prior to an additional layer being added, a nucleation centre must appear on the surface, termed a two-dimensional critical nucleus.[3,7]

1.3 Batch-wise Crystallization

Batch manufacturing is still the most common platform used in the pharmaceutical industry, particularly for crystallization processes, due to the simplicity of the equipment and relatively low start-up costs. Furthermore, API crystallization processes are developed in labs where batch processes are dominant due to the low volume imposed by the limited supply of material early on in development. As such, these batch processes are more likely to continue to be used at larger scales of production. The versatility of batch vessels also means that the same vessel can be used for multiple products (after cleaning of course) and/or a range of unit operations e.g. reactions, crystallization, mixing. For crystallization processes, supersaturation in the system can be generated by cooling the batch vessel by reducing the temperature, or by increasing the solution concentration by evaporative crystallization by heating the vessel.

Whilst crystallization processes conducted in batch are generally well understood in terms of the mechanisms and operating procedures, a major issue with batch operation is batch-to batch variability of the product, which can affect

downstream unit operations of the manufacturing process. This is an area where continuous manufacturing has an advantage over conventional batch processes.

1.4 Continuous Crystallization

Continuous manufacturing has gained huge interest in recent decades as a means to manufacture medicines in the pharmaceutical industry.[13–15] Such processes already exist in other industries (e.g. food and petrochemical industries), however, In recent years, both academic and industrial institutions have been collaborating to achieve a common goal for manufacturing processes of pharmaceutical products. The common goal is to achieve fully continuous operation from the addition of precursors and reagents at the synthesis stage of the process and collect the therapeutic product (tablet, capsule etc.) at the other end of the line. Such achievements have already been demonstrated by Mascia et al.[16] and, in doing so, the benefits of continuous operation over batch processes can be directly compared.[16] Continuous manufacturing has shown to provide greater reproducibility,[17] more consistent product, improved yield,[18] higher throughput,[19] as well as reduced facility costs[20,21] and a reduction in the number of process steps .[16,22]

There are two main classes of crystallizers used for continuous operation: mixed suspension mixed product removal (MSMPR) and plug flow (PF) crystallizers. MSMPRs have very good internal mixing and relatively long residence times, whereas PF have much shorter residence times and can produce product of much smaller size compared to MSMPRs.[18] MSMPR crystallizers are the most commonly used of the two classes.[23] They can be setup as a single stage or in a cascade arrangement, both of which as illustrated in Figure 1.4.

However, there are advantages of using a PF crystallizer over an MSMPR. One is that there is no impeller present causing crystal breakage or unwanted secondary nucleation.[24] Furthermore, whilst the process is in steady state, each individual particle experiences identical conditions through the lifetime of the crystallizer. This, in theory, leads to uniform and consistent product.[24]

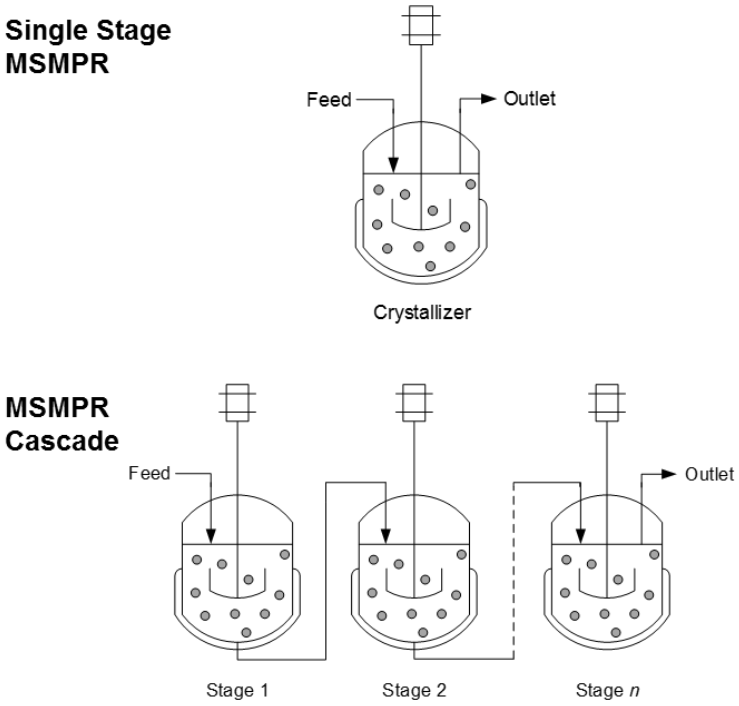

Figure 1.4. Single stage MSMPR (top) and MSMPR cascade (bottom).

1.4.1 Start-up Period of Continuous Processes

Before a continuous process reaches steady state, the system must go through a start-up period. During steady state, the desired process parameters such as concentration, CSD, crystal form etc. are all constant, and product of the desired specification is produced. However, during start-up, product out-with specification is being produced.[25] Therefore, it is of great importance that this period is as short as possible in order to minimize waste and reduce time such that steady state can be reached quickly. However, very few publications exist where the start-up of a continuous process for an MSMPR crystallizer has been the focus, given that it is such an important step in a continuous manufacturing process. Process integration studies to include the use of a wet-mill have been investigated[26,27] as well as demonstration of an automated direct nucleation control (ADNC) strategy.[27,28] Yang et al.[26] investigated the use of integrating a wet-mill into their setup in both upstream and downstream configurations against a conventional one stage MSMPR setup. They found that by integrating the wet mill upstream as a continuous nucleator, the start-up time can be significantly reduced (as well as achieving a high yield, narrow crystal size distribution and desired average crystal size). Yang et al.[28] al. found that using the ADNC approach on the start-up and steady state of a continuous process not only

demonstrated quick start-up time, but also suppressed disturbances. However, when Yang et al.[27] investigated the use of a wet milling-based ADNC approach, this did not improve the start-up time compared to using either process independently. Hou et al.[29] investigated how different start-up procedures for a continuous process affected the start-up time. They tried three different approaches: 1. starting from an unseeded saturated solution 2. Starting from batch suspension at equilibrium and 3. Using MSMPR product from a previous run as seed material. They found that using product material from one continuous process as seeds for a subsequent run provided the shortest start-up time. Similar results were found by Powell, who noted that the seed properties can influence the time to achieving steady state.[30] Furthermore, they found that the steady state reached in the process was independent of start-up mode used.

Several modelling studies have also investigated the start-up of a continuous process.[31,32] Yang and Nagy investigated the use of different dynamic cooling and anti-solvent addition profiles, as well as a combination of the two, and found that waste during start-up could be reduced by up to 50% by using dynamic anti-solvent profiles alone.[31] Su et al. developed a model for continuous MSMPR operation and proposed a concentration control strategy to aid in the design of a short start-up procedure.[32]

1.4.2 Steady State Monitoring

Once a continuous process reaches steady state, it is then important to ensure that the process is effectively monitored. This ensures that the parameters of the process remain constant, and that any perturbations in the steady state achieved can be quickly identified and, ideally, rectified. The most common way to monitor a crystallization process is to use process analytical technology (PAT) tools. PAT tools are very effective methods for monitoring continuous crystallization processes. They negate the need for manual sampling, which brings with it the possibility of human error during sample prep for offline analytical techniques. Furthermore, they can provide real-time feedback on the current state of the process. Therefore, PAT tools are very useful for steady-state detection in continuous crystallization processes.[25]

1.4.3 Steady State Control

Since PAT tools can obtain information in real-time from crystallization processes, they therefore offer the ability to be utilized for control.[33] The Nagy group

are at the forefront of such crystallization control systems. For concentration control in a crystallization process a strategy called supersaturation control (SSC) can be used.[34,35] By using a concentration monitoring method (e.g. UV-Vis or IR), the concentration can be fed back to a computer in real time such that the temperature in the reactor is controlled to keep the supersaturation in the system constant as growth of crystals occurs. This keeps the system within the metastable region of the phase diagram so that no unwanted secondary nucleation occurs.

A direct nucleation control (DNC) method can be used to control the particle counts within a system.[34,36] This indirectly controls the crystal size. This strategy uses heating and cooling cycles to dissolve or nucleate/grow crystals in the system, respectively. This way, the number of crystals is kept constant. Even when additional seed crystals are added to the crystallizer the control system heats to reduce the number to the target set-point of crystals, hence showing the ability of the control system in alleviating disturbances.[28,37]

Hansen et al.[38] have also demonstrated use of both DNC and SSC in combination with Raman spectroscopy in order to insure that the correct polymorph of a compound was being produced. Polymorphs are different crystal lattice arrangements of the same molecule. By packing differently, different crystal shapes and morphologies can be achieved. Different polymorphs of a compound will have different stabilities and hence different solubilities, melting points etc.

Although for chiral resolution processes it has been shown that they can be well monitored, no such control strategy exists for such a process in an event where something goes wrong i.e. unwanted nucleation of the counter enantiomer, either in batch or continuous crystallization processes. For further reading on PAT monitoring and control, readers should refer to several review papers that exist.[33,39]

1.5 Chirality

It seems inherent in life that everything has '*handedness*'. Studies have shown that most of the population on the planet are right-handed, but as of yet there has been no explanation as to why. Molecules are no different, and those that possess this handedness are termed *chiral*. Just like our own hands, chiral molecules are molecules which are non-superimposable mirror images of one another. And, just like our hands, there is evidence that nature also has a preference of *handedness*. Amino acids, for

example, are always found in the left-handed form in nature, whereas sugars are always found in the right handed form.

The cause of chirality in molecules is an asymmetric center on a carbon atom, where the carbon is surrounded by four different substituents, as shown in Figure 1.5.

Figure 1.5. A representation of an asymmetric carbon in an organic molecule bonded with four different substituents, causing its own mirror image to be non-superimposable.[40]

Enantiomers can be identified by D- and L- or *R*- and *S*-. The former notation comes from the direction in which the enantiomer rotates polarized light; *dextrorotatory* (+) or *levorotatory* (-) i.e. either left or right (see Section 2.3.1). The latter notation names each enantiomer based on the hierarchy of substituents around the asymmetric carbon (the higher the atomic number of the substituent the higher up in the hierarchy). Substituents are numbered 1 to 4 where the lowest atomic number substituent is facing away from the observer (e.g. where hydrogen is one of the substituents it will always numbered 4 since it has the smallest atomic number).The enantiomer is named *R*- if we move from 1 to 2 in the clockwise direction or *S*- if we move in the anti-clockwise direction from 1 to 2. It is important to note that each notation is not interchangeable and D- does not always equate to either *R*- or *S*- and vice versa i.e. it is possible to have S-(+)- or S-(-) compounds for example.

Both enantiomers have identical physical, chemical and structural properties. But why is all this important? From a pharmaceutical point of view, they are extremely important. In the 1960's it was discovered that a chiral drug called thalidomide was causing birth defects in newborn children. The drug was being administered by doctors as a treatment for morning sickness in pregnant women, however, their children were being born with partially developed limbs. The *R*-enantiomer of thalidomide administered achieved the desired therapeutic response, however, the *S*-enantiomer of thalidomide is teratogenic, which causes these birth defects.[41] For some drugs, both

enantiomers interact with the same receptor in the body meaning they produce the same therapeutic response. For most others, however, the opposite enantiomer does not react with its intended receptor site (see Figure 1.6) and either doesn't interact with any other receptor at all or interacts with one which doesn't produce any harmful effects. On the other hand the opposite enantiomer interacts with a receptor in such a way that a harmful (or even toxic) effect on the body is induced. Table 1.1 gives details of some other chiral drugs in which each enantiomer has an opposing pharmaceutical effect. Therefore, it is of great importance that in the latter two cases we are able to separate enantiomers from one another.

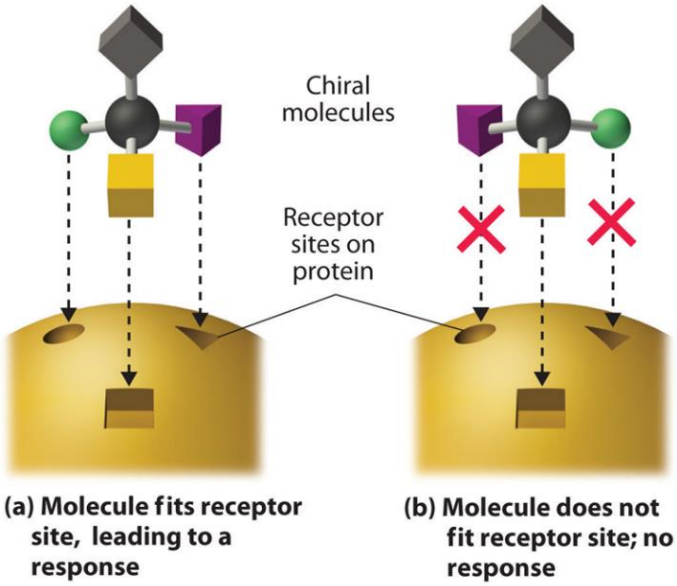

Figure 1.6. One form of the drug fits into the target receptor site (left) leading to a therapeutic response. The opposite chiral form (right) does not, meaning no therapeutic response at the intended site is achieved.[40]

Table 1.1. Examples of pharmaceutical compounds whose enantiomers have different therapeutic responses based on Marcellos et al.[42]

Drug	Preferred Enantiomer	Counter Enantiomer
Ibuprofen[43]	S-, Anti-inflammatory	R-, Inactive
Methamphetamine[44]	L-, Nasal decongestant	D-, Central nervous system stimulant
Ethambutol[45]	S,S-, Tuberculosis treatment	R,R-, Causes blindness
Naproxen[46]	S-, Arthritis treatment	R-,Causes liver damage

1.5.1 Chirality in Crystal Structures

When it comes to chirality within crystal structures, there are a few different scenarios. Enantiomers can either crystallize as a racemic compound; where each crystal lattice is composed of equal amounts of both enantiomers. Conglomerates, where each crystal lattice is enantiopure (contains only one of the enantiomers), or as a solid solution, where both enantiomers compete for the same space within the crystal structure i.e. it can be a random assortment of both enantiomers. An illustration of each of these crystal structures is shown in Figure 1.7. Racemic compounds make up around 90-95% of all pharmaceutical chiral compound crystal structures, conglomerates make up around 5-10% and solid solution make up less than 1% of pharmaceutical chiral compound crystal structures.

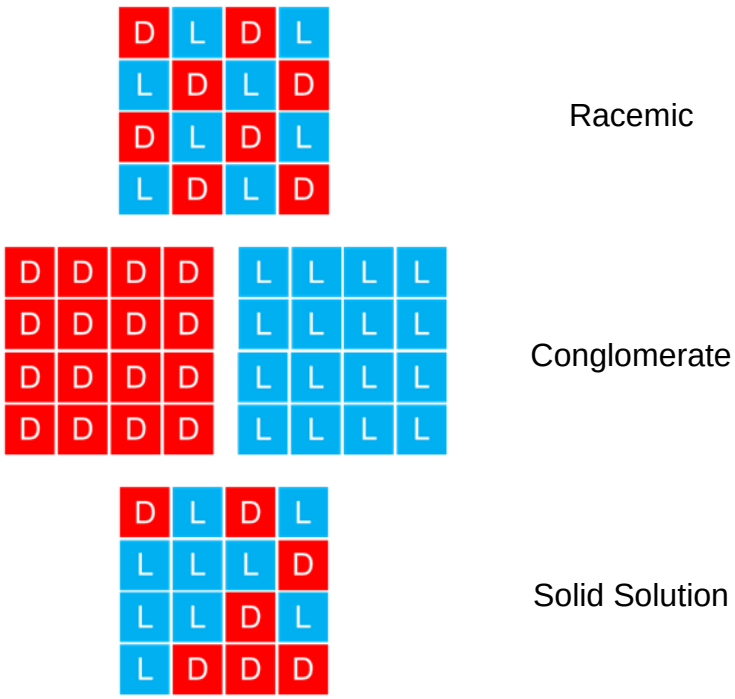

Figure 1.7. An example of a racemic (left), conglomerate (middle) and solid solution (right) crystal structure.

The form which is most stable depends on the properties of the chiral molecule itself, as well as temperature and enantiomer composition. This can be represented in the form of a ternary phase diagram for each system, as shown in Figure 1.8. Each corner of the phase diagram represents 100% of one of the three substituents in the system; the solvent (S), the D-enantiomer (D) and the L- enantiomer (L).

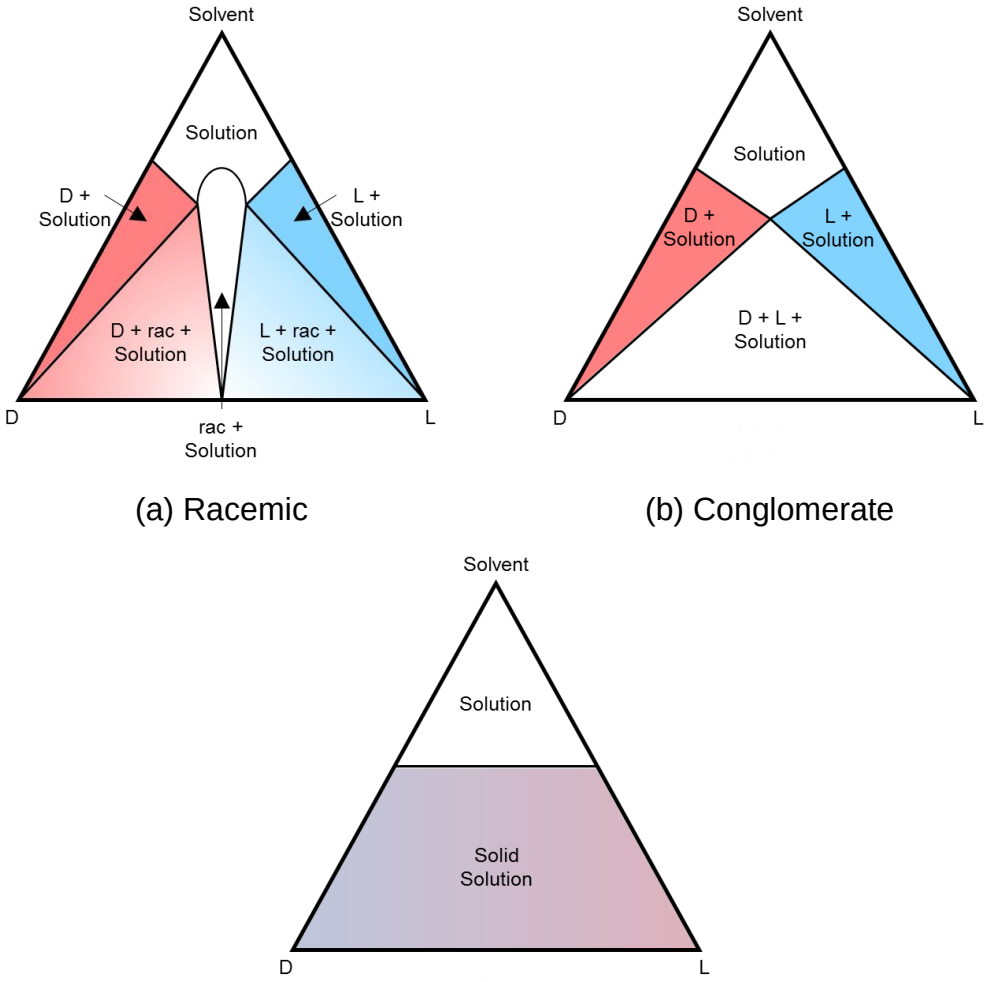

Figure 1.8. Ternary phase diagram of (a) racemic, (b) conglomerate and (c) solid solution forming compounds. Each axis is typically represented by either mole fraction or mass fraction.

1.5.2 Chiral Resolution Methods

Chiral resolution methods are processes by which we can separate chiral forms from one another.[1] There are a number of different resolution techniques, however, the most effective method will depend strongly on the chiral molecule of interest, and the properties is possess, both in solution and in the solid phase. Resolution methods are most commonly applied at the crystallization stage of production, however, asymmetric synthesis methods can used to obtain enantiopurity during synthesis of the

target molecule. However, this sometimes involves the use of toxic catalysts.[47] Crystallization techniques such as Viedma ripening[48–51] and preferential crystallization[52–57] have been extensively studied in the last 10-15 years. Whilst being able to achieve enantiopure product, Viedma ripening is a difficult approach to scale to the levels required for industrial product due to the large amount of grinding required in the system, even with use of an *in-situ* homogenizer.[58] However, similar deracemization techniques such as temperature-cycling induced deracemization has allowed such processes to be scaled since large levels of grinding are not required.[59] However, preferential crystallization is commonly used in industry due to its ease and scalability. For racemic compounds, a common separation technique is to add a conformer such that a diastereomeric salt is created, which can subsequently be preferentially separated. In this thesis, however, the preferential crystallization of a simple conglomerate forming compound will be used for investigation.

1.5.2.1 Preferential Crystallization (PC)

A batch preferential cooling crystallization process is most commonly carried out in a stirred tank reactor (STR). For a conglomerate forming system, a solution containing a racemic (50:50) mixture of both enantiomers is present in the reactor. In the case of preferentially crystallizing an enantiomer of a racemic compound, this solution may be enriched such that the process occurs in the region of the phase diagram where enantiopure crystals can crystallize. The solution is then cooled such that it becomes supersaturated, at which point seeds of the preferred enantiomer are added to create a suspension. In the case of an isothermal cooling crystallization, the solution will first be cooled to the desired crystallization temperature before seeds are added. In the case of a poly-thermal cooling method, seeds will be added just beyond the solubility curve as the solution becomes supersaturated. The reactor will then continue to be cooled to the desired temperature at a rate slow enough to keep the system inside the metastable zone as growth of the seed crystals. In either case, for a preferential crystallization it becomes inevitable that nucleation of the counter enantiomer (or racemic compound) will occur. Thus, the process must be terminated before this unwanted nucleation occurs.

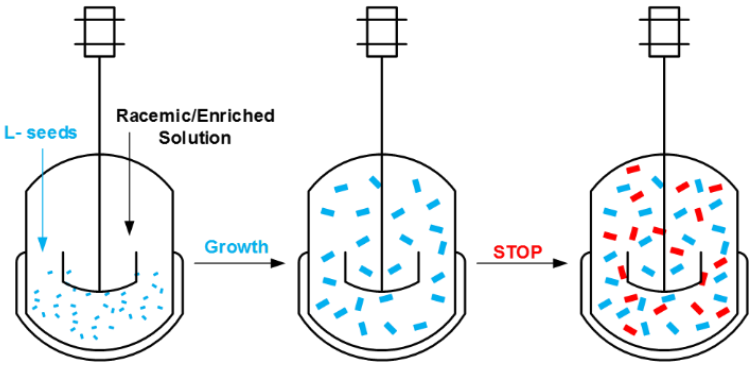

Figure 1.9. A batch preferential crystallization process seeded with one enantiomer. The process must be terminated after a period of time otherwise unwanted nucleation of the undesired enantiomer will occur.

Figure 1.10 shows the ternary phase diagram for a conglomerate system of enantiomers and the solution composition trajectory for the batch PC process described. Point A shows a racemic liquid composition within the supersaturated region of the phase diagram (grey area). At point A, seeds of the preferred enantiomer L are added to the system. As L crystallizes out, the solution composition fraction with respect to D increases, and the process tends towards point C, which is the point at which equilibrium is reached. However, at point B, nucleation of the counter enantiomer D occurs and the solution compositions tends towards point D, where a racemic composition is reached. Point B in the system can occur earlier (closer to point A) or later (closer to point C) depending on whether the initial supersaturation created in the system is higher, or lower, respectively.

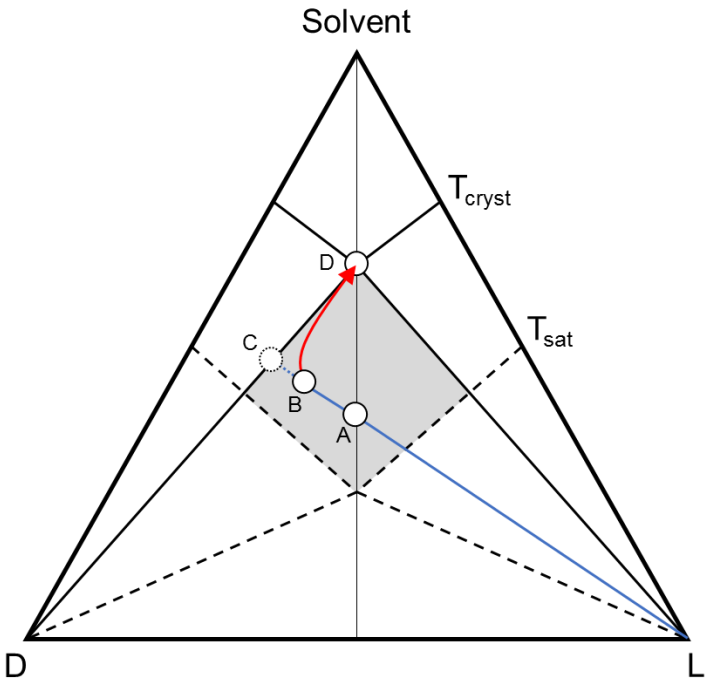

Figure 1.10. Ternary phase diagram of a conglomerate system of enantiomers illustrating the solution trajectory during a conventional batch preferential crystallization process seeded with the preferred enantiomer only (L in this case). Point A represents the racemic starting composition of the solution. Point B represents the point at which the counter enantiomer nucleates and the solution trajectory moves towards point D, which represents a racemic solution composition at the crystallization temperature. Point C represents the theoretical equilibrium in the system if all of L crystallizes out without the nucleation of D. The grey area represents the metastable region within the system.

1.5.2.2 Preferential Crystallization in Coupled Batch Mode

Performing a preferential crystallization process in a coupled vessel setup, a process first described experimentally by Elsner *et al.*[55], has been thoroughly studied in recent years, both experimentally[53,60,61] and through computational models.[62–64] The process is applicable to the separation of enantiomers of a conglomerate forming system and in separating a pure enantiomer from the racemic compound in a racemic compound forming system. A common setup consists of two batch STRs each connected to one another via solid free liquid exchange lines. An example of such a setup is shown in Figure 1.11. In the case of a separation of conglomerates, each

reactor contains a racemic solution composition that, like the simple batch process, is supersaturated to the metastable region of the phase diagram. Each reactor is then seeded with enantiopure seeds of one of the two enantiomers (e.g. L in vessel 1 and D in vessel 2).

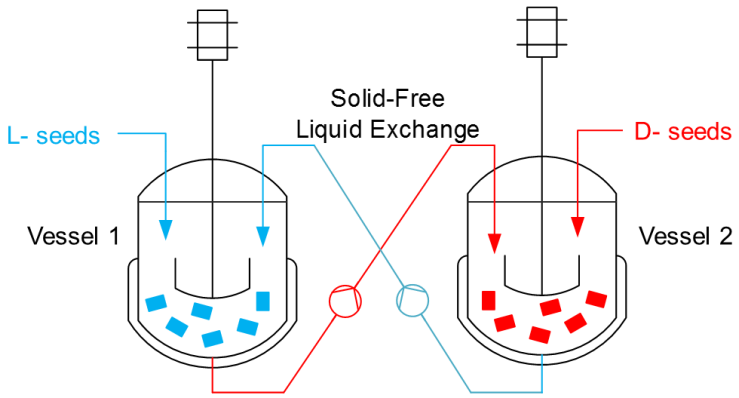

Figure 1.11. Schematic of a typical coupled batch preferential crystallization setup for the separation of a conglomerate forming system of enantiomers. Each tank is seeded with one of the enantiomers. Solid-free liquid exchange of enriched mother liquor occurs between each vessel keeping the overall solution composition close to racemic, thus reducing the risk of counter enantiomer nucleation in either vessel.

As growth of an enantiomer occurs in one of the vessels, thereby depleting the concentration of this enantiomer in the solution, the solution is then transferred to the other vessel via a filtered liquid exchange line. This allows movement of the mother liquor into the other vessel whilst keeping crystals in the vessel. Once the solution is transferred concentration of the other enantiomer in solution in then decreased by growth of the opposite enantiomer in this vessel. Since this happens simultaneously between each vessel, the solution is maintained at an almost racemic composition throughout the process. This is illustrated in Figure 1.12, which shows the ternary phase diagram for a conglomerate system of enantiomers and the solution composition trajectory during a coupled batch preferential process. Point A represents the starting racemic composition in each vessel, each of which is then seeded. The line from point A to point B, which indicates a racemic composition at the crystallization temperature

T_{cr}, is an ideal trajectory of the solution. This would be achieved by having an infinity high exchange rate between the vessels.

For the separation of an enantiomer from a racemic compound, the starting solution in each vessel would be at a eutectic composition. One vessel would be seeded with the pure enantiomer and the other vessel would be seeded with the racemic crystal form. The liquid free exchange would maintain the solution composition along the eutectic line to the eutectic point at the crystallization temperature.

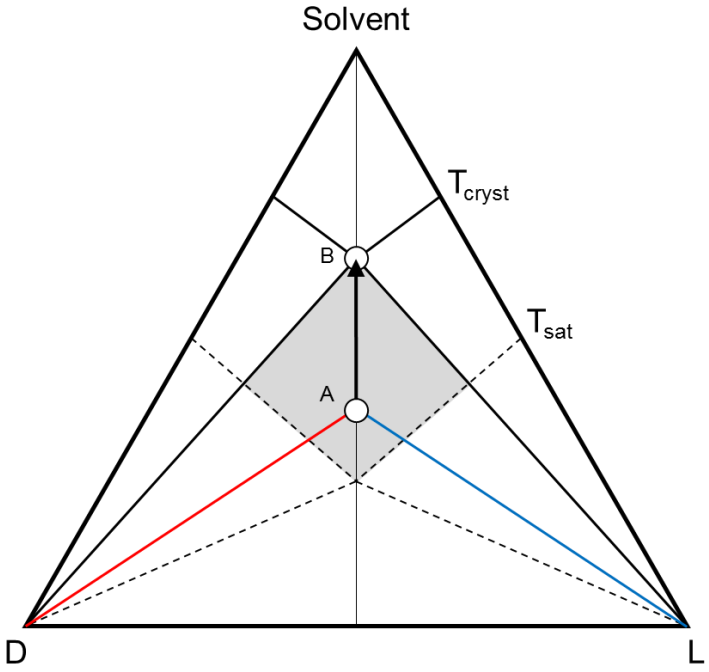

Figure 1.12. Ternary phase diagram of a conglomerate forming system of enantiomers showing the solution composition trajectory during a coupled batch preferential crystallization process. Each tank has a racemic starting composition represented by point A. Mother liquor transfers between the vessels meaning it maintains a racemic composition, and moves to point B, which represents a racemic solution composition at the crystallization temperature. The grey area represents the metastable region within the system.

1.5.2.3 Continuous Preferential Crystallization

In a single stage continuous preferential crystallization process, an MSMPR crystallizer is seeded with the preferred enantiomer (much like a batch-wise PC process). Slurry containing enantiopure solid product as well as solution now enriched

with the unwanted enantiomer is continuously removed from the crystallizer. Simultaneously, fresh racemic (or enriched) solution is fed into the crystallizer from a feed tank.[19]

A coupled batch setup can also be integrated into a continuous preferential crystallization setup as demonstrated by Galan et al.[54] Here, two MSMPR crystallizers are coupled in the same way as shown in Figure 1.11. However, as well as solid free liquid exchange between the vessels, product slurry is also removed from each individual crystallizer along with simultaneous addition of fresh racemic solution from a central feed tank. Similar setups have also been demonstrated in other studies.[19,60]

1.5.2.4 Second Order Asymmetric Transformation (SOAT)

As previously mentioned, it is inevitable in a PC that, given enough time, the unwanted counter enantiomer will crystallize and thus contaminate enantiopure product. However, the second-order asymmetric transformation (SOAT) process is a hybrid of PC and deracemization. Therefore, it offers great promise in achieving high yields and productivities compared to PC since it is possible to achieve a 100% yield of enantiopure material (compared with a maximum 50% yield in PC processes).[65] In a SOAT process, like PC, a racemic solution of enantiomers is seeded with enantiopure crystals of one enantiomer. These seed crystals grow and remove this enantiomer from solution. At the same time, racemization occurs in solution where counter-enantiomer molecules covert to molecules of the preferred enantiomer. This keeps the solution composition [close to] racemic and therefore significantly reduces the risk of unwanted counter enantiomer nucleation.[66] However, if the racemization kinetics of the molecule is slow, then care should be taken and the supersaturation in the system should be kept low in order to avoid unwanted counter-enantiomer nucleation.

Despite the benefits of SOAT, however, such a process requires a racemizing compound (or a racemizing agent to be added for compounds that don't have the ability to racemize). Therefore, PC processes are incredibly useful in obtaining enantiopure crystalline material. However, more control over PC processes must be attained so that higher productivities can be obtained whilst having a low risk of unwanted counter enantiomer nucleation. Furthermore, should the counter enantiomer crystallize, we should have such control over the process that this can be rectified.

1.6 Aims and Objectives

A controlled crystallization process is desired such that a certain product quality attribute (crystal size, shape, polymorphic form, crystal purity) is obtained or a specific process specification (process yield, productivity, process efficiency) is met. Achieving control in preferential crystallization means producing product of the desired chiral form whilst inhibiting and controlling unwanted nucleation of the counter enantiomer (which would contaminate enantiopure product) or, if unwanted nucleation does occur, applying appropriate controlling actions to rectify the situation.

The main aim of this thesis is to demonstrate control in both batch and continuous preferential crystallization processes by improving product enantiopurity and increasing the overall process yield and productivity compared to a conventional batch-wise preferential crystallization process. This aim is broken down into four objectives, as illustrated in Figure 1.5.1. Each experimental chapter of this thesis contributes to the overall aim through either a batch or continuous preferential crystallization process.

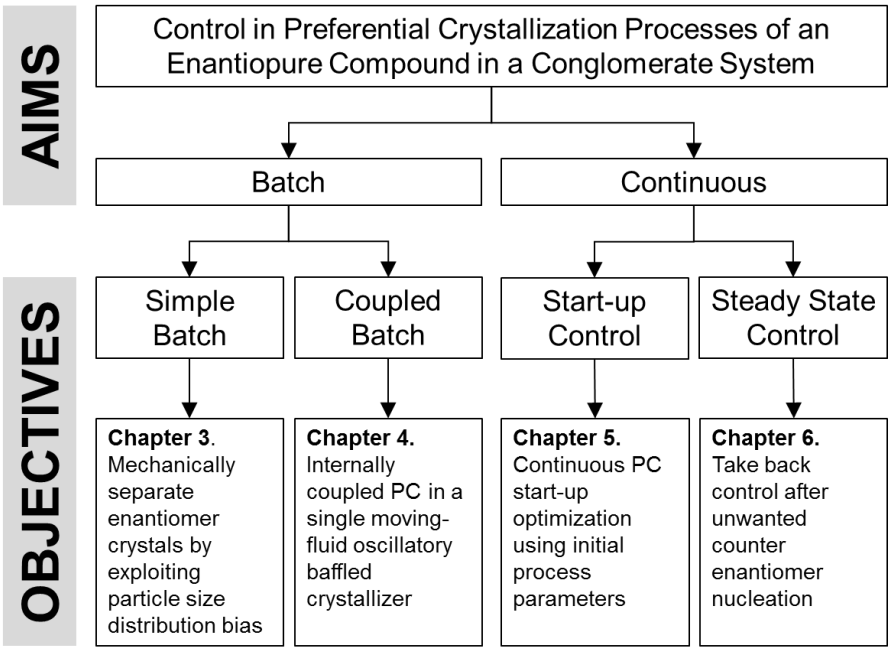

Figure 1.13. The main aim of this thesis is broken down into four specific objectives: two objectives contribute to demonstrating control in batch preferential crystallization

processes and two to demonstrating control in continuous preferential crystallization processes.

Chapter 3: Enabling Mechanical Separation of Enantiomers through Batch Controlled Concomitant Crystallization. This chapters addresses the issue of inevitable unwanted counter enantiomer nucleation in a batch preferential crystallization process and demonstrates a novel method in which this can be avoided. The strategy developed is to use a bias in the product size of each enantiomer in order to mechanically separate them after the crystallization process. By seeding a racemic solution with both enantiomer crystals using a large amount of small seeds of one enantiomer and a small amount of large seeds of the counter enantiomer, each enantiomer crystalline product develops in a distinct crystal size distribution during crystallization. The product consists of crystals of both the preferred and unwanted enantiomer and if there is a sufficiently large bias in their size, they can be mechanically separated by sieving, for instance. In such a process it is important to avoid nucleation in order to maintain control over the size distribution bias. A simple growth only population balance model can be applied such that, as long as the crystallization kinetic parameters of the system are known, the amount of seed required for each form as well as the optimal cooling profile in order to avoid any further nucleation (primary or secondary) can be determined.

Chapter 4: Coupled Batch-wise Preferential Crystallization in a Single Moving-Fluid Oscillatory Baffled Crystallizer. This chapter adopts the concept of a coupled batch preferential crystallization setup. By applying this concept to an oscillatory baffled crystallizer (OBC), however, a single reactor can be used, thus negating the need for a second vessel or additional pumps and tubing. This is achieved by placing a mesh filter between the seal of two connecting parts of the OBC. Seeds of one enantiomer can then be added to one side of the filter and seeds of the opposite enantiomer on the other side. The supersaturation of one enantiomer in solution can be reduced before crossing the filter and allowing the other enantiomer to grow. As long as the seed crystals are larger than the pore size of the filter, only solution will be exchanged between each side.

Chapter 5: Start-up and Steady State of a Continuous Preferential Crystallization in a Continuous Stirred Tank Reactor. This chapter investigates the effect of the initial process parameters (supersaturation, residence time, seed loading, seed size and initial counter enantiomer concentration) on the start-up time and steady state of a continuous preferential crystallization process and in turn develops a workflow for investigating the start-up of a continuous preferential crystallization process. Using a design of experiments (DoE) approach to conduct an experimental plan, a set of screening experiments will be described in order to determine the most important factors that affect the start-up time and steady robustness of a continuous preferential crystallization process. Using online PAT tools (focus beam reflectance measurement and polarimetry) the start-up time to steady state can be detected and, subsequently, the robustness of that steady state can be determined through online monitoring. In doing so, the most important process parameters can be further investigated to reduce waste and optimize the start-up time, as well as maintaining a robust metastable steady state for the duration of the process.

Chapter 6: Resolution Control in a Continuous Preferential Crystallization Process. Given time, nucleation of the counter enantiomer in a supersaturated solution is inevitable in any preferential crystallization process, batch or continuous. Therefore, this chapter investigates potential control strategies that can be applied in the event of such an inevitable occurrence in order to take back control. Control strategies are investigated for both batch and continuous seeded preferential crystallization processes. While in a batch process there are no available strategies, for a continuous process, the thermodynamics of the ternary phase diagram are exploited by switching the feed solution from a racemic feed to an enantiopure feed after nucleation of the counter enantiomer. The composition of the solution in the crystallizer, therefore, is adjusted in such a way that crystals of the counter enantiomer are dissolved after which the feed solution is reverted back to a racemic feed.

1.7 References

(1) Jacques, J.; Collet, A. *Enantiomers, Racemates and Resolutions*; John Wiley & Sons Ltd, 1981.

(2) Davey, R. J.; Schroeder, S. L. M.; ter Horst, J. H. Nucleation of Organic Crystals

- A Molecular Perspective. *Angew. Chemie* **2013**, No. 52, 2166–2179.

(3) Mullin, J. W. *Crystallization*, Fourth Edi.; Butterworth-Heinemann, 2001.

(4) Randolph, A. D.; Larson, M. A. *Theory of Particulate Processes*, Second.; Academic Press, Inc.: San Diego, 1988.

(5) Agrawal, S. G.; Paterson, A. H. J. Secondary Nucleation: Mechanisms and Models. *Chem. Eng. Commun.* **2015**, *202* (5), 698–706. https://doi.org/10.1080/00986445.2014.969369.

(6) Cruz, P.; Rocha, F.; Ferreira, A. Determination of the Critical Mixing Intensity for Secondary Nucleation of Paracetamol in an Oscillatory Flow Crystallizer. *CrystEngComm* **2018**, *20* (6), 829–836. https://doi.org/10.1039/C7CE01940H.

(7) Myerson, A. *Handbook of Industrial Crystallization*; Butterworth-Heinemann, 2002.

(8) Jones, A. G. *Crystallization Process Systems*; Butterworth-Heinemann, 2002.

(9) ter Horst, J. H.; Schmidt, C.; Ulrich, J. *Handbook of Crystal Growth*; Elsevier, 2015. https://doi.org/10.1016/B978-0-444-63303-3.00032-8.

(10) Noyes, A. A.; Whitney, W. R. The Rate of Solution of Solid Substances in Their Own Solutions. *J. Am. Chem. Soc.* **1897**, No. 19, 930–934.

(11) Veesler, S.; Puel, F. *Handbook of Crystal Growth*; Elsevier, 2015. https://doi.org/10.1016/B978-0-444-56369-9.00021-6.

(12) Volmer, M. *Kinetic der Phasenbildung*, Steinkopff, Leipzig, **1939**

(13) Plumb, K. Continuous Processing in the Pharmaceutical Industry: Changing the Mind Set. *Chem. Eng. Res. Des.* **2005**, *83* (6), 730–738. https://doi.org/10.1205/cherd.04359.

(14) Myerson, A. S.; Krumme, M.; Nasr, M.; Thomas, H.; Braatz, R. D. Control Systems Engineering in Continuous Pharmaceutical Manufacturing May 20-21, 2014 Continuous Manufacturing Symposium. *J. Pharm. Sci.* **2015**, *104* (3), 832–839. https://doi.org/10.1002/jps.24311.

(15) Wang, J.; Li, F.; Lakerveld, R. Process Intensification for Pharmaceutical Crystallization. *Chem. Eng. Process. - Process Intensif.* **2018**, *127*, 111–126. https://doi.org/10.1016/J.CEP.2018.03.018.

(16) Mascia, S.; Heider, P. L.; Zhang, H.; Lakerveld, R.; Benyahia, B.; Barton, P. I.; Braatz, R. D.; Cooney, C. L.; Evans, J. M. B.; Jamison, T. F.; et al. End-to-End Continuous Manufacturing of Pharmaceuticals: Integrated Synthesis,

Purification, and Final Dosage Formation. *Angew. Chem. Int. Ed. Engl.* **2013**, *52* (47), 12359–12363. https://doi.org/10.1002/anie.201305429.

(17) Li, J.; Lai, T. C.; Trout, B. L.; Myerson, A. S. Continuous Crystallization of Cyclosporine: Effect of Operating Conditions on Yield and Purity. *Cryst. Growth Des.* **2017**, acs.cgd.6b01212. https://doi.org/10.1021/acs.cgd.6b01212.

(18) Wang, T.; Lu, H.; Wang, J.; Xiao, Y.; Zhou, Y.; Bao, Y.; Hao, H. Recent Progress of Continuous Crystallization. *J. Ind. Eng. Chem.* **2017**, *54*, 14–29. https://doi.org/10.1016/J.JIEC.2017.06.009.

(19) Rougeot, C.; Hein, J. E. Application of Continuous Preferential Crystallization to Efficiently Access Enantiopure Chemicals. *Org. Process Res. Dev.* **2015**, *19* (12), 1809–1819. https://doi.org/10.1021/acs.oprd.5b00141.

(20) Alvarez, A. J.; Singh, A.; Myerson, A. S. Crystallization of Cyclosporine in a Multistage Continuous MSMPR Crystallizer. *Cryst. Growth Des.* **2011**, *11* (10), 4392–4400. https://doi.org/10.1021/cg200546g.

(21) Schaber, S. D.; Gerogiorgis, D. I.; Ramachandran, R.; Evans, J. M. B.; Barton, P. I.; Trout, B. L. Economic Analysis of Integrated Continuous and Batch Pharmaceutical Manufacturing: A Case Study. *Ind. Eng. Chem. Res.* **2011**, *50* (17), 10083–10092. https://doi.org/10.1021/ie2006752.

(22) Baxendale, I. R.; Braatz, R. D.; Hodnett, B. K.; Jensen, K. F.; Johnson, M. D.; Sharratt, P.; Sherlock, J.-P.; Florence, A. J. Achieving Continuous Manufacturing: Technologies and Approaches for Synthesis, Workup, and Isolation of Drug Substance May 20–21, 2014 Continuous Manufacturing Symposium. *Journal of Pharmaceutical Sciences*. 2015, pp 781–791. https://doi.org/10.1002/jps.24252.

(23) Zhang, D.; Xu, S.; Du, S.; Wang, J.; Gong, J. Progress of Pharmaceutical Continuous Crystallization. *Engineering* **2017**, *3* (3). https://doi.org/10.1016/J.ENG.2017.03.023.

(24) McGlone, T.; Briggs, N. E. B.; Clark, C. A.; Brown, C. J.; Sefcik, J.; Florence, A. J. Oscillatory Flow Reactors (OFRs) for Continuous Manufacturing and Crystallization. *Organic Process Research and Development*. 2015. https://doi.org/10.1021/acs.oprd.5b00225.

(25) Simon, L. L. Continuous Manufacturing: Is the Process Mean Stationary? *AIChE J.* **2018**. https://doi.org/10.1002/aic.16125.

(26) Yang, Y.; Song, L.; Gao, T.; Nagy, Z. K. Integrated Upstream and Downstream Application of Wet Milling with Continuous Mixed Suspension Mixed Product Removal Crystallization. *Cryst. Growth Des.* **2015**, *15* (12), 5879–5885. https://doi.org/10.1021/acs.cgd.5b01290.

(27) Yang, Y.; Song, L.; Zhang, Y.; Nagy, Z. K. Application of Wet Milling-Based Automated Direct Nucleation Control in Continuous Cooling Crystallization Processes. *Ind. Eng. Chem. Res.* **2016**, *55* (17), 4987–4996. https://doi.org/10.1021/acs.iecr.5b04956.

(28) Yang, Y.; Song, L.; Nagy, Z. K. Automated Direct Nucleation Control in Continuous Mixed Suspension Mixed Product Removal Cooling Crystallization. *Cryst. Growth Des.* **2015**, *15* (12), 5839–5848. https://doi.org/10.1021/acs.cgd.5b01219.

(29) Hou, G.; Power, G.; Barrett, M.; Glennon, B.; Morris, G.; Zhao, Y. Development and Characterization of a Single Stage Mixed-Suspension, Mixed-Product-Removal Crystallization Process with a Novel Transfer Unit. *Cryst. Growth Des.* **2014**, *14* (4), 1782–1793. https://doi.org/10.1021/cg401904a.

(30) Powell, K. A. Improving Continuous Crystallisation Using Process Analytical Technologies : Design of a Novel Periodic Flow Process, Loughborough University, 2017.

(31) Yang, Y.; Nagy, Z. K. Combined Cooling and Antisolvent Crystallization in Continuous Mixed Suspension, Mixed Product Removal Cascade Crystallizers: Steady-State and Startup Optimization. *Ind. Eng. Chem. Res.* **2015**, *54* (21), 5673–5682. https://doi.org/10.1021/ie5034254.

(32) Su, Q.; Nagy, Z. K.; Rielly, C. D. Pharmaceutical Crystallisation Processes from Batch to Continuous Operation Using MSMPR Stages: Modelling, Design, and Control. *Chem. Eng. Process. Process Intensif.* **2015**, *89*, 41–53. https://doi.org/10.1016/j.cep.2015.01.001.

(33) Nagy, Z. K.; Fevotte, G.; Kramer, H.; Simon, L. L. Recent Advances in the Monitoring, Modelling and Control of Crystallization Systems. *Chem. Eng. Res. Des.* **2013**, *91* (10), 1903–1922. https://doi.org/10.1016/j.cherd.2013.07.018.

(34) Abu Bakar, M. R.; Nagy, Z. K.; Saleemi, A. N.; Rielly, C. D. The Impact of

Direct Nucleation Control on Crystal Size Distribution in Pharmaceutical Crystallization Processes. *Cryst. Growth Des.* **2009**, *9* (3), 1378–1384. https://doi.org/10.1021/cg800595v.

(35) Saleemi, A. N. Strategic Feedback Control of Pharmaceutical Crystallization Systems, Loughborough University, 2011.PhD Thesis

(36) Acevedo, D.; Yang, Y.; Warnke, D. J.; Nagy, Z. K. Model-Based Evaluation of Direct Nucleation Control Approaches for the Continuous Cooling Crystallization of Paracetamol in a Mixed Suspension Mixed Product Removal System. *Cryst. Growth Des.* **2017**, acs.cgd.7b00860. https://doi.org/10.1021/acs.cgd.7b00860.

(37) Saleemi, A.; Rielly, C.; Nagy, Z. K. Automated Direct Nucleation Control for in Situ Dynamic Fines Removal in Batch Cooling Crystallization. *CrystEngComm* **2012**, *14* (6), 2196. https://doi.org/10.1039/c2ce06288g.

(38) Hansen, T. B.; Simone, E.; Nagy, Z.; Qu, H. Process Analytical Tools To Control Polymorphism and Particle Size in Batch Crystallization Processes. *Org. Process Res. Dev.* **2017**, *21* (6), 855–865. https://doi.org/10.1021/acs.oprd.7b00087.

(39) Simon, L. L.; Pataki, H.; Marosi, G.; Meemken, F.; Hungerbühler, K.; Baiker, A.; Tummala, S.; Glennon, B.; Kuentz, M.; Steele, G.; et al. Assessment of Recent Process Analytical Technology (PAT) Trends: A Multiauthor Review. *Organic Process Research and Development*. 2015. https://doi.org/10.1021/op500261y.

(40) Stoker, H. S. *General, Organic and Biological Chemistry*, Sixth.; White, A., Ed.; Brooks/Cole, 2013.

(41) Shekunov, B. Y.; York, P. Crystallization Processes in Pharmaceutical Technology and Drug Delivery Design. *J. Cryst. Growth* **2000**, *211* (1–4), 122–136. https://doi.org/10.1016/S0022-0248(99)00819-2.

(42) Curitiba Marcellos, C. F.; Durand, H.; Kwon, J. S.-I.; Gomes Barreto, A.; Lage, P. L. da C.; Bezerra de Souza, M.; Secchi, A. R.; Christofides, P. D. Optimal Operation of Batch Enantiomer Crystallization: From Ternary Diagrams to Predictive Control. *AIChE J.* **2017**. https://doi.org/10.1002/aic.16028.

(43) Chhabra, N.; Aseri, M. L.; Padmanabhan, D. A Review of Drug Isomerism and Its Significance. *Int. J. Appl. basic Med. Res.* **2013**, *3* (1), 16–18.

https://doi.org/10.4103/2229-516X.112233.

(44) Newmeyer, M. N.; Concheiro, M.; da Costa, J. L.; Flegel, R.; Gorelick, D. A.; Huestis, M. A. Oral Fluid with Three Modes of Collection and Plasma Methamphetamine and Amphetamine Enantiomer Concentrations after Controlled Intranasal L-Methamphetamine Administration. *Drug Test. Anal.* **2015**, *7* (10), 877–883. https://doi.org/10.1002/dta.1784.

(45) Raymond, K. W. *General, Organic & Biological Chemistry; An Intgerated Approach*, Fourth.; John Wiley & Sons, Inc., 2014.

(46) Masterton, W. L. *Chemistry: Principles and Reactions*, Eighth.; Brooks/Cole, 2016.

(47) Köllges, T.; Vetter, T. Model-Based Analysis of Continuous Crystallization/Reaction Processes Separating Conglomerate Forming Enantiomers. *Cryst. Growth Des.* **2017**, *17* (1), 233–247. https://doi.org/10.1021/acs.cgd.6b01487.

(48) Sögütoglu, L.-C.; Steendam, R. R. E.; Meekes, H.; Vlieg, E.; Rutjes, F. P. J. T. Viedma Ripening: A Reliable Crystallisation Method to Reach Single Chirality. *Chem. Soc. Rev.* **2015**, *44* (19), 6723–6732. https://doi.org/10.1039/C5CS00196J.

(49) Engwerda, A. H. J.; Meekes, H.; Kaptein, B.; Rutjes, F. P. J. T.; Vlieg, E. Speeding up Viedma Ripening. *Chem. Commun.* **2016**, *96*, 1659–1676. https://doi.org/10.1039/C6CC06766B.

(50) Xiouras, C.; Fytopoulos, A. A.; Ter Horst, J. H.; Boudouvis, A. G.; Van Gerven, T.; Stefanidis, G. D. Particle Breakage Kinetics and Mechanisms in Attrition-Enhanced Deracemization. *Cryst. Growth Des.* **2018**, acs.cgd.8b00201. https://doi.org/10.1021/acs.cgd.8b00201.

(51) Xiouras, C.; Ter Horst, J. H.; Van Gerven, T.; Stefanidis, G. D. Coupling Viedma Ripening with Racemic Crystal Transformations: Mechanism of Deracemization. *Cryst. Growth Des.* **2017**, acs.cgd.7b00908. https://doi.org/10.1021/acs.cgd.7b00908.

(52) Polenske, D.; Lorenz, H.; Seidel-Morgenstern, A. Potential of Different Techniques of Preferential Crystallization for Enantioseparation of Racemic Compound Forming Systems. *Chirality* **2009**, *21* (8), 728–737. https://doi.org/10.1002/chir.20672.

(53) Petruševska-Seebach, K.; Seidel-Morgenstern, A.; Elsner, M. P. Preferential Crystallization of L-Asparagine in Water. *Cryst. Growth Des.* **2011**, *11* (6), 2149–2163. https://doi.org/10.1021/cg101408e.

(54) Galan, K.; Eicke, M. J.; Elsner, M. P.; Lorenz, H.; Seidel-Morgenstern, A. Continuous Preferential Crystallization of Chiral Molecules in Single and Coupled Mixed-Suspension Mixed-Product-Removal Crystallizers. *Cryst. Growth Des.* **2015**, *15* (4), 1808–1818. https://doi.org/10.1021/cg501854g.

(55) Elsner, M. P.; Ziomek, G.; Seidel-Morgenstern, A. Efficient Separation of Enantiomers by Preferential Crystallization in Two Coupled Vessels. *AIChE J.* **2009**, *55* (3), 640–649. https://doi.org/10.1002/aic.11719.

(56) Levilain, G.; Eicke, M. J.; Seidel-Morgenstern, A. Efficient Resolution of Enantiomers by Coupling Preferential Crystallization and Dissolution. Part 1: Experimental Proof of Principle. *Cryst. Growth Des.* **2012**, *12* (11), 5396–5401. https://doi.org/10.1021/cg3009943.

(57) Lorenz, H.; Polenske, D.; Seidel-Morgenstern, A. Application of Preferential Crystallization to Resolve Racemic Compounds in a Hybrid Process. *Chirality* **2006**, *18* (10), 828–840. https://doi.org/10.1002/chir.20327.

(58) Steendam, R. R. E.; ter Horst, J. H. Continuous Total Spontaneous Resolution. *Cryst. Growth Des.* **2017**, *8*, 4428–4436. https://doi.org/10.1021/acs.cgd.7b00761.

(59) Steendam, R. R. E.; ter Horst, J. H. Scaling Up Temperature Cycling-Induced Deracemization by Suppressing Nonstereoselective Processes. *Cryst. Growth Des.* **2018**, acs.cgd.8b00121. https://doi.org/10.1021/acs.cgd.8b00121.

(60) Chaaban, J. H.; Dam-Johansen, K.; Skovby, T.; Kiil, S. Separation of Enantiomers by Continuous Preferential Crystallization: Experimental Realization Using a Coupled Crystallizer Configuration. *Org. Process Res. Dev.* **2013**, *17* (8), 1010–1020. https://doi.org/10.1021/op400087g.

(61) Elsner, M. P.; Ziomek, G.; Seidel-Morgenstern, A. Simultaneous Preferential Crystallization in a Coupled Batch Operation Mode. Part II: Experimental Study and Model Refinement. *Chem. Eng. Sci.* **2011**, *66* (6), 1269–1284. https://doi.org/10.1016/j.ces.2010.12.035.

(62) Elsner, M. P.; Ziomek, G.; Seidel-Morgenstern, A. Simultaneous Preferential Crystallization in a Coupled, Batch Operation Mode—Part I: Theoretical

Analysis and Optimization. *Chem. Eng. Sci.* **2007**, *62* (17), 4760–4769. https://doi.org/10.1016/j.ces.2007.05.035.

(63) Majumder, A.; Nagy, Z. A Comparative Study of Coupled Preferential Crystallizers for the Efficient Resolution of Conglomerate-Forming Enantiomers. *Pharmaceutics* **2017**, *9* (4), 55. https://doi.org/10.3390/pharmaceutics9040055.

(64) Chaaban, J. H.; Dam-Johansen, K.; Skovby, T.; Kiil, S. Separation of Enantiomers by Preferential Crystallization: Mathematical Modeling of a Coupled Crystallizer Configuration. *Org. Process Res. Dev.* **2014**, *18* (5), 601–612. https://doi.org/10.1021/op400286q.

(65) Oketani, R.; Marin, F.; Tinnemans, P.; Hoquante, M.; Laurent, A.; Brandel, C.; Cardinael, P.; Meekes, H.; Vlieg, E.; Geerts, Y.; et al. Deracemization in a Complex Quaternary System with a Second-Order Asymmetric Transformation by Using Phase Diagram Studies. *Chem. - A Eur. J.* **2019**, *25* (61), 13890–13898. https://doi.org/10.1002/chem.201903338.

(66) Oketani, R.; Hoquante, M.; Brandel, C.; Cardinael, P.; Coquerel, G. Resolution of an Atropisomeric Naphthamide by Second-Order Asymmetric Transformation: A Highly Productive Technique. *Org. Process Res. Dev.* **2019**, *23* (6), 1197–1203. https://doi.org/10.1021/acs.oprd.9b00133.

Chapter 2

2 Materials and Methods

2.1 Materials

The compound used in this work was asparagine monohydrate. This is a non-essential amino acid that forms a conglomerate in the crystalline phase. The structures of the asparagine monohydrate enantiomers are shown in Figure 2.1. DL-asparagine monohydrate (DL-asn), L-asparagine monohydrate (L-asn) and D-asparagine monohydrate (D-asn) were all purchased from Sigma-Aldrich (Germany) throughout the course of this study. De-ionized water, purified by an in-house Milli-Q gradient system from Millipore SAS (France), was used as the solvent throughout this work and was used as dispensed.

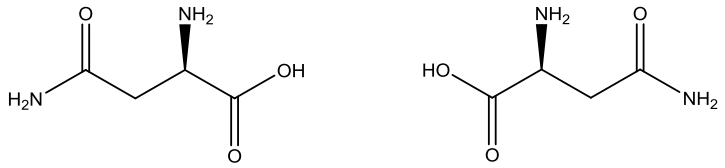

D-asparagine L-asparagine

Figure 2.1. Enantiomers of asparagine; D-asn (left) and L-asn (right).

Asparagine monohydrate has been used abundantly in literature, for both determination of crystallization kinetics as well as a model compound for both batch and continuous preferential crystallization processes. It is a popular model compound due to its low cost and extremely low toxicity. Its solubility in water and insolubility in organic solvents e.g. alcohols also makes it an ideal compound to use for anti-solvent crystallization studies. There are currently no known polymorphs of asparagine monohydrate.

2.2 Material Characterization

2.2.1 Solubility and Gravimetric Concentration Measurements

Effective crystallization processes cannot be conducted without sufficient and accurate knowledge of the chosen system's phase diagram. The first stage in developing a crystallization process is to obtain the solubility phase diagram for the chosen system. Solubility measurements are commonly carried out using gravimetric[1,2] or turbidity[3,4] methods. Gravimetric methods are conducted by adding an excess amount of solid to a solvent solution at a specific temperature. Agitation is applied and the system is allowed to equilibrate. After a significant period of time, agitation is stopped and any excess solid is allowed to settle in the tank/vial. Next, multiple solid free samples of the solution are taken and added to pre-weighed vials (A) and weighed (B). Evaporation then takes place and when all solvent has evaporated the vial with the remaining solid is then weighed again (C). Using the formula given in equation 2.1, the solubility can be obtained.

$$\text{Concentration} = \frac{\text{C}-\text{A}}{\text{B}-\text{C}} \tag{2.1}$$

However, due to the long experimental times required to conduct solubility measurements gravimetrically, in this work, solubility measurements were carried out using the turbidity method. This method is carried out by using multiple heating a cooling cycles on a solution of known concentration at specific heating and cooling rates. In doing so, the clear point (the temperature point at which no more crystals are present in solution) and the cloud point (the temperature at which the first appearance of crystals in suspension) of the system are measured. The difference between the clear and cloud point temperature which gives the metastable zone width (MSZW) of the system.

Solubility measurements were carried out using the Crystal16 (Technobis, Netherlands) which consists of four independent parallel blocks each able to hold four 1 ml vials. Samples of known concentration in 1 g water were added to each vial along with a 6 mm magnetic stirrer. Each vial was heated slowly at a rate of 0.3°C/min until the target temperature was reached at which point it was held at this temperature for 30 minutes (min). Each vial was then cooled at a rate of 0.3°C/min again and held for

30 min once the target temperature was reached. The cycle was repeated three times. The stirring rate was 700 rpm throughout each run. Microsoft Excel was used to analyse the data and determine the clear point and cloud point of each concentration.

The concentration of solution samples from crystallization processes was measured gravimetrically in this work. The method of doing so is similar to the gravimetric solubility determination method, the only exception being that a slurry (solid and solution) sample is taken from the reactor and filtered using a Buchner funnel and vacuum pump. Aliquots of the filtered solution are then taken and added to pre-weighed vials and allowed to evaporate as described previously, and the concentration was determined using Eq. 2.1. The recovered solid was then used for enantiomeric excess determination by HPLC analysis (see section 2.2.2).

2.2.2 High Performance Liquid Chromatography (HPLC)

HPLC is an analytical technique used to separate and quantify components in a sample mixture. It does this by carrying a sample (analyte) in a solution, known as the mobile phase, through a column at a constant flow rate using high pressure pump and allowing the sample to interact with solid adsorbent material, known as the stationary phase. The composition of the mobile and stationary phases depend on the analyte being measured.

Components in the sample that have a stronger affinity (preference) for the stationary phase than other components will take longer to pass through the column. Components with a stronger affinity for the mobile phase will pass through quickly. The longer the column, the more opportunities for interaction with the stationary phase for each component and therefore the greater the separation. Once through the column the analyte(s) are then detected by means of some physiochemical property of the analyte(s), most commonly a UV detector.

In this work, chiral HPLC was used to determine the enantiomeric excess of both solid and solution samples taken during a crystallization process. In a chiral column, each enantiomer has a different affinity for the stationary phase and can therefore be separated based on their independent retention times. In contrast if an "ordinary" column was used, both enantiomers would exit the column at the same time and thus would not be separated. The enantiomeric excess of a sample is determined

by the ratio of the difference in each peak area and the total peak area, as described in Eq. 2.2.

$$E\ [\%] = \left[\frac{(A_{Dasn} - A_{Lasn})}{(A_{Dasn} + A_{Lasn})}\right] x\ 100 \tag{2.2}$$

where E is the enantiomeric excess of the sample in percent, A_{Dasn} is the peak area of D-asn and A_{Lasn} is the peak area of L-asn. Chiral HPLC analysis was carried out using an Agilent HPLC instrument. Solid samples obtained from the filtered slurry were dissolved in water at a concentration of 0.5 - 1.5 mg/ml solvent. Solution samples were diluted to a concentration of 0.5 – 1.5 mg/ml solvent. A CHIROBIOTIC T column (Astec, 150 x 4.6 mm with 5 μm particle size) was used at 25.0°C with a 70/30 methanol/water (v/v) mobile phase (flow rate of 0.5 ml/min) with UV detection at 205 nm. The injection volume was 5 μl. Data was analysed using either the Agilent Masshunter Quantitative Workstation Software or the Agilent Chemstation software.

2.2.3 Scanning Electron Microscope (SEM)

Scanning electron microscopy (SEM) uses a focused beam of electrons to scan across the surface of a solid sample. These electrons strike the sample and interact with atoms on the surface. These collisions emit a range of signals (secondary electrons, backscattered electrons and X-rays) which are then detected. SEM is a useful technique to investigate crystal morphology and aspect ratio, as well as detailed information about the crystal surface such as imperfections, the presence of crystal fines and any damage incurred to product particles.

In this work, SEM analysis was carried out using a JOEL IT 100 scanning electron microscope in secondary electron mode at 10 keV. Images were taken at both x50 and x300 magnifications from at least two different positions. Prior to analysis, all samples were sputtered with gold to achieve a coated layer of 10 nm in thickness using a Leica EM ACE 200 sputter-coater and kept under vacuum for two minutes since asparagine crystals were found to be prone to charging.

2.2.4 Particle Size Analysis

2.2.4.1 Sieving

Crystal seed preparation and particle size analysis was carried out using a Fritsch Analysette 3 Pro sieve shaker. For seed preparation raw material was sieved for three 30 min cycles at an amplitude of 1 mm. For sieving of crystallization product, each sieve was pre-weighed and material was then sieved for 15 min cycles at an amplitude of 1 mm until the weight of each sieve was constant for three consecutive cycles.

2.3 Online Monitoring Methods

2.3.1 Polarimetry

A unique property possessed by chiral molecules is their ability to rotate polarized light.[5] A polarimeter is an instrument used to detect and measure this optical rotation and is a well-established on-line monitoring technique for monitoring preferential crystallization processes.[6–8] For enantiopure systems, polarimetry can give solution concentration information and for enantiomeric enriched systems, it can give an accurate determination of the concentration difference, ΔC, or enantiomeric excess, E, in the solution and therefore indirectly, the crystal E.

Within the polarimeter, a light source emits monochromatic light in all directions perpendicular to the plane of propagation. This light travels through a polarizer that allows only light on one plane through. On coming into contact with a chiral substance in the sample cell, it is rotated either right, *dextrorotatory* (+), or left, *levorotatory* (-). This is illustrated in Figure 2.2. One enantiomer of a compound will rotate this light in one direction, whilst the opposite enantiomer will rotate it in the other direction. For a given concentration, each enantiomer will rotate the light by the same magnitude. Hence, a racemic mixture of a compound will have a net rotation of zero. If this polarized light is passed through and empty cell or one filled with an optically inactive (achiral) compound, the polarized light will emerge unchanged.

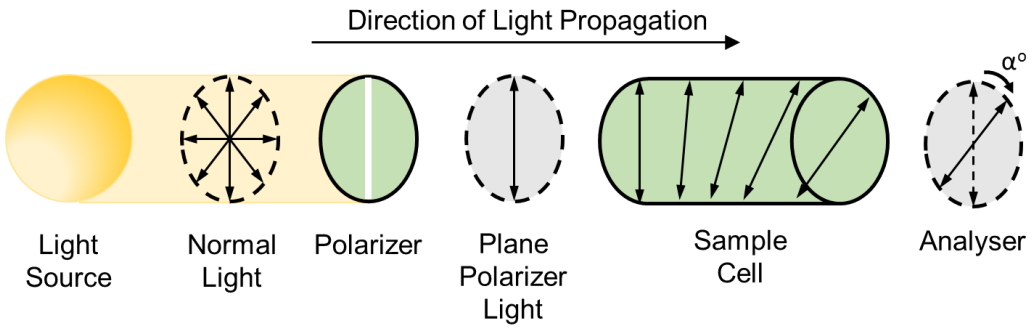

Figure 2.2. The plane polarized light is rotated clockwise or anti-clockwise by the presence of chiral molecules in the sample cell. The magnitude of this rotation is determined by the analyzer and gives information on the concentration or enantiomeric excess in the sample.

Optical rotation analysis was conducted using an AUTOPOL IV Polarimeter (Rudolph Research Analytical, UK) with a 100 mm optical rotation cell. Solid free solution was continuously removed from the crystallizer via a sintered glass filter (ROBU Glasfilter, Germany, 250 x 13 mm) of pore size 10-20 μm (porosity 4) and pumped through the polarimeter cell via a Watson-Marlow (UK) 520 DU peristaltic pump at a flow rate of 45 ml/min. Using these conditions, the solution from the reactor takes 20 seconds to reach the polarimeter to be measured. Optical rotation measurements were recorded every 10 seconds and each measurement was obtained at 30^{o}C and a wavelength of 436 nm.

2.3.2 Focus Beam Reflectance Measurement (FBRM)

Focus beam reflectance measurement (FBRM) is a real-time *in situ* particle tracking technique commonly used to monitor crystallization processes. It provides information on the approximate number and size distribution of particles. It does this by emitting a rotating infrared laser through a glass window at the tip of the probe at a speed of Vs m/s. When this laser comes into contact with a solid particle, that beam is reflected back into the probe to be detected. The length of time the laser is reflectedthe particle times the velocity of the laser is known as the chord length (equation 2.3).[9] This can give information about the approximate size of each particle and therefore can give information on the system e.g. nucleation, growth, agglomeration, breakage etc. This is illustrated in Figure 2.3.

$$\text{CLD} = v_s . \Delta t \tag{2.3}$$

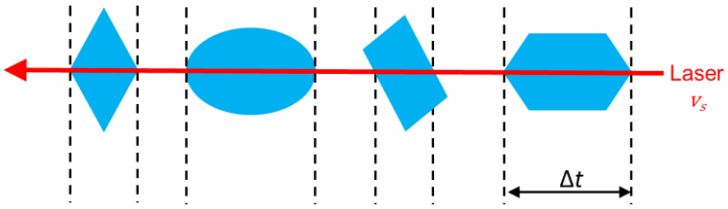

Figure 2.3. Chord length measurement by the FBRM probe.[9]

In-situ analyses was carried out using a Particle Track G400 FBRM immersion probe (Mettler-Toledo, UK). The probe utilizes an infrared laser with a wavelength of 785 nm through a sapphire window that rotates ate 2 m/s. Samples were recorded every 10 seconds for the duration of each crystallization process. For data processing, the iC FBRM software was used.

2.4 Data Analysis Methods

2.4.1 Design of Experiments (DOE)

Design of experiments (DOE) is a statistical method for obtaining the maximum amount of experimental detail as possible with minimum amount of experimental effort.[9] There are several DOE approaches that can be used, which depend on the desired outcome of the experiments e.g. from fractional-factorial (screening) designs, which are used to determine what effect (if any) a particular process parameter (variable) or combination of parameters has on the process of interest, to full factorial designs, which are used to optimize process parameters to achieve the best results for the desired outcome of the process. Such optimization approaches are best suited for a small number of variables and levels (low to high values), since, any increase in the number of levels or variables will exponentially increase the number of experiments required.

Four statistics are used to describe the generated model: R^2, Q^2, model validity and model reproducibility. R^2 is the goodness of fit of the model and measures how well the regression model fits the raw data:

$$R^2 = 1 - \frac{S_R}{S_T} \quad (2.4)$$

where S_R is the sum of squares of the residual, corrected for the mean and S_T is the total sum of squares of response Y, corrected for the mean. R^2 varies between 0 and 1, where 1 is a perfect model and 0 is no model at all. However, R^2 alone cannot be used to describe a model since it can be made artificially close to 1 by including more terms to the model. Therefore, the *goodness of prediction* Q^2 can give a better indication of the usefulness of the model as it estimates how well the model will predict future experiments:

$$Q^2 = 1 - \frac{S_{PR}}{S_T} \quad (2.5)$$

where S_{PR} is the prediction residual sum of squares. Q^2 also has an upper bound of 1 however it has a lower limit of minus infinity. For a model to be considered good, both R^2 and Q^2 should be high, and separated by no more than 0.3. A Q^2 value of >0.5 is regarded as good and >0.9 is excellent. The model validity is calculated once the replicate experiments have been completed and reflect whether the right type of model has been chosen. A value >0.25 indicates a valid model, <0.25 indicates a significant 'lack of fit' in the model:

$$\text{Model Validity} = 1 + 0.57647 \times \log_{10}(p) \quad (2.6)$$

where p is the p-value for the lack of fit of the model. Finally, the model reproducibility indicates how reproducible the model is. The larger the value the smaller the error between replicate experiments in relation to the variability across the remaining experiments in the design. A value <0.5 means that there is a large pure error and poor control over the experimental procedure.

$$\text{Model Reproducibility} = 1 - \frac{MS_{PE}}{MS_T} \quad (2.7)$$

where MS_{PE} is the mean square of the pure error and MS_T is the total mean square of response Y.

A fractional factorial (screening) DOE was conducted using MODDE Pro 11 software (UMetrics) and all data was analyzed using the partial least squares (PLS) method within the software.

2.5 References

(1) Powell, K. A. Improving Continuous Crystallisation Using Process Analytical Technologies : Design of a Novel Periodic Flow Process, Loughborough University, 2017. PhD Thesis.

(2) Lorenz, H.; Sapoundjiev, D.; Seidel-Morgenstern, A. Enantiomeric Mandelic Acid System - Melting Point Phase Diagram and Solubility in Water. *J. Chem. Eng. Data* **2002**, *47* (5), 1280–1284. https://doi.org/10.1021/je0200620.

(3) Srisanga, S.; ter Horst, J. H. Racemic Compound, Conglomerate, or Solid Solution: Phase Diagram Screening of Chiral Compounds. *Cryst. Growth Des.* **2010**, *10* (4), 1808–1812. https://doi.org/10.1021/cg901483v.

(4) Kongsamai, P.; Maneedaeng, A.; Flood, C.; ter Horst, J. H.; Flood, A. E. Effect of Additives on the Preferential Crystallization of L-Asparagine Monohydrate. *Eur. Phys. J. Spec. Top.* **2017**, *226* (5), 823–835. https://doi.org/10.1140/epjst/e2016-60257-3.

(5) Bruice, P. Y. Chiral Compounds Are Optically Active. In *Organic Chemistry*; Pearson, 2011; pp 206–208.

(6) Alvarez Rodrigo, A.; Lorenz, H.; Seidel-Morgenstern, A. Online Monitoring of Preferential Crystallization of Enantiomers. *Chirality* **2004**, No. 16, 499–508.

(7) Petruševska-Seebach, K.; Seidel-Morgenstern, A.; Elsner, M. P. Preferential Crystallization of L-Asparagine in Water. *Cryst. Growth Des.* **2011**, *11* (6), 2149–2163. https://doi.org/10.1021/cg101408e.

(8) Elsner, M. P.; Ziomek, G.; Seidel-Morgenstern, A. Efficient Separation of Enantiomers by Preferential Crystallization in Two Coupled Vessels. *AIChE J.* **2009**, *55* (3), 640–649. https://doi.org/10.1002/aic.11719.

(9) Saleemi, A. N. Strategic Feedback Control of Pharmaceutical Crystallization Systems, Loughborough University, 2011.

Chapter 3

3 Enabling Mechanical Separation of Enantiomers through Batch Controlled Concomitant Crystallization

Andrew S. Dunn, Botond Szilagyi[†], Zoltan K. Nagy[*], Joop H. ter Horst*

In the pharmaceutical industry the separation of chiral molecules is important due to the different physiochemical properties enantiomers of a chiral drug possess. Therefore, resolution techniques are used to separate such enantiomers from one another. In particular, preferential crystallization is a common technique used to separate conglomerate forming compounds, due to its high selectivity. However, efficient separation of enantiomers in a batch-wise preferential crystallization process through seeding with the preferred enantiomer alone is still inefficient since unwanted primary nucleation of the counter enantiomer is inevitable. Here we demonstrate a mechanical separation method for the separation of enantiomers for a conglomerate forming compound through the mechanical separation method of sieving enabled by a bias in the crystal size distributions of each enantiomer. This bias is created by a concomitant crystallization of both enantiomers using optimized seeding and cooling profiles obtained from a population balance model. In this way, a high level of control is attained over a batch-wise preferential crystallization process compared to preferential crystallization since the crystallization of both enantiomers is controlled. We show that through this separation method, material with impurity levels as low as 6 weight% can be obtained. To our knowledge this is the first demonstration of such a process to separate enantiomers of a conglomerate forming compound.

[*] Davidson School of Chemical Engineering, Purdue University, West Lafayette, Indiana 47907, United States
[†]Physical development and optimization of the process model was carried out by Dr. Botond Szilagyi

3.1 Introduction

The pharmaceutical industry requires the use of resolution processes in order to separate chiral molecules to obtain a homochiral product.[1] The importance of the access to efficient resolution processes is clear from the physiochemical properties of chiral drug substances. There are rare cases where both enantiomers (mirror image forms) of a chiral molecule induce the desired pharmaceutical response. In other cases one of the enantiomers has the desired pharmaceutical response while the other enantiomer is inactive. However, in the more serious case, the opposite enantiomer can induce a hazardous effect on the patient.[2] Such is the case of Naproxen: the *S*-enantiomer produces the desired anti-inflammatory response, whereas its mirror image *R*-enantiomer causes liver poisoning.[3]

There are a number of process techniques available to separate enantiomers, including deracemization[4–6] and chromatography[7–9] techniques. A common resolution technique used in industry is preferential crystallization (PC). In a PC process, a racemic or enantiomerically enriched solution is seeded with the preferred enantiomer, thereby allowing this form to crystallize out of solution and grow.[10] One aspect of the PC process which still causes problems, however, particularly in batch setups, is the unwanted primary nucleation of the counter enantiomer.[11] As the preferred enantiomer crystallizes, the supersaturation with respect to the counter enantiomer remains constant or, in the case of cooling or evaporative crystallization processes, increases in time. If the process is run for too long, this unwanted form will eventually crystallize via primary nucleation, in which case the process must be stopped. The likelihood of this occurring increases with increasing supersaturation and batch time. The risk of unwanted nucleation of the counter enantiomer can be reduced by running the PC process in a coupled batch[12–14] or continuous setups.[15,16] Recently, we demonstrated a control strategy that can be implemented in each of these setups that rectifies any occurrences of unwanted nucleation of the counter enantiomer.[16] Furthermore, the use of additives can be used to inhibit the crystallization of the unwanted chiral form.[17] However, the problem remains that the risk of unwanted counter enantiomer nucleation is ever present.

It is important, therefore, to investigate other methods to separate enantiomers, for example, through mechanical separation. Mastai et al.[18] exploited the difference in

densities between racemic and enantiopure crystals of a racemic forming compound based on a density gradient method to obtain up to 70% separation of forms. However, such exploitation of solid-state properties cannot be used for conglomerate forming compounds since the densities are equal for both enantiomers. Furthermore, manipulation of the size and shape is difficult to control for only one enantiomer without affecting the other. Therefore, manipulation of the crystal size distributions (CSDs) for each enantiomer can be used via seeded batch-wise concomitant crystallization. Recently, purification by mechanical separation based on particle size has been demonstrated for a binary eutectic mixture of fluorene and fluorenone by Zhang et al.[19] However, no such process has been applied to a more complex system where both compounds have the same crystallization behaviour i.e. a conglomerate forming system of enantiomers.

In this paper we demonstrate a mechanical separation strategy for a conglomerate forming system of enantiomers by creating a bias in the crystal size distribution of each enantiomer. This strategy removes the risk of unwanted primary nucleation of the counter enantiomer by obtaining control of the crystallization of both enantiomers simultaneously. First, we describe the formulation of a dynamic crystallization model of the process by means of population balance equations (PBEs) before performing a two-level model optimization in order to obtain optimum crystallization conditions for experimentation. Finally, we experimentally demonstrate use of the mechanical separation method in order to separate enantiomers of the conglomerate forming compound asparagine monohydrate.

3.2 Model Development and Numerical Solution

Population balance models (PBMs) are a widely used way to model crystallization processes. The PB equation (PBE) describes the evolution of the solid phase within the crystallizer; it is constructed by partial difference equations (PDEs) that describe the change in the number density function n in time. The number density gives the number of particles per unit of volume within the $L, L + dL$ size interval at time t. In a PC process for a conglomerate forming compound, the solute molecules of one enantiomer will only crystallize on the seeds of this particular enantiomer. Hence, in a PC process for a conglomerate systems two populations can be distinguished: the

population of L- and D- enantiomer crystals, for which the number densities are denoted by $n_L(L,t)$ and $n_D(L,t)$, respectively.

In this study, we assume a growth-only concomitant crystallization process with negligible agglomeration and breakage of particles. In such crystallization process, the number density of crystals remains constant and the seed crystals are grown during the process. This is a good approximation if the crystallization process is kept within the metastable zone in order to avoid nucleation. Furthermore, the agitation intensity must be high enough to keep the system well-mixed and minimize the agglomeration, but at the same time mild enough to prevent crystal breakage. This process will be referred to hereafter as a well-controlled crystallization. The one-dimensional growth only PBE for such a well-controlled batch-wise cooling crystallization, can be given by:

$$\frac{\partial n_I(L,t)}{\partial t} + G_I \frac{\partial n_I(L,t)}{\partial L} = 0, \qquad I = L, D \tag{3.1}$$

where the initial and boundary conditions are given as,

$$\begin{aligned} n_I(L,0) &= n_{I,0}(L) \\ n_I(L \to \infty, t) &= 0 \end{aligned} \tag{3.2}$$

The initial condition $n_{I,0}(L)$ gives the seed distribution of L-asn and D-asn whereas the boundary condition states that the crystals have finite size. In Eq. 3.1 G_I is the size independent growth rate (assuming size independent growth) of enantiomer *e* in µm/s, which is modeled by the power law equation:

$$G_I = k_g \left(\frac{C_I}{C_{I,sat}} - 1 \right)^g \tag{3.3}$$

where k_g and g are kinetic parameters, which are independent of enantiomeric form, C_I is the solution concentration of the L- and D- enantiomers and $C_{I,sat}$ is the saturation

concentration of an enantiomer. For the solubility description of asparagine the model equation given by Petruševska-Seebach et al. is used:[20]

$$w_{eq}^{L} = p_1 \times \exp(p_2 \mathrm{T}) + p_3 w^{D} \tag{3.4}$$

where w_{eq}^{L} denotes the solubility of L-asn in terms of weight fraction as a function of temperature (°C) and counter enantiomer weight fraction w^{D}. The weight fraction based solubility can easily be recalculated to match the unit of concentration for $C_{I,sat}$. According to the solubility equation, the L-asn solubility depends on temperature and the concentration of D-asn. A similar equation is applicable for a D-asn solubility calculation. Based on the solubility expression, the dynamics of two populations are not independent of each-other being linked through the solubility expressions. However, based on the solubility expressions this effect is small. The change in concentration inside the crystallizer as a function of time is given by the solute mass balance, which is written in the form of an ordinary differential equation (ODE):

$$\frac{dC_I}{dt} = -3\rho_c k_v G_I 10^{-18} \int_0^{\infty} L^2 n_I(L,t)\, dL, \qquad I = \mathrm{L}, \mathrm{D} \tag{3.5}$$

where ρ_c is the crystal density, k_v is the volume shape factor and 10^{-18} is a factor that transforms μm^3 to m^3. Here we assumed that the L-asn and D-asn crystals have identical densities and shapes. The initial condition of the mass balance is the initial concentration: $C_I(t=0) = C_{I,0}$.

3.2.1 Numerical Solution of the Model Equations

Various techniques have been developed to solve PBEs. One of the more popular methods is to use the standard method of moments (SMOM)[21] and its extensions.[22] This enables the exact calculation of moments of the distribution and the concentration however it fails to calculate the full CSD. Among the full PBE solvers the Method of Characteristics (MOC) is known to be the most accurate as it completely removes the convective term from the hyperbolic PBE.[23] For crystallization process simulation MOC can be numerically inaccurate because of the mass balance evaluation

of Eq. 3.5, unless a very fine discretization is applied, which in turn causes it to become numerically inefficient. In this work, SMOM is employed for concentration calculation, and the combined SMOM and MOC for the accurate and efficient full CSD calculation. These are well known techniques[24] and thus only a brief description is provided here.

3.2.1.1 SMOM for Solute Calculation

The SMOM relies on the moment transformation rule, given by the following equation:

$$\mu_{I,i} = \int_0^\infty L^i n_I(L,t)dL \tag{3.6}$$

Applying the moment transformation to PBE in Eq. 3.1 gives the moment equations system:

$$\frac{d\mu_{I,0}}{dt} = 0$$
$$\frac{d\mu_{I,i}}{dt} = iG_I\mu_{I,i-1} \qquad i = 1,2,3 \tag{3.7}$$

with the moment transformation, the mass balance in Eq. 3.5 becomes:

$$\frac{dC_I}{dt} = -3\rho_c k_v G_I \mu_{I,2} 10^{-18} \tag{3.8}$$

The system of moment equations for the two populations Eq. 3.7 with the corresponding mass balances Eq. 3.8 generates ten ordinary differential equations (ODEs) which consist of the closed model of the well-controlled PC process.

MOM is the computationally most effective PBE solution technique, and it has the advantage that it provides the accurate concentration profile. For numerous calculations in this work, the model equations are solved for the concentration profile,

and to those calculations the MOM is applied. However, exact CSD reconstruction from its moments is not possible.

3.2.1.2 Combined SMOM and MOC for full CSD Calculation

MOC is a well-suited solution method of the PB Eq. 3.1 for full CSD calculation. As this technique is routinely applied for crystallization modelling, here only a brief description is provided but interested readers can find a detailed description in literature.[25,26] Through the MOC approach we define CSD curves in the (*L*-*t*) plane, which reduces the PBE to a system of ODEs. The (*L*-*t*) plane can be expressed in a parametric form by $L = L(Z)$ and $t = t(Z)$, where the parameter Z gives the measure of distance along the characteristic curve. The number density n_I can be redefined as:

$$n_I(L,t) = n_I\big(L(Z), t(Z)\big) \tag{3.9}$$

Applying the chain rule on we obtain:

$$\frac{dn_I(L,t)}{dZ} = \frac{dt}{dZ}\frac{\partial n_I(L,t)}{\partial t} + \frac{dL}{dZ}\frac{\partial n_I(L,t)}{\partial L} \tag{3.10}$$

Comparing the coefficients of Eqs. 3.1 and 3.10 it can be concluded that:

$$\frac{dt}{dZ} = 1 \rightarrow dt = dZ \tag{3.11}$$

$$\frac{dL}{dZ} = G_I \leftrightarrow \frac{dL}{dt} = G_I \tag{3.12}$$

$$\frac{dn_I(L,t)}{dZ} = 0 \leftrightarrow \frac{dn_I(L,t)}{dt} = 0 \tag{3.13}$$

with initial conditions, corresponding to $t = Z = 0$, $L = L_0$ and $n_I(L,0) = n_{I,0}(L)$. Eq. 3.13 expresses that the number of crystals belonging to the characteristic lines

remain unchanged throughout the process. To obtain the dynamic evolution of the crystal size distribution, $n_I(L,0)$, equation 3.12, with prescribed growth expressions, can be integrated repeatedly for different initial values $[L_0]$. The mass balance Eq. 3.5 can be evaluated using the MOC based CSD. However, for accurate mass balance calculation a high number of characteristic lines have to be used i.e. Eq. 3.12 is solved for many different $[L_0]$ values, which degrades the overall computational efficiency. As a clever workaround, MOC can be effectively combined with the MOM as follows; firstly, the MOM solution is applied, which provides the accurate concentration profile as an input for the growth rate calculation within the MOC. This effectively decouples the accuracy of CSD dynamics from the MOC discretization coarseness and hence, the computational time.

3.3 Model-based Optimization

Model-based optimization was carried out for the determination of optimum process conditions subject to the set of constraints and objectives. The batch PC process to be optimized in which a racemic solution of enantiomers is seeded with crystals both chiral forms of different crystal sizes and seed loadings. In this way, we can create a bias in the product crystal size of each enantiomer and thus separate these enantiomer crystals by means of a mechanical process such as sieving. In this section, we briefly present the developed novel optimization. A schematic of the optimization procedure is shown in Figure 3.1.

It is important to understand that the product CSD of a growth-only batch crystallization process is fully determined by the seed CSD and operating concentration domain. In this context, one might have the impression that for the purpose of this work it is sufficient to use the traditional equations for the seed recipe design (Eq. 3.24). There are two problems with this assumption; first, this is valid if the crystallizer is operated within the metastable zone. This leads to the second issue; to ensure growth-only conditions i.e. low supersaturation throughout the process), large batch times must be applied. To improve the performance, dynamic simulation-based optimizations are required that can operate directly on nonlinear constraints, such as maximum allowed supersaturations, as well as various objectives.

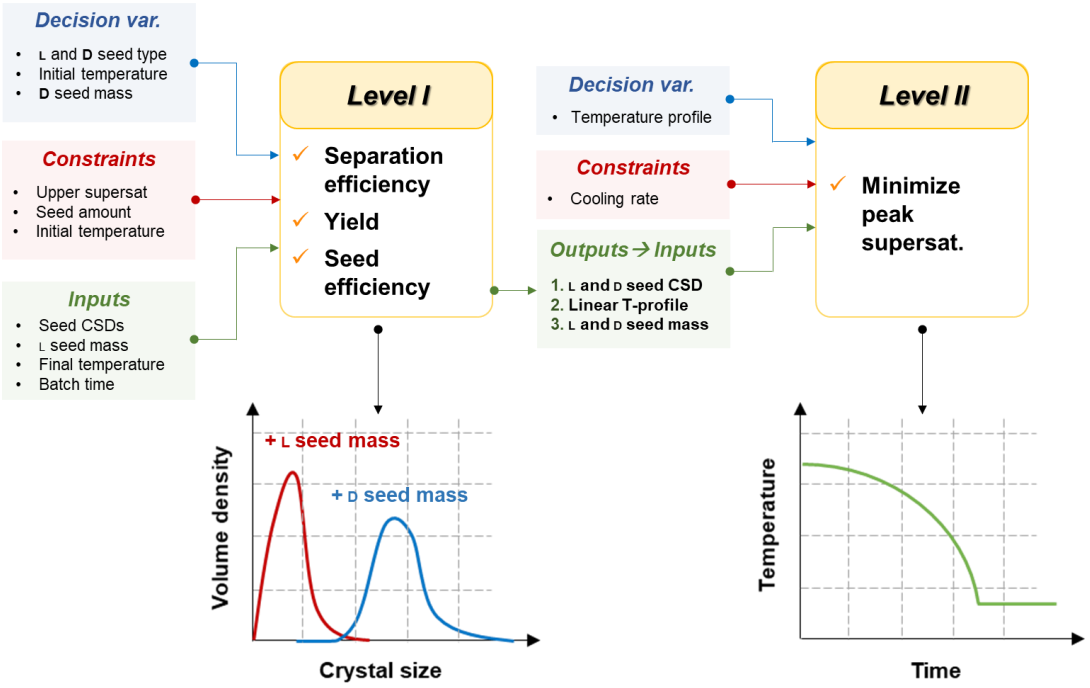

Figure 3.1. Schematic representation of the model optimization framework for the mechanical separation of enantiomers of a conglomerate forming compound. Input parameters, decision variables and constraints are applied to a Level 1 optimization to optimize the separation efficiency, yield and seed efficiency of the process. This initial optimization generates outputs of initial seed CSD and seed loading for each enantiomer as well as an optimized linear cooling profile. These Level 1 optimization outputs are then used as inputs alongside additional decision variables and constraints for a Level 2 optimization which generates the optimum dynamic cooling profiles in order to minimize the peak supersaturation achieved during the process.

3.3.1 The Objective

We aim to maximize three sub-objectives, namely, the separation efficiency *e*, the yield *y* and the seed efficiency *s*.

$$O = O_e + w_1 O_y + w_2 O_s \tag{3.14}$$

where w_1 and w_2 are weight factors that control the relative importance of each sub-objective. The separation efficiency is defined as the fraction of the crystallized product volume that is present in enantiopure sieve fractions:

$$O_e = \sum_{i=1}^{N} \varepsilon_i \Phi_i \tag{3.15}$$

where i stands for the i^{th} sieve fraction, ε_i is a binary variable that characterizes the separation in the i^{th} sieve fraction having the value $\varepsilon_i = 1$ if the solid enantiomer excess E_{cr} exceeds a threshold value in the given sieve fraction, and it is 0 otherwise:

$$\varepsilon_i = \begin{cases} 1, \text{if} \int_{L_{b,i}}^{U_{b,i}} \frac{\left|n_{L,v}(L,t_f) - n_{D,v}(L,t_f)\right|}{\left[n_{L,v}(L,t_f) + n_{D.v}(L,t_f)\right]} dL > E_c \\ 0, \text{otherwise} \end{cases} \tag{3.16}$$

where $n_{L,v}$ and $n_{D,v}$ are the volume based CSDs of L- and D- enantiomers, respectively and t_f is the final time. The sizes $L_{b,i}$ and $U_{b,i}$ are the lower and upper size limit of the i^{th} sieve fraction. The volume fraction Φ_i denotes the volume fraction of crystals in the given sieve fraction:

$$\Phi_i = \frac{\int_{L_{b,i}}^{U_{b,i}} \left[n_{L,v}(L,t_f) + n_{D,v}(L,t_f)\right] dL}{\mu_{L,3}(t_f) + \mu_{D,3}(t_f)} \tag{3.17}$$

It is assumed that the solution is in equilibrium i.e. there is no supersaturation at the beginning and the end of crystallization process. The yield, defined as the fraction of solute crystallized out, is expressed in terms of solubilities in the corresponding temperatures:

$$O_y = \frac{[C_{L,satS,L}(T_i) - C_{L,satS,L}(T_f)] + [C_{D,satS,D}(T_i) - C_{D,satS,D}(T_f)]}{C_{L,sat}(T_i) + C_{D,sat}(T_i)} \tag{3.18}$$

where T_i and T_f denote the initial and final temperatures.

The seed efficiency sub-objective expresses the mass of product obtained from unit mass of seed:

$$O_s = \frac{\mu_{L,3}(t_f) + \mu_{D,3}(t_f) - \mu_{L,3}(t_i) - \mu_{D,3}(t_i)}{\mu_{L,3}(t_i) + \mu_{D,3}(t_i)} \tag{3.19}$$

The introduction of seed efficiency term is necessary since the seeds are high quality crystals obtained from the product of previous batches, hence, the seed production reduces the overall productivity. The weight factors of the optimization were set based on preliminary optimizations such to assign the highest relative importance to separation efficiency, whereas slightly lower and relatively equal importance to yield (w_1 = 0.01) and seed efficiency (w_2 = 0.05).

3.3.2 The Decision Variables

In order to simplify the optimization problem, the following quantities were given fixed values: batch time (with a certain equilibrium time after the final temperature is reached for de-supersaturation), final crystallization temperature and seed loading of L-asn crystals. L-asn seed loading is fixed to give some level of control over the optimization to the human operator. The following continuous decision variables therefore still exist:

- D-asn seed loading,
- initial temperature and
- vector of temperatures that define the cooling profile

On a practical level. L-asn and D-asn seed crystals were obtained by sieving. There are no arbitrary sieve openings, therefore the seed distribution cannot be directly optimized. In contrast, different sieve fractions can be used as seeds. For example, one might apply 63-90 μm L-asn and 90-125 μm D-asn seed sieve fractions. Hence, the L-asn and D-asn seed type is an integer decision variable. The problem becomes a mixed integer nonlinear programming (MINLP).

3.3.3 Constraints and Solution Techniques

We used a two-level solution for the optimization problem that considerably improves the chance of finding the global optimum. As Figure 3.1 presents, the first level optimization results in a solution of the MINLP maximization problem by an exhaustive search i.e. carrying out optimization for every possible combination of L-asn and D-asn sieve fractions, based on the following objective:

$$O_1(T_i, \Phi_D, U_L, U_D) = O_e + w_1 O_y + w_2 O_{se} \tag{3.20}$$

In this optimization the linear cooling profile is applied with a fixed final temperature. T_i is the initial temperature (the final temperature is fixed at 20°C), Φ_D is the volume fraction of D-asn seeds in the total suspension volume (Φ of L-asn seeds is fixed at 0.0025) and U_L and U_D are the integer labels representing the sieve fractions for L-asn and D-asn seed types (seed sieve fractions). For example, U_L = 1 for the smallest available sieve fraction of L-asn seeds, U_L = 2 for the second smallest sieve fraction etc. The following constraints for the crystallization process were applied:

$$\max\{C_L(t), C_D(t)\} \leq C_{MS}(T(t))$$

$$T_{i,min} \leq T_i \leq T_{i,max} \tag{3.21}$$

$$\Phi_{D,min} \leq \Phi_D \leq \Phi_{D,max}$$

The first constraint avoids conditions for secondary nucleation or other nucleation processes to occur by limiting the process to operate within the metastable zone by avoiding the concentration to exceed the metastable limit. Secondary nucleation would generate new crystals to act as seeds which leads to a loss of control over the particle size distributions. The second constraint limits the saturation temperature T_{sat} by limiting the initial concentrations of the process. This allows for a sufficient amount of crystallization to occur during the process without wasting vast amounts of material by starting at significantly high solution concentrations. The third constraint limits the volume fraction of D-asn seed crystals.

The second optimization O_2 was carried out to find the optimal temperature profile. The temperature profile is defined as a vector of temperatures (T_V) in the intermediate time moments corresponding to the elements of the time vector (t_V). t_v is the vector of evenly spaced time moments between the initial and final process time. The objective O_2 is the minimization of peak supersaturation by re-adjusting the temperature profile between the fixed initial and final temperatures, which further reduces the chance of unwanted secondary nucleation:

$$O_2(T_V) = \max\{S_L(t_v), S_D(t_v)\} \tag{3.22}$$

where $S_L(tv)$ and $S_D(tv)$ denote the vectors of supersaturation throughout the batch for both enantiomers. The second optimization has the constraints:

$$c_{r,min} \leq c_r = -\frac{\Delta T}{\Delta t} \leq c_{r,max} \tag{3.23}$$

where c_r is the cooling rate. The second optimization readjusts the temperature profile to minimize the peak supersaturations. To reduce calculation time while retaining accuracy the computationally more expensive MOC was applied only in the evaluation of Eq. 3.16 to calculate the Level 1 objectives. The nonlinear constraint of the first optimization as well as the second optimization objective were calculated using the SMOM solver.

The kinetic and process parameters used in the simulation case study are listed in Table 3.1. It is important to highlight that the solubility and growth kinetics are directly taken from literature[20,27] and are used without re-adjustment.

Table 3.1. Model parameters applied in this study, taken from the literature.[20,27]

Parameter	Symbol	Value	Units
Growth rate constant	k_g	5.044	µm/s
Growth rate supersaturation exponent	g	1.48	-
Crystal volume shape factor	k_v	1.87	-
Crystal density	ρ_c	1.554×10^{3}	kg/m^3
Solubility parameter	p_1	9.2×10^{-3}	-
Solubility parameter	p_2	4.43×10^{-2}	-
Solubility parameter	p_3	3.048×10^{-2}	-

3.4 Experimental

3.4.1 Materials and Methods

DL-asparagine monohydrate (DL-asn) and L-asparagine monohydrate (L-asn) and D-asparagine monohydrate (D-asn) were purchased from Sigma-Aldrich (Germany). Seed crystals of L-asn were prepared through subsequent sieving using the Fritsch Analysette 3 Pro sieve shaker to obtain the desired sieve fractions described in Table 3.2. De-ionised water, purified by Milli-Q gradient system from Milipore SAS (France), was used as a solvent.

Chiral HPLC analysis was carried out using an Agilent HPLC instrument to determine enantiomeric excess of the solution and recovered solid product. Solid samples obtained from the filtered slurry were dissolved in water at a concentration of 1 mg/ml solvent. A CHIROBIOTIC T column (Astec, 150 x 4.6 mm with 5 µm particle size) was used at 25.0°C with a 70/30 methanol/water (v/v) mobile phase (flow rate of 0.5 ml/min) with UV detection at 205 nm. The injection volume was 5 µl.

3.4.2 Separation Experiments

Separation experiments were performed in a Mettler Toledo OptiMax™ workstation of 1 L capacity, equipped with an in-line Hastelloy® Pt100 temperature sensor. The system was operated and controlled using iControl V5.2 software. For in-situ particle tracking a Mettler-Toledo FBRM probe (G400 series) was inserted into the reactor and added to the workstation with iC FBRM V4.3 incorporated into the iControl software. For in-situ particle imaging a Mettler-Toledo Particle Viewing

Microscope (PVM) was inserted into the reactor and added to the workstation with iC PVM V7.0 incorporated into the iC Control Software. DL-asn was added to water in the OptiMax™ reactor such that an overall composition required as dictated by Table 3.2 was obtained. The solution was heated to 10°C above the saturation temperature T_s to ensure all particles dissolved and a clear solution was obtained. The temperature was the reduced to T_s and held for 10 minutes. The optimized temperature profile was then started. At this point seeds of both L-asn and D-asn were added in accordance with Table 3.2. Experiments were carried out using different volume fraction seed loadings of L-asn and D-asn seeds and different seed sizes of each.

Table 3.2. Experimental parameters for the experimental demonstration of the separation strategy. The seed volume fraction Φ is define as the ratio between the volume of seed of L-asn or D-asn and the total volume of the suspension.

Experiment	T_s [°C]	L-asn		D-asn		Cooling Time [hours]
		Seed Size [μm]	Volume Fraction Φ_L	Seed Size [μm]	Volume Fraction Φ_D	
1	44.8	63-90	0.0017	180-250	0.0025	5
2	42.6	45-63	0.0025	125-180	0.0010	5
3	37.2	45-63	0.0025	180-250	0.0011	5
4	40.9	20-45	0.0025	90-125	0.0010	3
5	35.0	355-500	0.0025	63-90	0.0013	3

Once the process was complete, the suspension was removed from the vessel and filtered using the Buchner funnel. The filtrated solid was washed once with solvent (water) and three times with anti-solvent, isopropanol (IPA), and left to dry overnight in a vacuum oven. It was found during experimentation that filtration and washing of the product crystals is extremely important; in preliminary experiments, no optimized washing procedure was in place and after drying the product crystals were heavily agglomerated. Therefore, the separation results obtained for these experiments were quite poor. However, once an improved washing regime was established, crystals were observed to be un-agglomerated and free flowing. After drying the product was sieved

using a Fritsch Analysette 3 Pro sieve shaker. Each sieved fraction was tared and weighed after sieving to determine the mass of product collected in each fraction. Finally, solid samples from each sieved fraction were taken for HPLC analysis to determine the solid enantiomeric excess. Product collected in a particular sieve fraction was considered impure if the enantiomeric excess obtained was less than 80%. A schematic of the experimental setup and process procedure is shown in Figure 3.2.

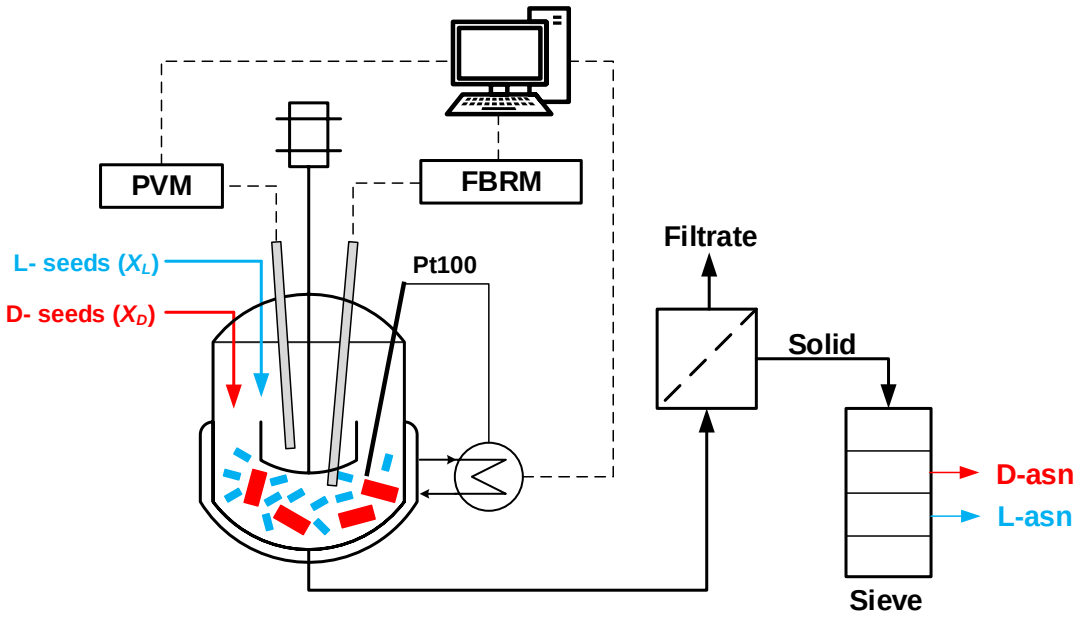

Figure 3.2. Batch PC setup for the mechanical separation of D-asn and L-asn enantiomers. A 1 L Optimax reactor was used for the crystallization process which was seeded with both D-asn and L-asn crystals as detailed in Table 3.2. Once the cooling profile was complete the suspension was collected, filter and washed. Product crystals were left to dry in a vacuum oven at 25°C overnight before being sieved. Samples of product collected in each sieve fraction were collected for enantiomeric excess determination by chiral HPLC.

3.5 Results

3.5.1 Concomitant Crystallization Simulations

The performed simulation case study demonstrates the capabilities of the developed two-level optimization strategy. The first level optimization determines the optimum input seed size and mass of L-asn and D-asn. The level two optimization then

optimizes the cooling profile to minimize the peak supersaturation in order to avoid unwanted nucleation during the process. Four seed distributions are chosen for the L-asn and D-asn with volume based average size of 100 (CSD1), 150 (CSD2), 200 (CSD3) and 250 µm (CSD4), which are plotted in Figure 3.3. This translates to 10 possible L-asn-D-asn seed pair CSD combinations.

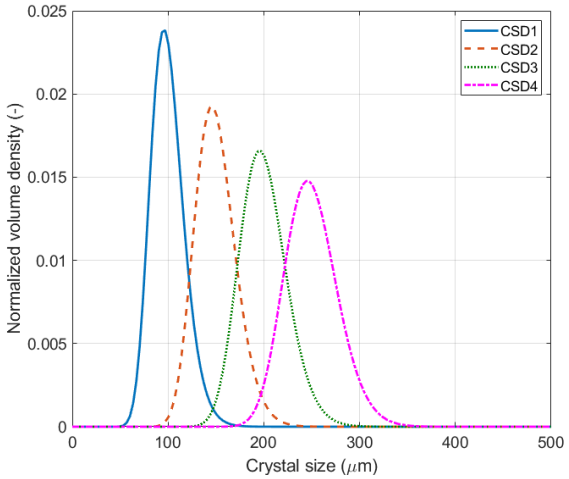

Figure 3.3. Seed distributions n_0 for both L-asn and D-asn in the simulation case study.

Table 3.3 lists the conditions and constraints of the process optimizations. In the simulation case study, the batch cooling time was set to 5 hours. However, in the experiments conducted both 3- and 5-hour batch cooling times were applied. The constraints for the initial temperature were set to lower and upper boundaries of 35 and 45°C, respectively, whereas the final temperature was fixed. The maximum cooling rate was set such as to be well within the cooling capacity of the system. L-asn seed volume fraction and the critical enantiomer excess were set intuitively. D-asn seed volume fraction limits were defined as a symmetrical interval around the L-asn seed volume fraction.

The Level 1 optimization results for a crystallization with initial temperature T_i = 41.63 and batch time of 5 h are presented in Table 3.4. Following the nomenclature of Figure 3.3, the optimal D-asn seed distribution is CSD3, whereas the optimal L-asn seed is CSD4. Naturally, these CSDs are optimal only in combination with the optimal initial temperature (41.63°C) and D-asn seed volume fraction (Φ_D = 0.0043).

Table 3.3. Parameters and constraints for optimization of the concomitant crystallization process

Parameter	Symbol	Value	Units
Batch time	t_b	3 or 5	h
Equilibration time	t_e	2	h
Initial temperature	T_i	35 - 45	°C
Final temperature	T_f	20	°C
L-asn seed volume fraction*	Φ_L	0.0025	-
D-asn seed volume fraction*	Φ_D	0.001 – 0.005	-
Minimal cooling rate	$c_{r,min}$	0.01	°C/min
Maximal cooling rate	$c_{r,max}$	0.3	°C/min
Critical enantiomeric excess	E_c	0.99	-
Sieve fractions boundaries	-	{20, 45, 63, 90, 125, 180, 250, 355, 500}	μm

*seed volume fraction is the volume fraction of seed crystals in respect to the total volume of solution and seed crystals

Table 3.4. Level 1 optimization results for the simulation-based case study. The nomenclature for L-asn and D-asn seeds is taken from Figure 3.3.

L-asn seed	D-asn seed	D-asn Volume Fraction Φ_D	T_i (°C)
4	3	0.00435	41.63

Figure 3.4a represents the normalized volume densities of the product crystal populations obtained in the two-level optimization together with the available sieve fraction boundaries. According to the results, the 500 μm sieve fraction is able to perfectly separate the two populations. Crystals of D-asn would be collected in the 355-500 μm sieve, with a very small portion collected in the 250-355 μm sieve whilst the L-asn crystals would be collected in the 500-710 μm sieve fraction. Hence, perfect separation of the enantiomer crystals is achieved using the optimized crystallization conditions. The level 1 optimized supersaturation of each enantiomer throughout the

process is plotted in Figure 3.4b. Due to the constraint on the concentration (Eq. 3.20) in the Level 1 optimization, the supersaturation profile during the crystallization nicely stays within the metastable zone.

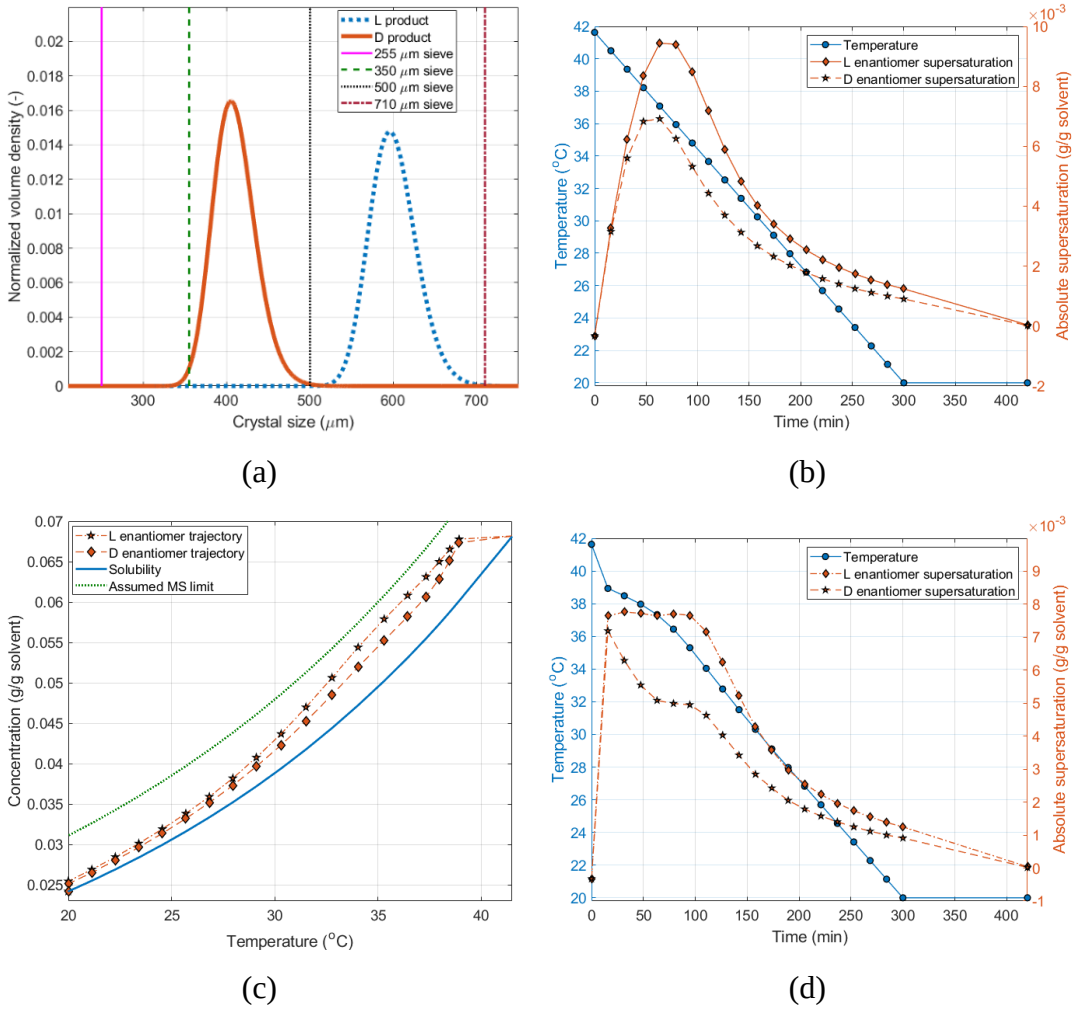

Figure 3.4. Level 1 (a and b) and Level 2 (c and d) optimization results for the simulation with CSD3 seeds for D-asn and CSD4 seeds for L-asn: (a) the optimized product distributions and available sieve fraction boundaries, (b) optimized linear cooling profile and the resulting supersaturations for the L- and D- enantiomers, (c) phase diagram of the Level 2 optimized process and (d) The optimized temperature profile and the resulting supersaturations for the L-asn and D-asn after the level 2 optimization.

The Level 2 optimization minimizes the peak supersaturation by optimizing the temperature profile within the set constraints of cooling rate and process time. Figure 3.4c illustrates that the operating trajectories in the solubility curve are well within the (assumed) secondary nucleation metastable zone. Therefore, the probability of unwanted secondary nucleation is minimized in the Level 2 optimization. The optimized temperature cooling profile (Figure 3.4d) has parabolic shape, which is known to be the most effective for avoiding unwanted nucleation in seeded cooling crystallization. It is interesting to observe how the peak supersaturation (which, in this case is for L-asn) plateaus at ~7.8 x 10^{-3} g/g solvent between 10-90 minutes of the process. The peak supersaturation in Level 1 optimization was ~9.2 x 10^{-3} g/g solvent, therefore, the Level 2 optimization reduced the peak supersaturation in the system by ~15 % through small adjustments in the temperature profile.

3.5.2 Parametric Study for Separation Efficiency

According to case study of Section 3.5.1 of this chapter, the developed optimization framework is suitable for calculating the optimal process conditions for efficient concomitant PC process design. However, from a process understanding point of view, the optimum operation represents only a narrow slice of the operating space. A parametric study was carried out to analyze the process in a substantially broader space.

Figure 3.5 presents the weight fraction of enantiopure product obtained by sieving with the sieve fractions defined in Table 3.3. The initial temperature and seed CSDs were set based on the optimization results in Table 3.4 in order to obtain results comparable to the optimization section. While in Figure 3.5a the critical enantiomeric excess was set to 99%, the critical enantiomeric excess for Figure 3.5b was set to 90%. According to the results, by increasing the critical enantiomeric excess, the domain in which enantiopure product can be obtained decreases. As the rest of the process parameters of these simulations were set based on the optimization results, the seed loadings corresponding to the optimal values on the surface of Figure 3.5b represent the optimum solution. As the separation efficiency was the main objective, it is not surprising that the optimum solution as at a plateau (100% separation). This parametric study also reveals that at the given initial temperature and seed CSDs there are many

other seed loadings that yield in 100% separation. This leaves room for the optimization of secondary objectives, such as yield and seed efficiency. Although, these surfaces do not consider the supersaturation and other constraints (Eq. 3.21), therefore some parts of the space might be infeasible for the optimization.

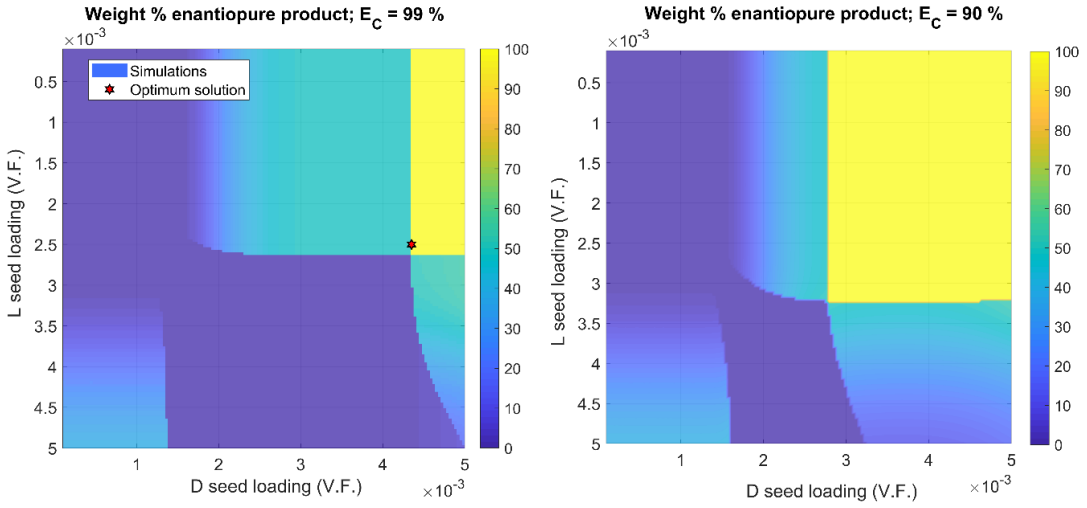

Figure 3.5. Achievable separation performance by sieving as a function of enantiomer seed loadings. The simulation conditions are based on Table 4: L-asn seed distribution = CSD4, D-asn seed distribution = CSD3, batch time = 5-hour, linear cooling from 41.63 to 20°C.

3.5.3 Concomitant Crystallization Experiments

The input seed CSDs and seed volume fractions, as well as the optimum cooling temperature profile determined in the optimization simulations were carried forward for experimental demonstration. A total of five experiments were carried out, the details of which are given in Table 3.2. Figure 3.6 shows the separation results of each experiment where the mass fraction of total product mass is shown for each product sieve fraction and, within each sieve fraction, the enantiomeric excess. If product collected in a sieve fraction has an enantiomeric excess of less than 80% then that material is considered to be impure. This purity threshold is also shown in each plot in Figure 3.6a-e for both L-asn (+80%) and D-asn (-80%).

In experiment 1 (Figure 3.6a) 100% D-asn product was collected in both the 355-500 μm and >500 μm sieve fractions. Pure L-asn product was collected in the 90-125 μm sieve fraction and below. Some D-asn product was collected in sieve fractions 125-

180 μm and 180-250 μm however there was still an enantiomeric excess >80% with respect to L-asn product. Impure product was collected only in the 250-355 μm sieve fraction meaning only 8.1% of the total product mass collected was impure.

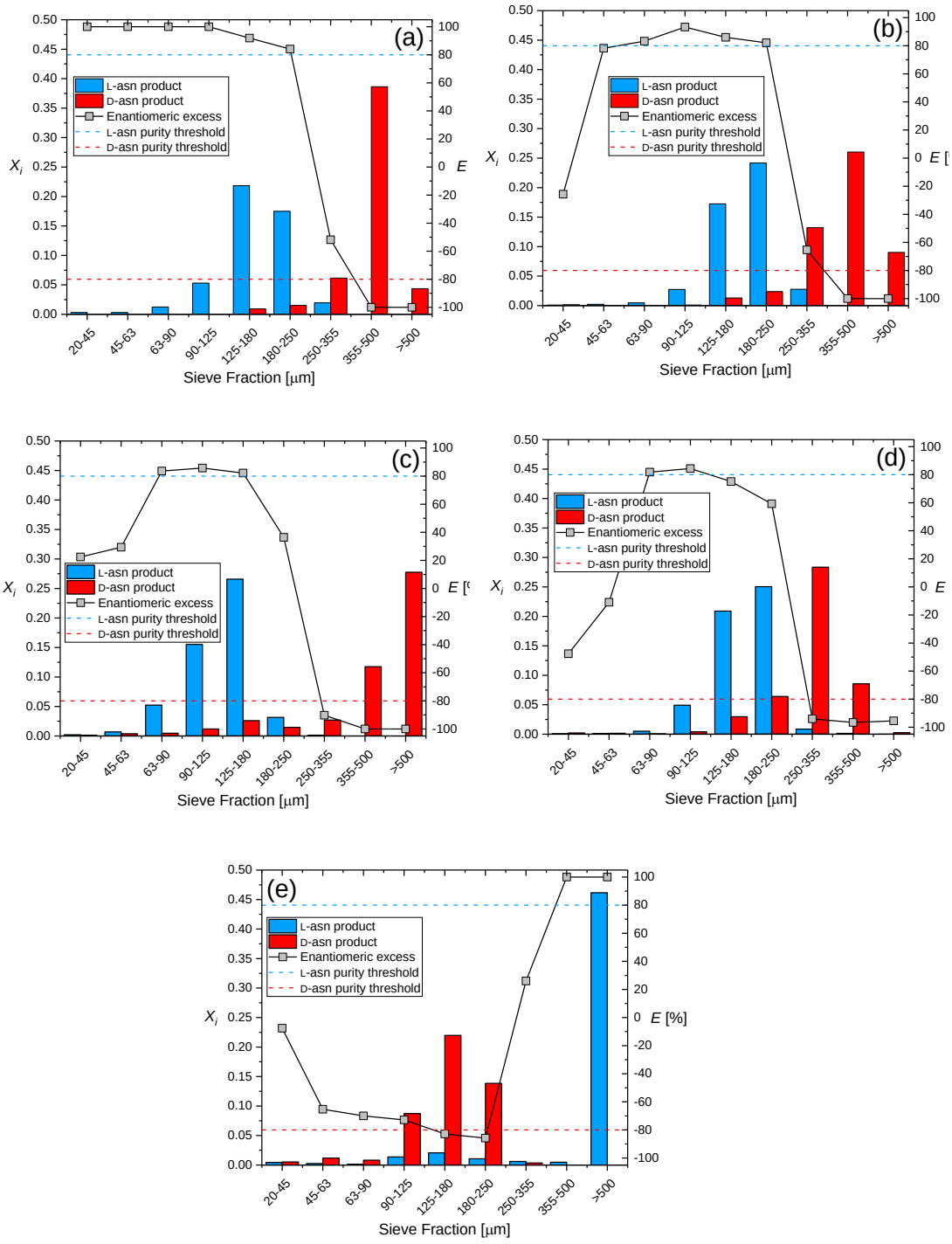

Figure 3.6. Product CSDs for L-asn (■) and D-asn (■) crystals collected via sieving after filtration washing and drying for experiments 1-5 (a-e, respectively) in Table 3.2.

Each sieve column shows the mass fraction X_i of total product obtained for L-asn and D-asn as well as the enantiomeric excess (-■-) of product in each sieve fraction. A purity threshold is set for both L-asn (--) at +80% enantiomeric excess and D-asn (--) at -80% enantiomeric excess.

A similar result was obtained for experiment 3, where only 6.0% of the total product mass collected was impure (product in sieve fractions 20-45 μm, 45-63 μm and 180-250 μm). In experiments 2 and 5 (Figure 3.6b and 3.6d, respectively), the percentage of impure product collected was 16.5% and 14.4% of the total product mass, respectively. Of the five experiments carried out in Table 3.2, only one experiment produced more than 20 wt% impure product; in experiment 4, 55.9% of the total product mass collected was impure.

Figure 3.6 shows that in all the experiments only a small fraction of product has been collected in the sieve fraction lower than the lowest input seed size (with the exception of experiment 2, where product has been collected in the sieve fraction equal to the seed input size). This observation gives a strong indication that secondary nucleation is taking place in the crystallizer. Evidence that secondary nucleation occurred is also observed in the FBRM count (Figure 3.7) and chord length distribution (CLD) trends (Figure 3.8) from each experiment.

Each plot in Figure 3.7a-e shows the FBRM count trends and cooling profiles for experiment 1-5. Count trends are shown for the corresponding sieve fractions available: 45-63, 63-90, 90-125, 125-180 and 180-250 μm. FBRM is a useful PAT tool than can give a good indication of the mechanisms occurring in the process e.g. crystal growth, nucleation, dissolution etc. However, it cannot give accurate size information since a 10 μm chord length might have been measured at the edge of a 100 μm crystal.

In the FBRM count trends in Figure 3.7a, a sharp increase in the number of counts for each sieve fraction chord length bin can be seen at around 20 min; this is the point at which seed crystals were added to the crystallizer (see Table 3.2 for seed loading details). After seeding, there is a decrease in the number of counts for chord lengths 45-63 μm and 63-90 μm. This could indicate growth of the seed crystals since, at the same time, we see an increase in the number of counts for 90-125 μm, 125-180 μm and 180-250 μm. Over time in each experiment we see continued increase in the

number of counts for 90-125 µm 125-180 µm and 180-250 µm chord lengths. However, there is also an increase in the number of counts for chord lengths 45-63 µm and 63-90 µm. This would indicate that the number of smaller particles in the crystallizer is increasing, most likely due to secondary nucleation in the system. Similar trends can be seen in experiments 2-5 (Figure 3.7b-e, respectively).

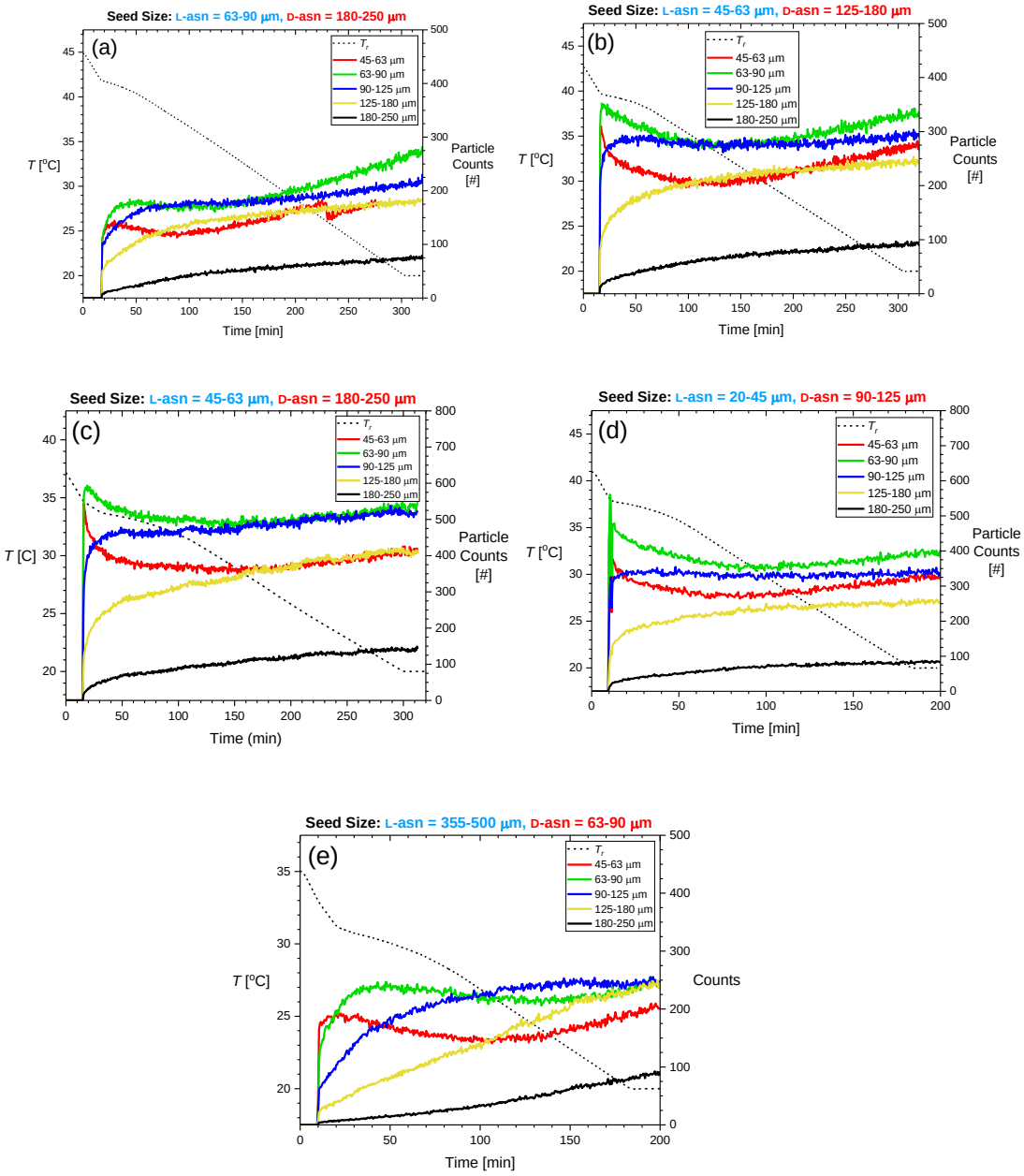

Figure 3.7. Temperature and FBRM count trends for experiments 1-5 (a-e, respectively) in Table 3.2. Each plot shows T_r = reactor temperature (--) as a function

of time and the measured particle chord lengths, (-) 45-63 μm, (-) 63-90 μm, (-) 90-125 μm, (-) 125-180 μm and (-) 180-250 μm as a function of time.

For each plot in Figure 3.8a-e, the seed CLD is shown (black dashed line) as well as CLDs are various time intervals throughout each experiment. For experiments with a 5-hour cooling profile, CLDs are shown at 1-hour intervals. For experiments with a 3-hour cooling profile, CLDs are shown at 30 min intervals. In each experiment 1-5 (Figure 3.8a-e, respectively) there is an overall trend in each experiment with time that the CLD shifts to the right, indicating crystal growth during the process. However, the inset of each plot on Figure 3.8a-d expands the region of the each CLD front.

In experiment 1 (Figure 3.8a), whilst there is an overall shift of the whole CLD to the right, we see that over time the CLD front shifts to the left with each sample point. This indicates that over time there are also more and more small particles being produced; another indication of secondary nucleation. In Figure 3.8b-e (experiments 2-5, respectively), there is an initial shift to the right of the CLD front (following the trend of the overall CLD) meaning that initially only growth is occurring. Then the CLD front starts trending to the left at 180 min in experiment 2 (Figure 3.8b), 240 min in experiment 3 (Figure 3.8c) and 120 min in experiment 4 (Figure 3.8d) and 150 min in experiment 5 (Figure 3.8e) indicating that secondary nucleation has started to occur in each of these experiments.

The effect of secondary nucleation can also be seen in the average product crystal sizes obtained from each enantiomer and comparing this value to the predicted average crystal size expected to be obtained. This predicted size can be investigated with Eq. 3.24:

$$L_p^3 = L_s^3 \times \frac{\Delta m + m_s}{m_s} \tag{3.24}$$

where L_p is the average size of the product crystals p, L_s is the average size of the seed crystals s, Δm is the change in mass due to crystallization from solution and m_s is the mass of seeds added at the start of the crystallization. Use of this equation assumes that throughout the process there is a constant number of particles i.e. no nucleation or agglomeration.

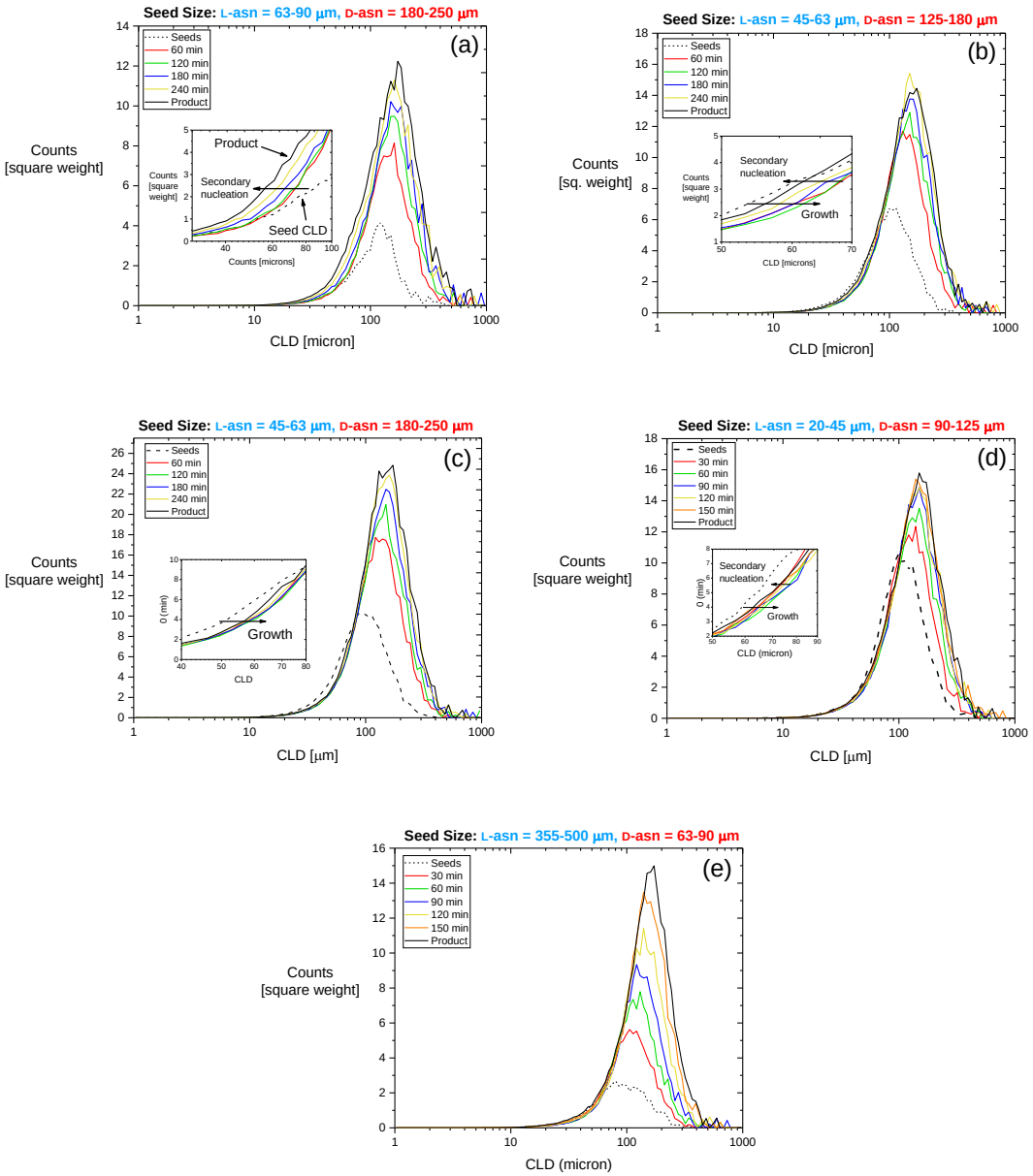

Figure 3.8. Chord length distribution (CLD) trends for experiments 1-5 (a-e, respectively) in Table 3.2. For experiments with a 5-hour cooling profile (experiments 1-3) the measured CLD at 60 min intervals in plot a-c: (--) seed (0 min), (-) 60 min, (-) 120 min, (-) 180 min, (-) 240 min and (-) product. For experiments with a 3 hour cooling profile (experiments 4 and 5) the measured CLD at 30 min intervals is shown in plots d and e: (--) seed (0 min), (-) 30 min, (-) 60 min, (-) 90 min, (-) 120 min, (-) 150 min and (-) product. The inset of each plot highlight any shifts in the CLD trend for each experiment that indicate any potential secondary nucleation.

Figure 3.9 illustrates the plot of obtained average crystal size versus predicted average crystal size. The straight line through the origin indicates that the predicted size is equal to the experimental size of the product for a point which lies on that line. Points which lie below this line indicate that the predicted average crystal size is greater than experimentally obtained average crystal size, meaning that it is likely that crystals have been formed during the process by means of secondary nucleation or breakage. Points which lie above the line indicate that the obtained average crystal size is larger than the predicted average crystal size, indicating that the number of crystals has decreased during the process, most likely due to agglomeration of crystals. The obtained average crystal size of each enantiomer $\bar{x}_{CSD}^{(e)}$ was calculated by:

$$\bar{x}_{CSD}^{(e)} = 2 \times \sum X_i^{(e)} \cdot \bar{x}_F \tag{3.25}$$

where $X_i^{(e)}$ is the mass fraction of enantiomer e in sieve fraction F and $\bar{x}_F$ is the average size in sieve fraction F assuming a normal distribution within the sieve fraction. Figure 3.9 shows that in all experiments, crystals of D-asn undergo secondary nucleation. In experiments 2 and 3, L-asn crystals are shown to undergo ideal growth. However from the separation plots in Figure 3.6b and 3.6c, respectively, we can see that some secondary nucleation of L-asn does occur. Figure 3.9 also shows that for experiment 4 some agglomeration of L-asn crystals may have occurred since the obtained average product crystal size is larger than the predicted average crystal size in this experiment.

3.6 Discussion

Whilst the model-based optimization generates the optimal process conditions (initial seed CSDs and seed loadings of both enantiomers as well as initial temperature and temperature cooling profile) to achieve chiral separation through sieving, experimentally, the actual separation efficiency achieved depends on several additional factors. First, it is important to maintain a constant number of crystals during the process i.e. no nucleation or agglomeration, so that only growth of the crystals occurs and therefore separation of the CSDs at the end of the process yields enantiopure material. In this work, seeds were prepared by sieving the raw material

obtained from the supplier. No further pre-treatment of the seeds was carried out. Therefore, it is possible that small fines could exist on the surface of the seeds. These fines can become dislodged during mixing and act as secondary nuclei.[28,29] This is known as initial breeding.[30] In addition, although the simulations suggest conditions to avoid secondary nucleation, this experimentally still may occur, compromising the CSD of both enantiomers. Furthermore, if any of the pre-sieved seed crystals are agglomerates (meaning they would not pass through the sieve shaker during seed preparation), they could become de-agglomerated by fluid mixing in the crystallizer during the process. However, this mechanism is least likely to occur. PVM images from each experiment 1-5 in Table 3.2 are shown in Figure 3.10. Images of the suspension both just after seeding and just before product was collected are shown. Although the PVM images are useful in allowing the process to be generally visualized, the quality of the images was not sufficiently good enough to allow the above hypothesis to be verified.

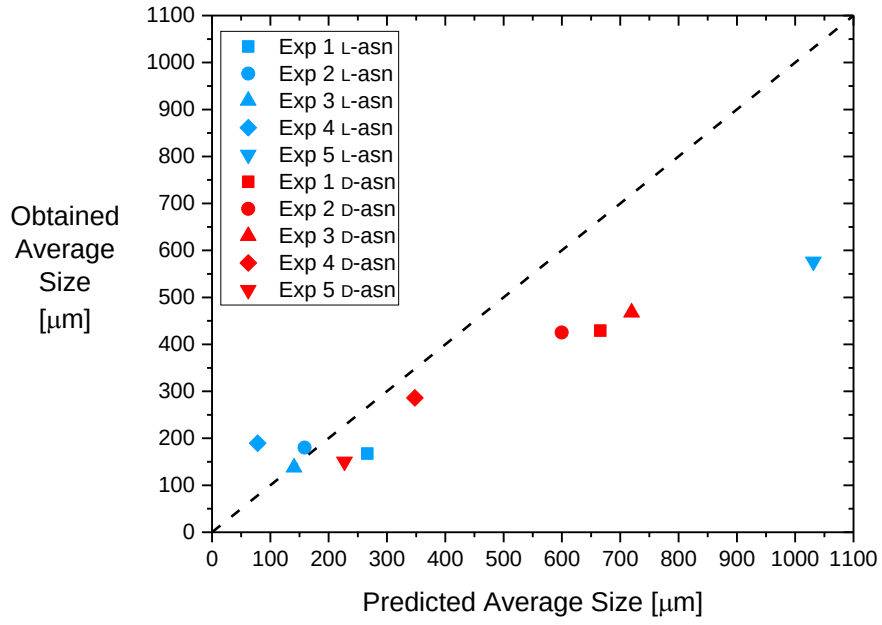

Figure 3.9. Obtained versus predicted average product particle size of both L-asn and D-asn crystals from the separation experiments carried out in Table 3.2 calculated from Eq. (3.25): L-asn (blue) and D-asn (red) average crystal sizes for experiment 1 (■,■), experiment 2 (●,●), experiment 3 (▲,▲), experiment 4 (♦,♦) and experiment 5 (▼,▼). The straight line through the origin indicates the predicted average crystal size is equal

to the experimentally obtained average crystal size. Points which show the predicted size is greater than the obtained size indicate formation of crystals during the process by secondary nucleation.

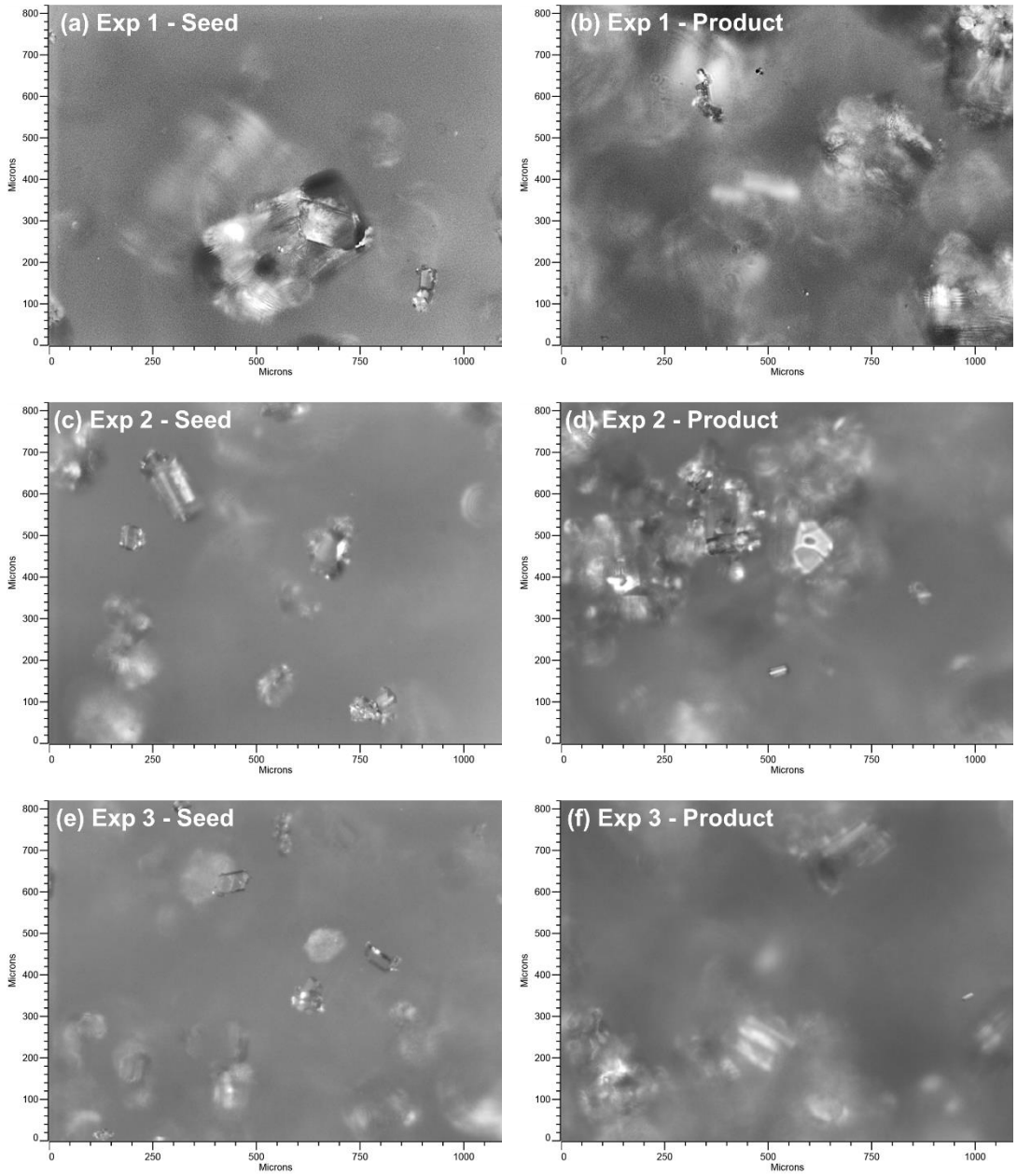

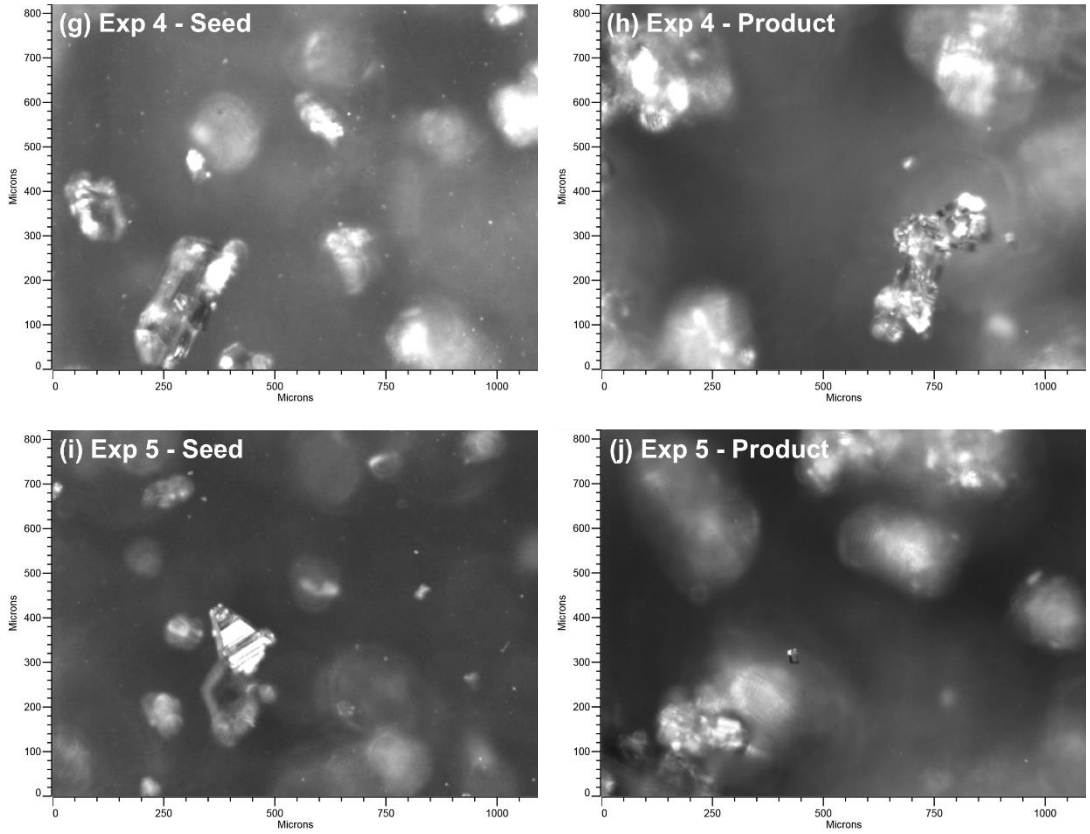

Figure 3.10. PVM images of seed and product for experiments 1-5 in Table 3.2.

Secondly, it is important to consider all the crystallization mechanisms that could be occurring in the system during process. The optimization model developed incorporates growth of the seed crystals only. Therefore, no agglomeration, breakage, primary of secondary nucleation mechanisms are taken into consideration as they are assumed to be negligible. In reality, however, these mechanisms may occur (with the exception of primary nucleation since we remain close to the solubility curve during cooling and therefore far away from the metastable limit). Since agglomeration, breakage and secondary nucleation may occur, they are likely to affect the separation results obtained e.g. secondary nuclei from larger crystals of one enantiomer will be collected in a smaller sieve fraction containing crystals of the opposite enantiomer, as was observed in experiments 2-5. In future work, therefore, it may be useful to also incorporate each of these crystallization mechanisms (secondary nucleation, agglomeration, breakage) into the optimization model before conducting experiments. However, computationally this may take more time. Furthermore, what we have shown in this work is that even a simple growth only optimization model allows the

experimental design of successful separation results, therefore addition of these other crystallization mechanisms may not be required.

Finally, the results for experiment 4, however, seem to suggest that L-asn product crystals underwent some agglomeration since the obtained average crystal size in the L-asn sieve fraction was higher than the predicted average crystal size. This is likely due to any variances that were experienced during the filtration, washing and drying stage of the process since agglomeration was not observed in any other experiments in Table 3.2. These variances could be due to differences in drying time since product was only left to dry in a vacuum oven overnight and not for a specific length of time. For further optimization of this type of separation process, it is important to consider each of these aforementioned factors. Of course, depending on the compound of interest, each factor may be more or less significant than observed in this work.

For future processes of this kind, it would also be useful to perform this separation approach in two stages: the first stage would be carried out as described in the paper, where a substantial enantiomeric excess is achieved in a number of sieve fractions using different combinations of pure enantiomer seed sizes and seed loadings. The next stage would be to then carry out a conventional preferential crystallization process for each of the sieve fractions where material is obtained. As long as the enantiomeric excess achieved in a sieve fraction is large enough, the second preferential crystallization process would be carried out in the region of the phase diagram where pure material can be obtained. This way an enantiomeric excess of commercial significance could be achieved.

3.7 Conclusion

We have demonstrated a strategy for separating enantiomers of a conglomerate forming compound via controlled seeded concomitant crystallization flowed by sieving. Through the use of a two-level optimization using a population balance model, experimental conditions such as seed size and loading of each enantiomer and the temperature profile were optimized to achieve separation of enantiomers based on their product crystal size. Although our model considers crystal growth only, and assumes the absence of nucleation (primary or secondary), agglomeration or breakage, it has

been shown to be effective in providing optimized crystallization conditions. Through this process, unwanted primary nucleation is inhibited since we seed with both enantiomers and through the optimized cooling profile, remain close to the solubility curve. However, for future use of this method the crystallization process should be optimized (through the use of process modelling) so that the risk of nucleation and agglomeration is minimized e.g. through the use of slower cooling profiles. In reality, these other mechanisms do occur, as we experience some secondary nucleation in our experiments.

3.8 References

(1) Srisanga, S.; ter Horst, J. H. Racemic Compound, Conglomerate, or Solid Solution: Phase Diagram Screening of Chiral Compounds. *Cryst. Growth Des.* **2010**, *10* (4), 1808–1812. https://doi.org/10.1021/cg901483v.

(2) Nguyen, L. A.; He, H.; Pham-Huy, C. Chiral Drugs: An Overview. *Int. J. Biomed. Sci.* **2006**, *2* (2), 85–100.

(3) Curitiba Marcellos, C. F.; Durand, H.; Kwon, J. S.-I.; Gomes Barreto, A.; Lage, P. L. da C.; Bezerra de Souza, M.; Secchi, A. R.; Christofides, P. D. Optimal Operation of Batch Enantiomer Crystallization: From Ternary Diagrams to Predictive Control. *AIChE J.* **2017**. https://doi.org/10.1002/aic.16028.

(4) Spix, L.; Alfring, A.; Meekes, H.; Van Enckevort, W. J. P.; Vlieg, E. Formation of a Salt Enables Complete Deracemization of a Racemic Compound through Viedma Ripening. https://doi.org/10.1021/cg4018882.

(5) Li, W. W.; Spix, L.; de Reus, S. C. A.; Meekes, H.; Kramer, H. J. M.; Vlieg, E.; ter Horst, J. H. Deracemization of a Racemic Compound via Its Conglomerate-Forming Salt Using Temperature Cycling. *Cryst. Growth Des.* **2016**, *16* (9), 5563–5570. https://doi.org/10.1021/acs.cgd.6b01034.

(6) Spix, L.; van Enckevort, W. J. P.; van der Wal, L. J. M.; Meekes, H.; Vlieg, E. Resolution of Asparagine in a Coupled Batch Grinding Process: Experiments and Modelling. *CrystEngComm* **2016**, *18* (48), 9252–9259. https://doi.org/10.1039/C6CE02043G.

(7) Xie, S.-M.; Yuan, L.-M. Recent Progress of Chiral Stationary Phases for Separation of Enantiomers in Gas Chromatography. *J. Sep. Sci.* **2017**, *40* (1),

124–137. https://doi.org/10.1002/jssc.201600808.

(8) Huang, X.-Y.; Di, D.-L. Chiral Separation by Counter-Current Chromatography. *TrAC Trends Anal. Chem.* **2015**, *67*, 128–133. https://doi.org/10.1016/J.TRAC.2015.01.009.

(9) Patel, D. C.; Wahab, M. F.; Armstrong, D. W.; Breitbach, Z. S. Advances in High-Throughput and High-Efficiency Chiral Liquid Chromatographic Separations. *J. Chromatogr. A* **2016**, *1467*, 2–18. https://doi.org/10.1016/J.CHROMA.2016.07.040.

(10) Jacques, J.; Collet, A. *Enantiomers, Racemates and Resolutions*; John Wiley & Sons Ltd, 1981.

(11) Levilain, G.; Coquerel, G. Pitfalls and Rewards of Preferential Crystallization. *CrystEngComm* **2010**, *12* (7), 1983. https://doi.org/10.1039/c001895c.

(12) Elsner, M. P.; Ziomek, G.; Seidel-Morgenstern, A. Efficient Separation of Enantiomers by Preferential Crystallization in Two Coupled Vessels. *AIChE J.* **2009**, *55* (3), 640–649. https://doi.org/10.1002/aic.11719.

(13) Chaaban, J. H.; Dam-Johansen, K.; Skovby, T.; Kiil, S. Separation of Enantiomers by Continuous Preferential Crystallization: Experimental Realization Using a Coupled Crystallizer Configuration. *Org. Process Res. Dev.* **2013**, *17* (8), 1010–1020. https://doi.org/10.1021/op400087g.

(14) Elsner, M. P.; Ziomek, G.; Seidel-Morgenstern, A. Simultaneous Preferential Crystallization in a Coupled Batch Operation Mode. Part II: Experimental Study and Model Refinement. *Chem. Eng. Sci.* **2011**, *66* (6), 1269–1284. https://doi.org/10.1016/j.ces.2010.12.035.

(15) Galan, K.; Eicke, M. J.; Elsner, M. P.; Lorenz, H.; Seidel-Morgenstern, A. Continuous Preferential Crystallization of Chiral Molecules in Single and Coupled Mixed-Suspension Mixed-Product-Removal Crystallizers. *Cryst. Growth Des.* **2015**, *15* (4), 1808–1818. https://doi.org/10.1021/cg501854g.

(16) Dunn, A. S.; Svoboda, V.; Sefcik, J.; Ter Horst, J. H. Resolution Control in a Continuous Preferential Crystallization Process. *Org. Process Res. Dev.* **2019**, acs.oprd.9b00275. https://doi.org/10.1021/acs.oprd.9b00275.

(17) Kongsamai, P.; Maneedaeng, A.; Flood, C.; ter Horst, J. H.; Flood, A. E. Effect of Additives on the Preferential Crystallization of L-Asparagine Monohydrate.

Eur. Phys. J. Spec. Top. **2017**, *226* (5), 823–835. https://doi.org/10.1140/epjst/e2016-60257-3.

(18) Mastai, Y.; Völkel, A.; Cölfen, H. Separation of Racemate from Excess Enantiomer of Chiral Nonracemic Compounds via Density Gradient Ultracentrifugation. *J. AM. CHEM. SOC* **2008**, *130*, 2426–2427. https://doi.org/10.1021/ja067905i.

(19) Zhang, S.; Huang, Y.; Zhou, L.; Yang, Y.; Xie, C.; Wang, Z.; Hou, B.; Hao, H.; Bao, Y.; Yin, Q. Novel Technology for Separation of Binary Eutectic-Forming Mixture by Cocrystallization into Different Sizes Combined with Particle Size Fraction. *Ind. Eng. Chem. Res.* **2019**, acs.iecr.9b01293. https://doi.org/10.1021/acs.iecr.9b01293.

(20) Petruševska-Seebach, K.; Seidel-Morgenstern, A.; Elsner, M. P. Preferential Crystallization of L-Asparagine in Water. *Cryst. Growth Des.* **2011**, *11* (6), 2149–2163. https://doi.org/10.1021/cg101408e.

(21) Randolph, A. D.; Larson, M. A. *Theory of Particulate Processes*, Second.; Academic Press, Inc.: San Diego, 1988.

(22) Wright, D. L.; McGraw, R.; Rosner, D. E. Bivariate Extension of the Quadrature Method of Moments for Modeling Simultaneous Coagulation and Sintering of Particle Populations. *J. Colloid Interface Sci.* **2001**, *236* (2), 242–251. https://doi.org/10.1006/JCIS.2000.7409.

(23) Aamir, E.; Nagy, Z. K.; Rielly, C. D.; Kleinert, T.; Judat, B. Combined Quadrature Method of Moments and Method of Characteristics Approach for Efficient Solution of Population Balance Models for Dynamic Modeling and Crystal Size Distribution Control of Crystallization Processes. *Ind. Eng. Chem. Res.* **2009**, *48* (18), 8575–8584. https://doi.org/10.1021/ie900430t.

(24) Mesbah, A.; Kramer, H. J. M.; Huesman, A. E. M.; Van den Hof, P. M. J. A Control Oriented Study on the Numerical Solution of the Population Balance Equation for Crystallization Processes. *Chem. Eng. Sci.* **2009**, *64* (20), 4262–4277. https://doi.org/10.1016/J.CES.2009.06.060.

(25) Omar, H. M.; Rohani, S. Crystal Population Balance Formulation and Solution Methods: A Review. *Cryst. Growth Des.* **2017**, *17* (7), 4028–4041. https://doi.org/10.1021/acs.cgd.7b00645.

(26) Porru, M.; Özkan, L. Monitoring of Batch Industrial Crystallization with Growth, Nucleation, and Agglomeration. Part 1: Modeling with Method of Characteristics. *Ind. Eng. Chem. Res.* **2017**, *56* (20), 5980–5992. https://doi.org/10.1021/acs.iecr.7b00240.

(27) Temmel, E.; Gänsch, J.; Lorenz, H.; Seidel-Morgenstern, A. Measurement and Evaluation of the Crystallization Kinetics of l -Asparagine Monohydrate in the Ternary l -/ d -Asparagine/Water System. *Cryst. Growth Des.* **2018**, *18* (12), 7504–7517. https://doi.org/10.1021/acs.cgd.8b01322.

(28) Cruz, P.; Rocha, F.; Ferreira, A. Determination of the Critical Mixing Intensity for Secondary Nucleation of Paracetamol in an Oscillatory Flow Crystallizer. *CrystEngComm* **2018**, *20* (6), 829–836. https://doi.org/10.1039/C7CE01940H.

(29) Frawley, P. J.; Mitchell, N. A.; Ó'Ciardhá, C. T.; Hutton, K. W. The Effects of Supersaturation, Temperature, Agitation and Seed Surface Area on the Secondary Nucleation of Paracetamol in Ethanol Solutions. *Chem. Eng. Sci.* **2012**. https://doi.org/10.1016/j.ces.2012.03.041.

(30) Steendam, R. R. E.; Frawley, P. J. Secondary Nucleation of Sodium Chlorate: The Role of Initial Breeding. *Cryst. Growth Des.* **2019**, acs.cgd.9b00317.

Chapter 4

4 Coupled Batch-wise Preferential Crystallization in a Single Moving-Fluid Oscillatory Baffled Crystallizer

Andrew S. Dunn, Ali Anwar, Cameron J. Brown, Joop H. ter Horst

Crystallization is a highly selective separation technique used in the pharmaceutical industry to obtain pure product crystals of active pharmaceutical ingredients. Therefore, it is often used to separate chiral molecules. Enantiomers of such molecules can have different physiochemical responses and thus it is important to separate them. A process such as preferential crystallization in two coupled vessels has been shown to be an efficient and effective method to separate enantiomers from one another. Previously this type of separation has been conducted with two coupled batch stirred tank crystallizers. However, such separations are complex to control due to the pumps, tubing and additional heating to transfer line that is required. Here we show that an integrated internally coupled batch crystallization process in an oscillatory baffled crystallizer (OBC) is an effective alternative for the coupled batch stirred tank crystallizers, avoiding the need for pumps, tubing and additional heaters. By inserting a filter between two connections of the OBC, effective separation can be achieved by allowing the liquid phase to cross. By using an OBC, we have achieved higher productivities and yields compared to values obtained in literature for the coupled batch stirred tank crystallizers.

4.1 Introduction

Crystallization processes are used in the pharmaceutical industry as purification and separation techniques, usually for an active pharmaceutical ingredient (API) or its pre-cursors.[1] Chiral compounds are an example of drug substances that need to be separated. However, such processes are challenging and complex due to the identical physical properties of chiral molecules. On a molecular level, both enantiomers of a chiral compound exhibit non-superimposable mirror imagery compared to each other. Since life is chiral, one enantiomer may be designed to target the intended biological receptor to provide the desired pharmaceutical response, while the opposite enantiomer can lack biological response or, in more serious cases, a potentially hazardous response e.g. naproxen.[2] Therefore, it is of major importance to separate such compounds.

Resolution techniques are used to separate enantiomers from one another in order to achieve enantiopure product.[3–6] For a conglomerate system of enantiomers, in which each individual crystal is composed of one chiral from,[4] preferential crystallization (PC) is a common separation technique due to its ease and highly selective nature.[7] In a PC process, enantiopure seeds of the desired enantiomer are added to a racemic (equal mixture) or enriched solution of enantiomers in the crystallizer and allowed to grow. However, over time it becomes increasingly more likely that the unwanted enantiomer will nucleate. Therefore, the process must be stopped before this unwanted nucleation occurs.

PC is commonly carried out in a single stirred tank crystallizer. In recent years, coupling two batch reactors together via a solid-free liquid exchange between the vessels has been extensively studied, both through modelling[8–11] and experimentally.[12–16] This type of setup has proven to be a much more efficient way of separating enantiomers in order to achieve enantiopure product compared to a single batch stirred tank crystallizer since the counter enantiomer supersaturation decreases in the coupled vessel before solution enriched with the preferred enantiomer is transferred back to the original vessel.[14] However, such a setup can be complex to control as it requires a number of pumps and tubes to connect the vessels, as well as additional heating to these connections to avoid any unwanted nucleation and therefore blockages during solution transfer. Furthermore, such systems are run at low initial

supersaturations in order to avoid the risk of nucleation of the counter enantiomer in each vessel before the system reaches equilibrium.

In this work, we demonstrate an innovative way to separate a conglomerate system of enantiomers through coupled preferential crystallization in a single moving fluid oscillatory baffled crystallizer (OBC) setup using a mesh filter between the connecting sections of the OBC. In this way, similarly to the coupled batch preferential crystallization approach, crystals of each opposing enantiomer can be kept separate, whilst allowing the mother liquor to flow freely between each side of the setup. First, we compare use of the filter between sections of the OBC against a simple batch isothermal PC process in the OBC. Next we determine the effect of seed loading in coupled batch mode and finally the effect of the initial supersaturation on yield, productivity and product purity.

4.2 Experimental

4.2.1 Materials and Methods

DL-asparagine monohydrate (DL-asn), D-asparagine monohydrate (D-asn) and L-asparagine monohydrate (L-asn) were purchased from Sigma-Aldrich (Germany). The solubility of L-asn and DL-asn have been determined previously.[15,17] Seeds of size 250-355 μm of D-and and L-asn were obtained through sieving of the raw material. Deionised water, purified by Milli-Q gradient system from Milipore SAS (France), was used as a solvent.

4.2.2 Experimental OBC Setup

Experiments were conducted in a 15 mm internal diameter OBC. A schematic of the experimental setup is shown in Figure 4.1. The OBC consisted of two jacketed straights each of length 700 mm and four jacketed bends (one connecting the piston to straight 1, two connecting each straight to one another in a U-bend formation and a final one at the end of straight 2). This gives the OBC a total working volume of approximately 400 ml. Once the reactor was filled with solution the piston was set at a frequency of 2.0 Hz and a peak to peak amplitude of 35 mm. This gave a Reynolds number Re_o of around 4300 as determined by Eq. 4.1.

$$Re_o = \frac{2\pi f x_o D \rho}{\mu} \quad (4.1)$$

Where f is the oscillation frequency (Hz), x_o is the centre to peak amplitude (17.5 mm), D is the tube diameter (15 mm), ρ is the solution density (1.035 g/cm^3) and μ is the solution viscosity (0.7978 mPa/s). The Reynolds number describes the mixing intensity in the column. The power input (power density) in a system describes the power P applied per unit volume V in the system. Such a model is useful in scaling up a crystallization process. Also, such a calculation is useful when comparing results obtained in an OBC and stirred tank crystallizer systems operating at these power densities.[18] In an OBC the power density is determined using the quasi steady flow model given by Baird and Stonestreet:[19]

$$\frac{P}{V} = \frac{2\rho N_b}{3\pi C_D^2}\left(\frac{1-\alpha^2}{\alpha^2}\right) x_o^3 (2\pi f)^3 \quad (4.2)$$

Where N_b is the number of baffles per unit length of the reactor, C_D is the coefficient of discharge of the baffles (normally given as 0.7) and α is the baffle orifice tube cross-section area ratio i.e. the ratio between the diameter of the OBC (d) and the diameter of the baffle opening (d_o) where d = 15 mm and d_o = 7 mm. A mesh filter of pore size 180 μm (Mesh Direct, UK) was inserted between the two bends connecting the straights. The jacket temperature of the setup was controlled by a Lauda Eco630 (Germany) heater-chiller.

4.2.3 Experimental Procedure

Feed solution for each experiment was prepared in a 1 L stirred tank crystallizer (Radleys, UK). For this, 77 g of DL-asn was added to the reactor before 1 kg of water was added, giving a saturation concentration C_s of 77 mg/ml solvent. The temperature of the reactor was increased to 10°C above the saturation temperature T_s = 30°C while stirring the suspension until a clear solution was obtained. The temperature was then reduced to the saturation temperature of the solution. The clear solution was then transferred into the OBC setup using a peristaltic pump (Masterflex L/S, USA) via P1 of the OBC, of which the jacket temperature was set to the saturation temperature of

the solution. Approximately 600 ml solution was pumped through the setup in order to flush the setup to avoid any cross contamination from any solution left over from the previous experiment.

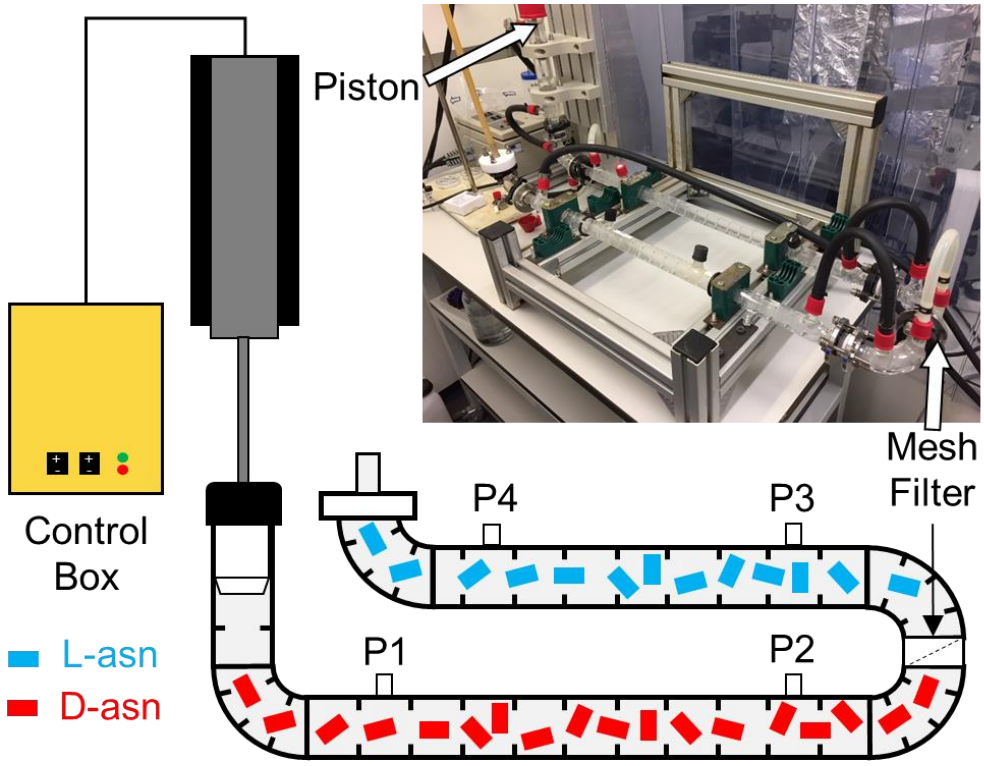

Figure 4.1. Schematic and image of the OBC setup used for coupled batch preferential crystallization of asn. The mesh filter is placed between the connection of the straight seeded with D-asn (red side) and the straight seeded with L-asn (blue side). This allows movement of the mother liquor between each side whilst the crystals of each enantiomer are retained in the sections separated by the filter. P1 = port 1, P2 = port 2, P3 = port 3, P4 = port 4.

For this an inlet tube is attached the P1 and an outlet tube is attached to the end of the OBC. The transfer line was then closed and the outlet of the OBC was raised so that no further solution could enter or exit the setup.

The temperature of the reactor was then reduced to the isothermal crystallization temperature, as detailed in Table 4.1. Once the crystallization temperature of the reactor was reached, seeds of size 250-355 μm of each enantiomer

were added to the appropriate side of the filter; D-asn seeds were added at P1 and L-asn were added at P4. In the case of experiment 1, a total of 2 g of L-asn seeds only were added to P1. In the other experiments one half of the total seed mass was added as L-asn seeds at P4 and the other half was added as D-asn seeds at P1. A small amount of slurry (approximately 5-7 ml) was taken from each straight at various time points during each experiment for solid and solution enantiomeric excess determination as well as solution concentration determination by chiral HPLC (see section 2.4). Suspension samples from the D-asn seeded straight were taken from P1 and samples from the L-asn seeded straight were taken from P4 (in experiment 5 samples were taken from P4 only). Due to the removal of several samples through the duration of each run, the oscillation efficiency of the OBC was affected by more air entering the system each time a sample was taken. Since the process was conducted in batch mode, suspension removed by sampling was not replenished. Therefore, for the repeat experiment, a sample was taken at the end of the process only.

4.2.4 Process Analysis

Chiral HPLC analysis was carried out using an Agilent UPLC instrument to determine the concentration and enantiomeric excess of the mother liquor and the enantiomeric excess of the recovered solid product. Solid samples obtained from the filtered slurry were dissolved in water at a concentration of 1.5 - 2 mg/ml solvent (in line with the HPLC calibration). A CHIROBIOTIC T column (Astec, 150 x 4.6 mm with 5 μm particle size) was used at 25.0°C with a 70/30 volume% methanol/water mobile phase (flow rate of 0.5 ml/min) with UV detection at 205 nm. The injection volume was 5 μl.

Gravimetric analysis was conducted to determine total solution concentration. For this, a slurry sample was filtered and a known amount of the filtrate was added to a pre-weighed vial and left to evaporate. The ratio of remaining mass and evaporated solvent volume is the overall concentration in mg/ml of asn.

SEM analysis was carried out using a JOEL IT 100 scanning electron microscope in secondary electron mode at 10 keV. Images were taken at both x50 and x300 magnifications from at least two different positions. Prior to analysis, all samples were sputtered with gold to achieve a coated layer of 10 nm in thickness using a Leica

EM ACE 200 sputter-coater and kept under vacuum for two minutes since asparagine crystals were found to be prone to charging.

4.2.5 Enantiomeric Excess, Productivity and Yield

Enantiomeric Excess. The enantiomeric excess of the solution E_s and the solid phase E_{cr} were determine using HPLC and calculated as the ratio between the difference in peak areas between each enantiomer and the total peak area:[17,20]

$$E = \frac{A_D - A_L}{A_D + A_L} \times 100\% \quad (4.3)$$

Where A_D is the peak area of D-asn and A_L is the peak area of L-asn in the HPLC chromatogram. In this work a positive E_s or E_{cr} value indicates an excess of L-asn and a negative E_s or E_{cr} value indicates an excess of D-asn.

Productivity. The productivity $P_e(t_{end})$ for enantiomer *e* is calculated as the ratio between the difference in the total mass of product $m_p^{(e)}$ and the initial seed mass $m_{seeds}^{(e)}$ and the initial mass $m^{(e)}_i$ of the enantiomer multiplied by the batch time.[14]

$$P_e\,(t_{end}) = \frac{m_p^{(e)} - m_{seeds}^{(e)}}{m_i^{(e)} \cdot t_{end}} \times 10^3 \quad (4.4)$$

Yield. The yield Ye for enantiomer e is calculated as the ratio between the mass of each enantiomer that has crystallized out i.e. the difference in the total mass of product $m_p^{(e)}$ and the initial seed mass $m_{seeds}^{(e)}$, and the theoretical mass of each enantiomer $m_t^{(e)}$ that can be crystallized out i.e. the difference in the starting mass of each enantiomer in solution and mass of enantiomer in solution at equilibrium.

$$Y_e = \frac{m_p^{(e)} - m_{seeds}^{(e)}}{m_t^{(e)}} \times 100\% \quad (4.5)$$

Table 4.1. Experimental parameters, process yield, productivity and product enantiomeric excess for experiments conducted in the OBC setup. For all experiments the saturation temperature T_s = 30°C, seed size of each enantiomer was 250-355 μm and frequency and amplitude of the piston was 2.0 Hz and 35 mm, respectively. The pore size of the filter was 180 μm for all experiments.

Experiment	T_{cryst} [°C]	S [C/C^*]	Total Seed Mass [g]	Filter [Y/N]	Process Time (t_{end}) [min]	Mass of Product [g]		Yield[b] [%]		Productivity[c] [mg/(g min)]		E_{cr} [%]	
						L-asn	D-asn	L-asn	D-asn	L-asn	D-asn	L-asn	D-asn
1	22	1.48	2[a]	N	25	3.11	-	22.1	-	2.855	-	20	-
2	22	1.48	2	Y	205	5.43	5.49	88.0	89.4	1.394	1.415	90	92
3	22	1.48	4	Y	200	6.11	6.62	79.2	89.0	1.311	1.472	2	53
4	25	1.28	4	Y	181	4.89	5.27	80.3	90.9	1.022	1.157	100	95
5	28	1.10	4	Y	185	2.60	2.45	38.6	28.5	0.209	0.155	92	100

[a]Experiment 1 used 2 g of enantiopure L-asn seeds only.

[b]The percentage yield is calculated based on the ratio between the amount of enantiomer crystallized (mass of enantiomer product minus the mass of enantiomer seeds) and theoretical mass of each enantiomer that can crystallize out at equilibrium.

[c]The productivity for each experiment utilizing the filter is calculated based on an approximate process time of 200 min. This is due to similar sampling times in each experiment of 200 min and given the fact that the time of obtaining the final sample for each experiment varies greatly. In doing so the productivity values for each experiment are more comparable.

4.3 Results and Discussion

Asparagine monohydrate is a conglomerate forming compound where each chiral form has, independently, an identical solubility curve. However, based on the solubility expression determined by Petruševska-Seebach et al.[15] and the solubility of DL-asn determine by Kongsamai et al.,[17] the solubilities of each enantiomer are not independent of one another when both are present, and depend on both the temperature and the amount of counter enantiomer.

Figure 4.2 shows a partial segment of the solubility curve of a racemic mixture of DL-asn monohydrate, including the metastable zone. The crystallization conditions of each experiment are shown, with T_s (30°C) and the starting concentration 77 mg/ml solvent is highlighted. Although the experiments are performed within the metastable zone, in a batch PC process nucleation of the counter enantiomer under these conditions will eventually occur.

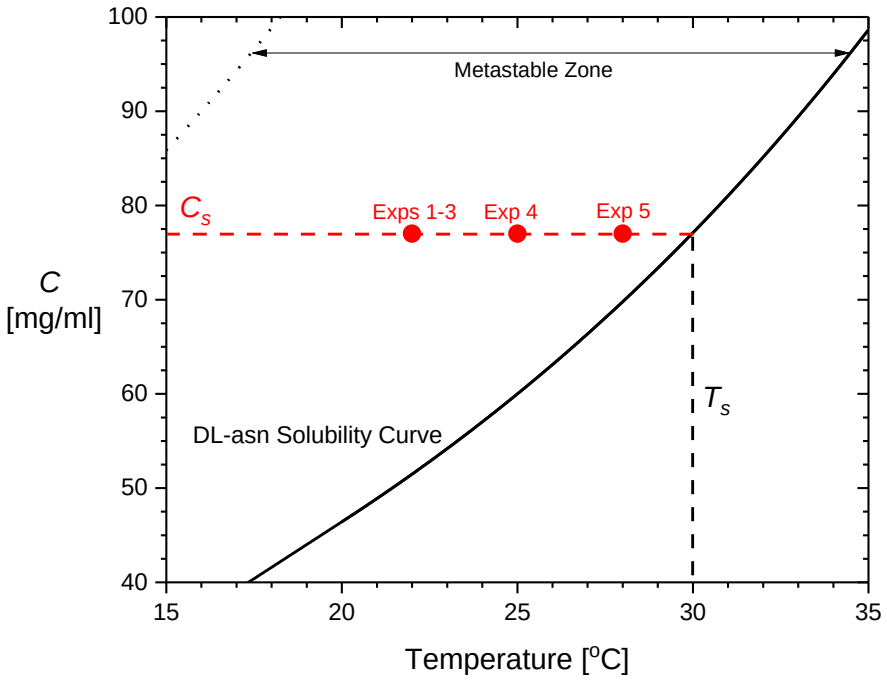

Figure 4.2. A section of the DL-asn monohydrate solubility curve and metastable zone illustrating the initial crystallization conditions for each experiment in Table 1, showing T_s 30°C and C_s 77 mg/ml solvent.

4.3.1 Batch Preferential Crystallization in the OBC

Experiment 1 in Table 4.1 details the conditions used for a basic isothermal batch preferential crystallization process in the OBC. The product enantiomeric excess E_{cr} and solution enantiomeric excess E_s as a function of time for this process at an initial supersaturation S = 1.48 and using an L-asn seed mass of 2 g are shown in Figure 4.3 (left). Approximately for the first 25 minutes of the process, the solid product remains enantiopure while solution enantiomeric excess decreases slightly to -4%. This decrease is due to L-asn being removed from solution as seed crystals grow, meaning there is an increasing excess of D-asn in solution over time. If equilibrium had been reached i.e. all possible L-asn crystallized out whilst D-asn remained in solution, the E_s value would have increased to around -21%, based on Eq. 4.1 (substituting peak area A for the concentration of each enantiomer in solution C).

Sometime between 25 and 50 min in the crystallization the unwanted primary nucleation of the counter enantiomer occurs causing the solid product enantiomeric excess to decrease to approximately E_{cr} = 85% at 50 min. During this time the solution enantiomeric excess increases further to around -5%, after which it decreases, reaching a final value of around 1.5% whilst solid product enantiomeric excess decreases to approximately E_{cr} = 20%. Table 4.1 details the product purity and process productivity result for this experiment 1.

In the process, we do not reach equilibrium for L-asn before D-asn nucleates. Since we have a high initial supersaturation S = 1.48 there is a shorter induction time for the nucleation of D-asn compared to running the process at a lower initial supersaturation. However, by running at a lower initial supersaturation, less L-asn would be able to crystallize. Therefore, a balanced initial supersaturation is required to achieve a high production value of L-asn and low nucleation probability of D-asn. Such a balance can be achieved by coupling the PC process.

4.3.2 Coupled Preferential Crystallization in the OBC

Effect of the Filter. Experiment 2 in Table 4.1 describes the conditions used for the isothermal coupled batch preferential crystallization at S = 1.48. In the supersaturated solution 1 g of enantiopure seeds of D-asn and of L-asn were introduced to the straight on either side of the mesh filter, respectively. The enantiomeric excess of the product

from each side as well as the overall solution enantiomeric excess as a function of time are shown in Figure 4.3 (right).

With use of the filter in experiment 2, pure product remains on either side of the filter even after 200 min. During this time the solution composition in both straights of the crystallizer remains close to racemic. Since product is produced this means that exchange of solution across the filter is successful and very efficient.

Solution in the L-asn straight of the OBC is depleted of L-asn due to growth of the L-asn crystals on this side. At the same time solution in the D-asn straight of the OBC is depleted of D-asn due to growth of the D-asn crystals. The filter allows these depleted solutions rich in unwanted enantiomers to be almost immediately exchanged between the two sections of the OBC while the growing crystals remain in their dedicated OBC sections. This exchange of solution reduces the supersaturation for the unwanted enantiomer on both sides of the filter. This can be seen by the close to racemic solution compositions maintained throughout the entire process (Figure 4.3, right). This reduction in supersaturation for the unwanted enantiomer on both sides of the filter is sufficient to avoid unwanted nucleation of the counter enantiomer for a significant period of time compared to the basic batch process. This is shown in the close to (>95%) enantiopure product obtained from both sides of the filter.

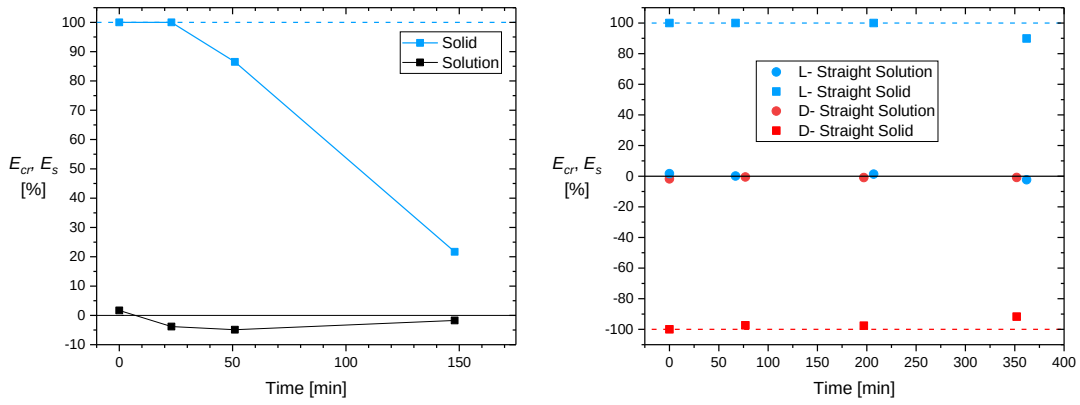

No Filter (Exp 1) Filter (Exp 2)

Figure 4.3. ***Left*****:** Solid (■) and solution (■) enantiomeric excesses E_{cr}, E_s, 100% solid product purity for L-asn (---) and racemic solution composition (-) for experiment 1 (see Table 1 for process conditions). ***Right*****:** L-asn seeded straight (■) and D-asn seeded straight (■) solid product and L-asn seeded straight (●) and D-asn seeded straight (●)

solution enantiomeric excess, product purities of 100% are shown for D-asn (---) and L-asn (---) and racemic solution composition is also shown (-) for experiment 2. Lines are a guide to the eye. Both experiments are performed with an initial supersaturation S = 1.48 and a total seed loading of 2 g.

Only in the final sample from experiment 2 (around 375 min) the enantiomeric excess of the solid in both straights drops to around 90%. Since the pore size of the filter is 180 μm, any particles smaller than this can pass through. Small particles could be generated by either primary or secondary nucleation. If solution exchange through the filter is not sufficiently fast enough to transfer solution enriched with counter enantiomer, then primary nucleation of the counter enantiomer in each straight could occur. However, if primary nucleation occurred the E_{cr} value in each straight would decrease significantly. Therefore, in this process secondary nucleation is the more likely mechanism of small particle production. Since crystals have grown larger during the process time, secondary nucleation through attrition via crystal-crystal or crystal-wall collisions becomes more likely. Attrition of the seed crystals would produce secondary nuclei of the same chiral handedness and these small attrition fragment might move through the filter. It could also be that secondary nuclei were generated through initial breeding, since seed crystals were prepared through sieving only with no further pre-treatment. SEM images of the seeds crystals in Figure 4.4 show the presence of small fines on the surface of the seed crystals which were likely to have been dislodged during mixing. If these fines are larger than the critical radius size required for crystal growth, then they will act as secondary nuclei.[21] To reduce the risk of contamination due to small particles passing through the filter, a smaller filter pore size could be used. However, a smaller size of filter pore could have an effect on the mixing of the system, due to a larger pressure drop when using a very small pore size. Therefore, this is something that should be taken into account along with initial seed size and mixing conditions (frequency and amplitude of the piston and therefore the Re_o and power density value). A very small pore size would require a high mixing intensity to account for the pressure drop experienced across the filter.

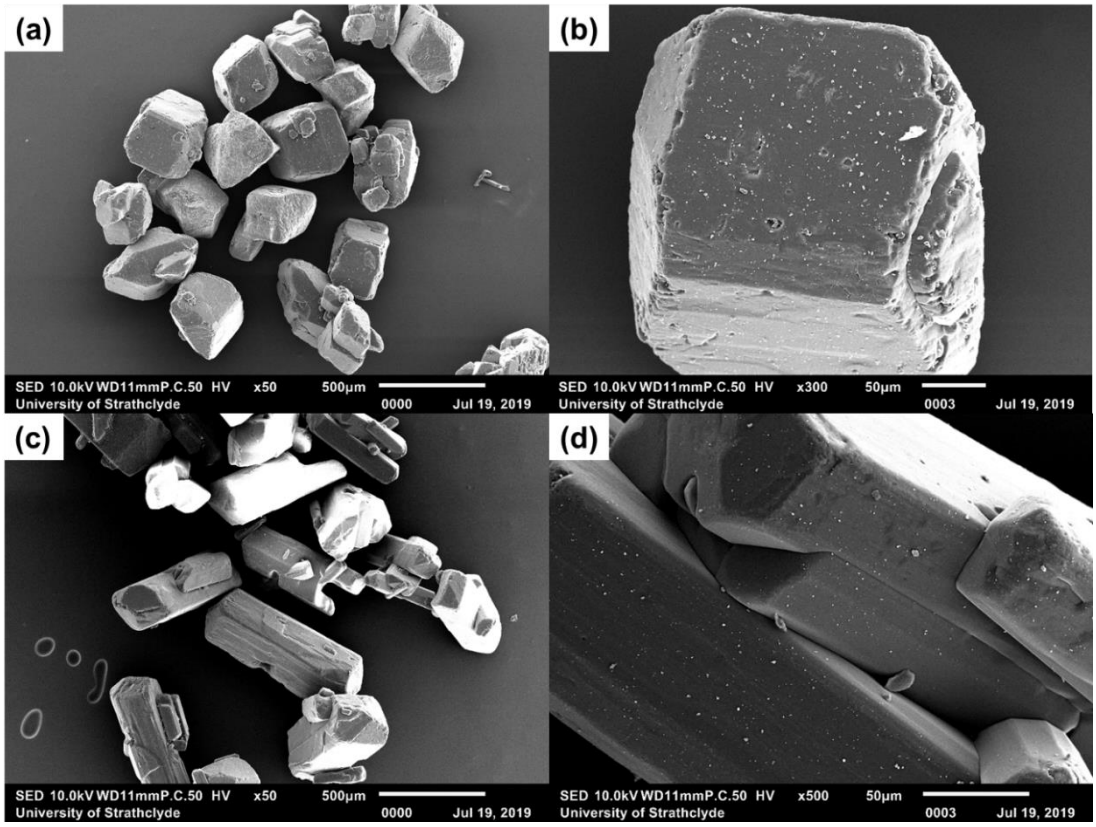

Figure 4.4. SEM images of L-asn seed crystals at (a) x50 and (b) x300 magnification and D-asn seed crystals of (c) x50 and (d) x500 magnification. Particle fines can be seen on the surface of the seed crystals, which may have cause secondary nucleation through initial breeding.

In order to assess the efficiency of the coupled batch process in the OBC using a filter against a basic isothermal batch PC process, the process yield, productivity and product enantiomeric excess of both processes are compared in Table 4.1. In the first 25 min of experiment 1, the point at which the process is considered to stop since unwanted crystallization of the counter enantiomer occurs after this, the total amount of L-asn produced is 3.11 g. This gives a yield of 22.1% productivity value of 2.855 mg/(g min). In experiment 2 (which incorporates use of the filter) 5.43 g and 5.49 g of L-asn and D-asn were produced, respectively. These values correspond to yield of 88.0% of L-asn and 89.4% of D-asn, giving productivity values of 1.394 mg/(g min) and 1.415 mg/(g min), respectively. Given that the final solution composition in each straight is extremely close to racemic, the slight differences in productivity can be

attributed to slight variances in the mass of seeds of each enantiomer added or inaccuracies during solid solution separation when sampling.

The productivity values calculated using equation 4.4 show that the productivity of experiment 1 is higher than that of experiment 2. However, it should be highlighted that the process time (t_{end}) for experiment 1 is significantly shorter than that of experiment 2 (25 min vs. 205 min). This low process time therefore increases the productivity value obtained as determined by equation 4. Furthermore, although the productivity in experiment 1 is higher, the mass of product obtain and the process yield are significantly lower. Also in experiment 2 we see that product purity remains close to 100% for the duration of the experiment. This means that by coupling the PC process a greater amount of pure product can be obtained for a longer period of time.

Effect of Seed Loading. Figure 4.6a and 4.6b show the enantiomeric excess results for experiments 2 and 3 in Table 4.1 respectively. In experiment 3 (like in experiment 2) a crystallization temperature of 22°C was used generating an initial supersaturation S = 1.48. However, experiment 3 uses a total seed mass of 4 g (2 g of each enantiomer) which is twice that of experiment 2. In experiment 3, the solid enantiomeric excess within each straight of the OBC drops to approximately 80% after 100 minutes into the process, showing that apparently the solid enantiopurity cannot be maintained for the same period of time as in experiment 2. In both experiments, solution composition remains close to racemic during the process.

This smaller time period in which enantiopurity can be maintained would suggest that the increase in the number of crystals is responsible for the rapid formation of impure product in either straight, rather than any unwanted primary nucleation, given that the seed crystals in both experiments were the same size. Since there are more crystals present in each straight in experiment 3 at the beginning of the experiment, initially crystal-crystal collisions and crystal-wall collisions will be more frequent and therefore the initial secondary nucleation rate via attrition will be higher.[22–25] Again, if these secondary nuclei are smaller than the pore size of the filter they are potentially able to pass through.

Since, however, there are fewer crystals present in experiment 2 i.e. a lower seed loading, it is to be expected that more secondary nucleation via attrition should

occur compared to experiment 3. With a lower seed loading, crystals will grow larger, therefore secondary nucleation via attrition will be higher due to an increase in the number of crystal-crystal collisions. Frawley et al. found that at lower seed loadings a higher volume of new i.e. secondary, nuclei was present in the product due to an increase in the secondary nucleation rate via attrition.[22] However, secondary nucleation via attrition does not depend solely on the seed loading but also on other factors like the mixing intensities induced in the crystallizer[26] (it is a mechanical process and therefore does not depend on supersaturation like contact nucleation or fluid shear).[21] A critical Reynolds number Re_o^c exists that is used to describe the transition from crystal growth dominance to secondary nucleation dominance. By operating at a Reynold number below Re_o^c crystal growth will be dominant in the system (however, secondary nucleation can still occur via other mechanisms such as contact nucleation and/or fluid shear).The Re_o^c value for asparagine monohydrate is currently unknown, but the Reynolds number calculated for the chosen frequency and amplitude in each experiment in this work is the same (approx.. 4300) as determined by Eq. 4.1. Furthermore, as found by Cruz et al.,[26] the critical Reynolds number required for the transition from growth dominance to secondary nucleation via attrition dominance in an OBC decreases with increasing supersaturation above a minimum supersaturation value. Below this minimum supersaturation value, the Re_o^c value needed for the transition from crystal growth dominance to secondary nucleation via attrition dominance is constant. Cruz et al. found that for paracetamol, the Re_o^c at initial supersaturation values of 1.10 and below was slightly under 4000, and decreased with increasing supersaturations.[26] Therefore, it could be that in this work even though experiment 2 has a lower seed loading than experiment 3, the operating Reynolds number is above Re_o^c for asparagine monohydrate at this supersaturation, and thus secondary nucleation via attrition will still occur.

SEM images in Figure 4.5 show a sample of the product crystals obtained from experiment 2 (Figure 4.5a and 5b) and experiment 3 (Figure 4.5c and 5d). In Figure 4.5a there are a number of large crystal present in the product sample, which are seed crystals that have grown during the process. In Figure 4.5b, damage to the corner of the seed crystal can be seen, which is likely due to attrition during the process as a result of collisions in the crystallizer. The smaller crystals present in Figure 4.5a and

4.5b are likely to have been produced through a combination of attrition, contact nucleation and fluid shear to the seed crystals and through initial breeding of crystal fines on the seed crystal surface identified in Figure 4.4. In Figure 4.5c and 4.5d, there are no crystals present that could be identified as seed crystals which have grown. Under the experimental conditions in experiment 3 (power density, initial supersaturation, seed size and seed loading) it is likely that the secondary nucleation mechanisms (initial breeding, attrition, contact nucleation and fluid shear) are occurring simultaneously. Thus, in future experiments conditions should be used to decouple these mechanisms in order to control the crystallization process and therefore optimize it.

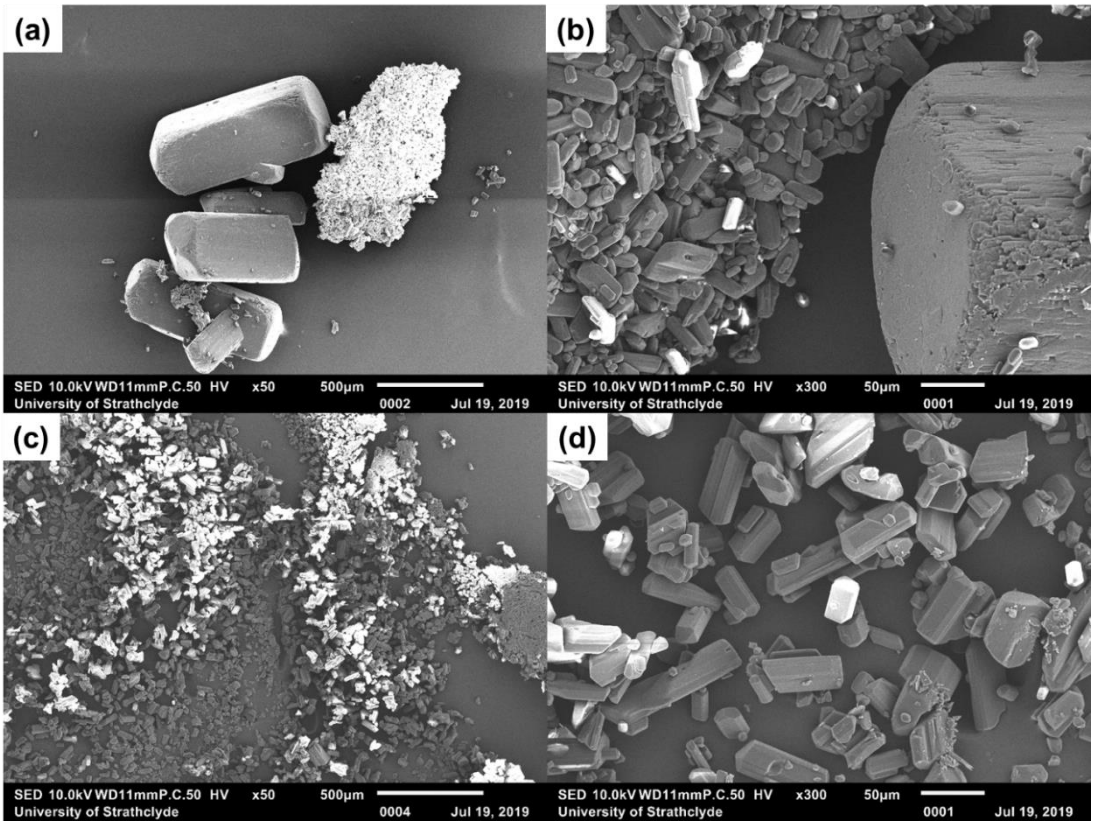

Figure 4.5. SEM images of product crystals obtained from D-asn seeded straight in experiment 2 at (a) x50 and (b) x300 magnification and product crystals obtained from L-asn seeded straight in experiment 3 at (c) x50 and (d) x300 magnification.

Table 4.1 details the process yield and productivity for experiments 2 and 3. In both experiments, a similar amount of product was obtained; 6.07 g and 5.49 g for the

L-asn and D-asn straights in experiment 2, respectively and 6.11 g and 6.62 g for the L-asn and D-asn straights in experiment 3, respectively. Since both experiments have the same T_s and T_c (and therefore the same initial supersaturation), the same amount of material is available for crystallization. However, small variances in the initial solution concentration as well the differences in the mass of seeds used contribute to the differences in the percentage yield obtained. The results also show that the productivity for experiment 3 is lower than that for experiment 2. This is due to the increased amount of seed material used in experiment 3. Since equation 4 takes into account the mass of seed material used, a higher amount of seed material will lower the productivity compared to an identical process that uses less seed material.

Effect of Supersaturation. Experiments 3-5 in Table 4.1 detail the conditions for assessing the effect of supersaturation on the efficiency of the filter. The corresponding results for these experiments are shown in Figure 4.6b-d (experiments 3-5, respectively). For experiment 5 (initial $S = 1.10$), the overall solution enantiomeric excess remains close to zero and solid product enantiomeric excess remains at 100% for each enantiomer for the duration of the process. Similarly, for experiment 4 (initial $S = 1.28$), the same trends for solution and solid product are observed. In both experiments 4 and 5, some minor solid impurity is observed (at 100 min for L-asn solid in experiment 5 and both L-asn and D-asn solid in experiment 4). Although the same mass of seeds was used in experiments 4 and 5 as was used in experiment 3, the lower initial supersaturation values used means that there is less solute available for growth. As such, crystals remain smaller compared to use of a lower seed loading under the same conditions. Therefore, secondary nucleation via attrition is less likely to occur. There are minor decreases in purity observed at 100 min in both straights as well as product in the D-asn straight in experiment 4 and at 100 min and product in the L-asn straight in experiment 5. These deviations are therefore likely to be due to initial breeding of crystals fines on the seed crystal surface observed in Figure 4.4.

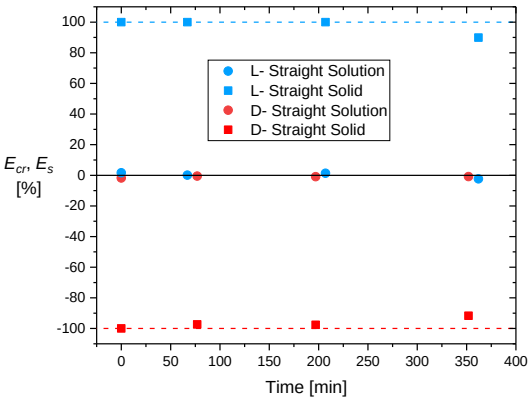

(a) Exp 2: S= 1.48
2 g Seeds

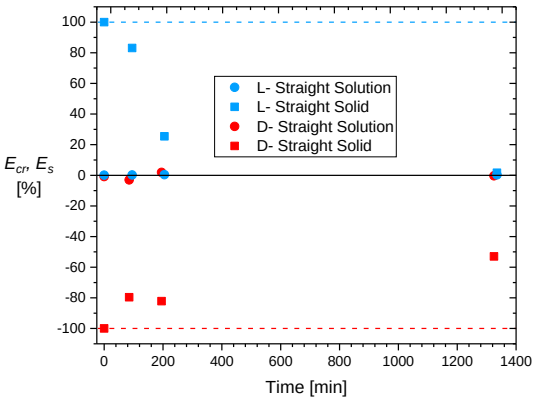

(b) Exp 3: S = 1.48
4 g Seeds

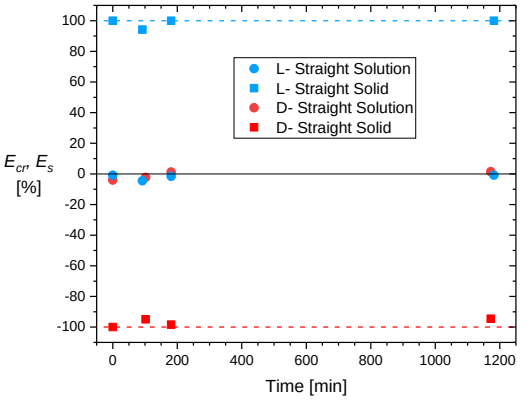

(c) Exp 4: *S* = 1.28
4 g Seeds

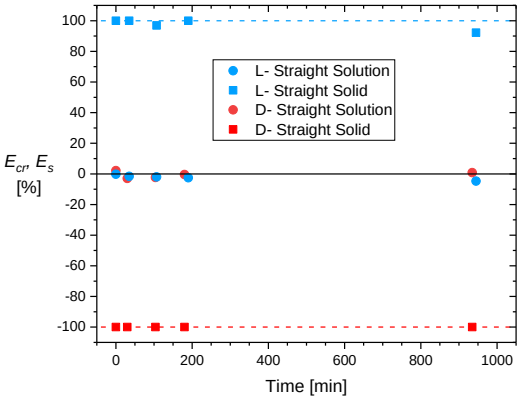

(d) Exp 5: *S* = 1.10
4 g Seeds

Figure 4.6. L-asn seeded straight (■) and D-asn seeded straight (■) solid product enantiomeric excess and L-asn seeded straight (●) and D-asn seeded straight (●) solution enantiomeric excess results for experiments 2-5 (plots a-d, respectively) in Table 1. Supersaturations (a) and (b) = 1.48, (c) = 1.28 and (d) = 1.10. Seed mass of (a) = 2 g and (b) to (d) = 4 g. Product purities of 100% are shown for L-asn (---) and D-asn (---). Racemic composition is also shown (-). Lines are a guide to the eye.

As detailed in Table 4.1, the productivity as function of supersaturation can be realized as it increases with increasing supersaturation. In experiment 4 (initial *S* = 1.28) 4.89 g and 5.27 g of L-asn and D-asn was crystallized, respectively. This corresponds to a yield of 80.3 % and 90.9 % of L-asn and D-asn, respectively, giving

productivity values of 1.022 mg/(g min) and 1.157 mg/(g min), respectively. In experiment 5 (initial S = 1.10) 2.60 g and 2.45 g of L-asn and D-asn product was collect, respectively. This corresponds to a yield of 38.6 % and 28.5 % of L-asn and D-asn, respectively, giving productivity values of 0.209 mg/(g min) and 0.155 mg/(g min), respectively. This trend in results is expected since each experiment uses the same mass and size of seed material, and the duration of each experiment is similar. Therefore, the increase in productivity is attributed to more material is available to crystallize out of solution at higher supersaturations. Therefore, in Eq. 4.2 a higher $m_p^{(e)}$ value is obtained for each increasing supersaturation value whilst the other values in the equation are constant which in turn means a higher productivity value is obtained.

4.4 Outlook

In this work the coupled batch PC process was run isothermally. However, if the process was run using controlled cooling profiles secondary nucleation in the process could be inhibited since the operating trajectory of the process would remain close to the solubility curve and thus the purity of the product would be maintained in each straight (this is also provided that the seed crystals are pre-treated to avoid any secondary nucleation via initial breeding). Additionally, by investigating the Re_o^c for asparagine monohydrate as a function of both supersaturation and initial seed loading in order to obtain curves similar to the one obtained by Cruz et al.,[26] in future experiments the frequency and amplitude of the mixing can be set such that growth of the seed crystals is dominant in the process.

The process could also be run as a continuous process using a continuous OBC (COBC). Similarly to this work, filters can be inserted between adjacent sections of the COBC, thus keeping opposite enantiomers separated, whilst racemic feed solution is continuously fed though the crystallizer and recycled at the outlet back to the feed tank, similar to the MSMPR setup used by Galan et al.[16]

4.5 Conclusions

We have demonstrated efficient separation of enantiomers of the conglomerate forming compound asparagine monohydrate in an OBC using a mesh filter between

reactor straights. In this way, solution is allowed to pass between the straights whilst pure crystals of each enantiomer are kept separate. This method has been compared to a standard simple batch isothermal preferential crystallization and shows that at the same initial supersaturation in a coupled isothermal batch-wise preferential crystallization in the OBC enantiopure product can be obtained and the process can run for much longer periods of time. Furthermore, this new setup uses the same principle as the coupled batch reactor setup previously studied, however, it negates the need for additional tanks, pumps or tubing due to its direct exchange of solution in the single piece of equipment. Compared to the previous coupled batch setup, it has been shown in this work that enantiopure product can be obtained operating at higher supersaturations under isothermal conditions. However, at high initial supersaturations and seed loadings secondary nucleation and mixing time mean that small crystals are produced such that they can pass through the filter, contaminating pure product in the opposite straight. Therefore, by using less seeds the process can become more efficient and secondary nucleation via attrition is less likely to occur. To optimize the process, varying the filter pore size along with the mixing intensity should be investigated in order to determine the critical mixing intensity at which secondary nucleation via attrition becomes dominant as a function of supersaturation and seed loading. Conducting the process using controlled cooling profiles as opposed to isothermal conditions would also improve process performance.

4.6 References

(1) Wang, J.; Li, F.; Lakerveld, R. Process Intensification for Pharmaceutical Crystallization. *Chem. Eng. Process. - Process Intensif.* **2018**, *127*, 111–126. https://doi.org/10.1016/J.CEP.2018.03.018.

(2) Nguyen, L. A.; He, H.; Pham-Huy, C. Chiral Drugs: An Overview. *Int. J. Biomed. Sci.* **2006**, *2* (2), 85–100.

(3) Coquerel, G. Novel Optical Resolution Technologies; Sakai, K., Hirayama, N., Tamura, R., Eds.; Springer Berlin Heidelberg, 2006; pp 1–51. https://doi.org/10.1007/128_2006_077.

(4) Jacques, J.; Collet, A. *Enantiomers, Racemates and Resolutions*; John Wiley & Sons Ltd, 1981.

(5) Fogassy, E.; Nógrádi, M.; Kozma, D.; Egri, G.; Pálovics, E.; Kiss, V. Optical Resolution Methods. *Org. Biomol. Chem.* **2006**, *4* (16), 3011–3030. https://doi.org/10.1039/B603058K.

(6) Mane, S. Racemic Drug Resolution: A Comprehensive Guide. *Anal. Methods* **2016**, *8* (42), 7567–7586. https://doi.org/10.1039/C6AY02015A.

(7) Levilain, G.; Coquerel, G. Pitfalls and Rewards of Preferential Crystallization. *Cryst Eng Comm* **2010**, *12* (7), 1983. https://doi.org/10.1039/c001895c.

(8) Qamar, S.; Galan, K.; Peter Elsner, M.; Hussain, I.; Seidel-Morgenstern, A. Theoretical Investigation of Simultaneous Continuous Preferential Crystallization in a Coupled Mode. *Chem. Eng. Sci.* **2013**, *98*, 25–39. https://doi.org/10.1016/J.CES.2013.05.010.

(9) Chaaban, J. H.; Dam-Johansen, K.; Skovby, T.; Kiil, S. Separation of Enantiomers by Preferential Crystallization: Mathematical Modeling of a Coupled Crystallizer Configuration. *Org. Process Res. Dev.* **2014**, *18* (5), 601–612. https://doi.org/10.1021/op400286q.

(10) Majumder, A.; Nagy, Z. A Comparative Study of Coupled Preferential Crystallizers for the Efficient Resolution of Conglomerate-Forming Enantiomers. *Pharmaceutics* **2017**, *9* (4), 55. https://doi.org/10.3390/pharmaceutics9040055.

(11) Elsner, M. P.; Ziomek, G.; Seidel-Morgenstern, A. Simultaneous Preferential Crystallization in a Coupled, Batch Operation Mode—Part I: Theoretical Analysis and Optimization. *Chem. Eng. Sci.* **2007**, *62* (17), 4760–4769. https://doi.org/10.1016/j.ces.2007.05.035.

(12) Chaaban, J. H.; Dam-Johansen, K.; Skovby, T.; Kiil, S. Separation of Enantiomers by Continuous Preferential Crystallization: Experimental Realization Using a Coupled Crystallizer Configuration. *Org. Process Res. Dev.* **2013**, *17* (8), 1010–1020. https://doi.org/10.1021/op400087g.

(13) Elsner, M. P.; Ziomek, G.; Seidel-Morgenstern, A. Simultaneous Preferential Crystallization in a Coupled Batch Operation Mode. Part II: Experimental Study and Model Refinement. *Chem. Eng. Sci.* **2011**, *66* (6), 1269–1284. https://doi.org/10.1016/j.ces.2010.12.035.

(14) Elsner, M. P.; Ziomek, G.; Seidel-Morgenstern, A. Efficient Separation of

Enantiomers by Preferential Crystallization in Two Coupled Vessels. *AIChE J.* **2009**, *55* (3), 640–649. https://doi.org/10.1002/aic.11719.

(15) Petruševska-Seebach, K.; Seidel-Morgenstern, A.; Elsner, M. P. Preferential Crystallization of L-Asparagine in Water. *Cryst. Growth Des.* **2011**, *11* (6), 2149–2163. https://doi.org/10.1021/cg101408e.

(16) Galan, K.; Eicke, M. J.; Elsner, M. P.; Lorenz, H.; Seidel-Morgenstern, A. Continuous Preferential Crystallization of Chiral Molecules in Single and Coupled Mixed-Suspension Mixed-Product-Removal Crystallizers. *Cryst. Growth Des.* **2015**, *15* (4), 1808–1818. https://doi.org/10.1021/cg501854g.

(17) Kongsamai, P.; Maneedaeng, A.; Flood, C.; ter Horst, J. H.; Flood, A. E. Effect of Additives on the Preferential Crystallization of L-Asparagine Monohydrate. *Eur. Phys. J. Spec. Top.* **2017**, *226* (5), 823–835. https://doi.org/10.1140/epjst/e2016-60257-3.

(18) McGlone, T.; Briggs, N. E. B.; Clark, C. A.; Brown, C. J.; Sefcik, J.; Florence, A. J. Oscillatory Flow Reactors (OFRs) for Continuous Manufacturing and Crystallization. *Organic Process Research and Development*. 2015. https://doi.org/10.1021/acs.oprd.5b00225.

(19) MH, B.; P, S. Energy-Dissipation in Oscillatory Flow Within a Baffled Tube. *Chem. Eng. Res. Des.* **1995**, *73* (5), 503–511.

(20) Kongsamai, P.; Flood, C.; ter Horst, J. H.; Flood, A. E. Particle Size Distributions and Performance of Preferential Crystallization of *L*-Asparagine·H_2O with Tailor-Made Additives. *Chem. Eng. Technol.* **2018**, *41* (6), 1173–1179. https://doi.org/10.1002/ceat.201700668.

(21) Agrawal, S. G.; Paterson, A. H. J. Secondary Nucleation: Mechanisms and Models. *Chem. Eng. Commun.* **2015**, *202* (5), 698–706. https://doi.org/10.1080/00986445.2014.969369.

(22) Frawley, P. J.; Mitchell, N. A.; Ó'Ciardhá, C. T.; Hutton, K. W. The Effects of Supersaturation, Temperature, Agitation and Seed Surface Area on the Secondary Nucleation of Paracetamol in Ethanol Solutions. *Chem. Eng. Sci.* **2012**. https://doi.org/10.1016/j.ces.2012.03.041.

(23) Evans, T. W.; Sarofim, A. F.; Margolis, G. Models of Secondary Nucleation Attributable to Crystal-Crystallizer and Crystal-Crystal Collisions. *AIChE J.*

1974, *20* (5), 959–966. https://doi.org/10.1002/aic.690200517.

(24) Mersmann, A. Fundamentals of Crystallization. In *Crystallization Technology Handbook*; Mersmann, A., Ed.; Marcel Dekker, Inc.: New York, 1995; pp 1–78.

(25) Ayazi Shamlou, P.; Jones, A. G.; Djamarani, K. Hydrodynamics of Secondary Nucleation in Suspension Crystallization. *Chem. Eng. Sci.* **1990**, *45* (5), 1405–1416. https://doi.org/10.1016/0009-2509(90)87134-E.

(26) Cruz, P.; Rocha, F.; Ferreira, A. Determination of the Critical Mixing Intensity for Secondary Nucleation of Paracetamol in an Oscillatory Flow Crystallizer. *CrystEngComm* **2018**, *20* (6), 829–836. https://doi.org/10.1039/C7CE01940H.

Chapter 5

5 Start-up and Steady State of a Continuous Preferential Crystallization in a Continuous Stirred Tank Reactor

Andrew S. Dunn, René R. E. Steendam, Joop H. ter Horst

Continuous manufacturing has been adopted by the pharmaceutical industry in recent years as the way forward in order to reduce waste and improve process conditions. Compared to batch processes, continuous processes can cut costs, reduce space requirements and produce more consistent product as well as higher yields of more uniform particles. By running preferential crystallization processes in continuous mode over batch, risk of unwanted crystallization of the counter enantiomer can be reduced and productivity of the process can be significantly improved compared to batch-wise preferential crystallization processes. One issue still concerning continuous crystallization processes is the start-up time state, which, on average, takes 6 residence times to reach steady state. In this work, we show how the initial process parameters (initial supersaturation, residence time, seed loading, sieve fraction and initial counter enantiomer concentration) affect the start-up time to steady state and the robustness of the steady state achieved. The results show that the main factors affecting the start-up time of a continuous crystallization process is parameter-parameter interactions involving properties of the seed material, with an interaction between the solid seed loading and the initial counter enantiomer concentration having the largest effect on reducing the start-up time. However, the robustness of the steady state is more affected by individual parameters, with the initial concentration of counter enantiomer in the starting solution having the biggest effect in reducing the robustness of the steady state. In order to obtain a fully robust process, therefore, a balance must be found between the desire for a short start-up time and the need for a robust steady state in the process.

5.1 Introduction

The pharmaceutical industry has begun to adopt continuous manufacturing as the way forward to reduce waste and improve product consistency. Although continuous processes are already implemented in other industries (e.g. food, agrochemical, petrochemical), it is only recently that pharmaceutical companies have begun to integrate continuous processes as part of their production.[1–3] As research into continuous API manufacture expands, more and more confidence in its abilities and advantages compared to batch processes within the industry are being acknowledged.[4] Continuous crystallization processes have the upper hand over batch processes in that the consistency and reproducibility of the process, as well as the particle uniformity and yield of the product produced is in potential superior to that of batch.[1] Furthermore, batch-to-batch inconsistencies are overruled by continuous manufacturing as the desired product specification can be acquired consistently in steady state.

Preferential crystallization (PC) is a chiral resolution process that can be used as an example to show the advantages of continuous processes over batch processes. Chiral molecules are molecules that are identical in their chemical properties e.g. solubility and melting point, but differ in their structural arrangement such that they are non-superimposable images of one another. As such, the biological response induced by each of these *enantiomers* is potentially different; one enantiomer produces the desired therapeutic response whereas the opposite enantiomer can have potentially harmful effect e.g. ethambutol; one enantiomer is a treatment for tuberculosis but the opposite enantiomer causes visual disturbance and may cause blindness. It is therefore important to separate enantiomers from one another.

In a batch PC process, a supersaturated racemic (an equal mixture of both enantiomers) solution is seeded with enantiopure crystals of the preferred enantiomer. The seed crystals grow by removing molecules of the preferred enantiomer from solution. However, since the other enantiomer remains in solution at a constant supersaturation, it is inevitable that over time it will crystallize. The risk of unwanted nucleation can be lowered by running a PC continuously. In a continuous PC process, the initial supersaturation generated by the temperature difference between the feed tank and the crystallizer can be lower compared to a batch PC process, since the solution removed from the crystallizer can be recycled, thus increasing the productivity

and yield of the process compared to a batch PC process. However, unwanted nucleation of the counter enantiomer is still inevitable, if enough time has passed.

Despite its many advantages, however, there are areas of continuous manufacturing that still require improvement. One issue concerning continuous processes is that the start-up period preceding steady state takes considerable time during which the product is typically out of specification.[5] The start-up of a continuous stirred tank reactor (CSTR), as a rule of thumb, is said to need an average of 6 residence times to reach steady state. During start-up, a large amount of waste product is therefore produced or, if the product produced during start-up is recycled, a large amount of time is wasted that could be otherwise spent producing the required product with the correct specifications.

To date, few publications on the start-up of continuous crystallization processes have been reported.[5–8] Previous work by Yang et al.[6] has shown that through the use of automated direct nucleation control, the start-up time to steady state can be significantly reduced. Another study by Yang et al.[9] investigated the use of a wet mill in a continuous crystallization setup in conjunction with the automated direct nucleation control. It was found that the use of the wet mill did not improve the start-up time of the process but instead was effective in maintaining steady state. In a different study it was found that use of different start-up procedures that can be effective in reducing the time to steady state. Hou et al.[7] found that by using material produced by the continuous process as seed material for the subsequent run was more effective in reducing the start-up process than starting the process from a batch suspension or from a supersaturated solution alone. They also found that the steady state achieved by the process was independent of the start-up method used. Yang and Nagy[5] investigated the use of dynamic cooling and anti-solvent profiles during start-up. They found that dynamic anti-solvent addition profiles reduced the waste produced during start-up by up to 50% since the addition rate of the anti-solvent also had an effect on the residence time, which temperature did not. Su et al. developed a mathematical model through which a concentration control strategy was used to enhance the start-up procedure.[8] However, to the author's knowledge it is not yet know how initial process parameters affect the start-up time and steady state of the process.

In this article, the influence of process parameters on the start-up and steady state of a continuous preferential cooling crystallization process in order to reduce the start-up time to achieving a robust steady state was investigated. DL-asparagine monohydrate is used as the model compound for this study. The continuous crystallization of L-asparagine monohydrate was studied from both enantiopure and racemic solutions. First, this article will focus on the effect of the initial process parameters on the start-up time to steady state for a given start-up procedure. The parameters that were varied were initial supersaturation, seed sieve fraction, seed loading, residence time and initial solution enantiomeric excess. Finally, we focus on the robustness of the steady state in each experiment, and how the parameters influenced the steady state that was achieved.

5.2 Experimental

5.2.1 Materials and Methods

DL-asparagine monohydrate (DL-asn) and L-asparagine monohydrate (L-asn) were purchased from Sigma-Aldrich (Germany) and used as received. Seed crystals of L-asn were prepared through sieving of the raw material using a Fritsch Analysette 3 Pro sieve shaker to obtain the seed sieve fractions of 180-250 (small), 250-355 (medium) and 355-500 (large) μm. Water, purified by Milli-Q gradient system from Milipore SAS (France), was used as a solvent.

5.2.2 Experimental Setup

The experimental setup depicted in Figure 5.1 consisted of two jacketed continuous stirred tank reactors (CSTR) (Radleys, UK). The feed vessel had a volume of 5 L whilst the crystallizer had a working volume of 250 ml. Baffles were inserted into both vessels in order to aid mixing. In the feed tank an anchor impeller was used at a constant stirring rate of 200 rpm, which was deemed sufficient to ensure good mixing throughout the reactor. In the crystallizer, a switch blade impeller was used at a constant stirring rate of 300 rpm. The temperature in each vessel was controlled by a thermocouple which was connected to a Lauda Alpha RA8 heater-chiller and a Lauda Eco630 heater-chiller connected to the feed tank and the crystallizer, respectively. The feed and outflow were controlled by Watson Marlow (UK) 520Du peristaltic pumps,

with 7 mm tubing carrying solution from the feed tank to the crystallizer and 5 mm tubing (3.2 mm inner diameter) sufficiently large to remove suspension from the crystallizer to a collection unit. A pump calibration was carried out prior to the experiment in order to ensure the flow rate in each tube was the same so that the suspension volume in the crystallizer remained constant. A focus beam reflectance measurement (FBRM) probe (Mettler-Toledo, UK) was used in the crystallizer to monitor particle counts within the system over time. A polarimeter (Rudolph Research Analytical, UK) was connected to the crystallizer via a sinter glass filter (Sigma-Aldrich), pore size 10-20 μm, submerged below the suspension surface. Solid free solution was carried to the polarimeter in order to monitor the solution enantiomeric excess within the crystallizer. To prevent crystallization during analysis the pipeline was heated.

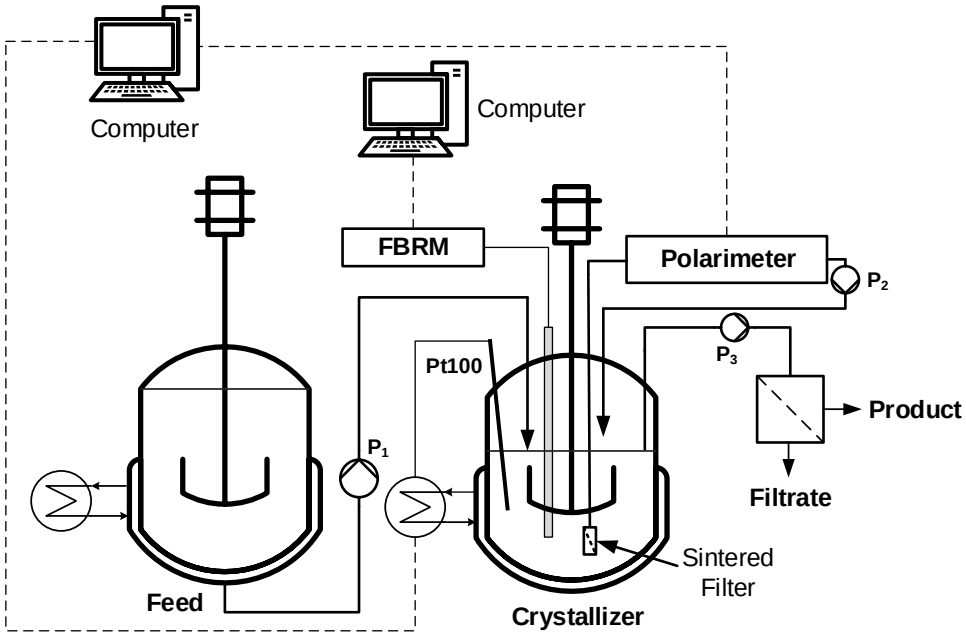

Figure 5.1. Schematic overview of the experimental setup for continuous crystallization experiments. Pump P_1 carries feed solution to the crystallizer seeded with L-asn. A FBRM probe is used to monitor particle counts over time. A polarimeter continuously withdraws solid free solution from the crystallizer via a sintered glass filter and pump P_2 to monitor the optical rotation over time. The outlet of the crystallizer is level controlled by pump P_3 which removes suspension from the crystallizer solid-liquid separation.

5.2.3 Experimental Procedure

A saturated solution of L-asn in water was prepared at 10.0°C above the saturation temperature T_s of the solution. Once clear, the solution was added to the feed vessel and heated to equilibrate with the temperature of the feed vessel (also set to 10.0°C above T_s). The saturation temperature required was given by the feed concentration C needed to obtain the required supersaturation ratio S, and is shown in Table 5.1. The crystallization temperature T_{cr} was 25.0°C for all experiments giving an equilibrium concentration C^* of 29.9 mg/ml. Therefore, C was calculated by $C = C^* \times S$. Initially, 250 ml of the saturated solution prepared was added to the crystallizer and the solution temperature was allowed to equilibrate with the crystallizer vessel temperature, set to 5.0°C above T_s. Once the solutions in both vessels reached the required temperature, the temperature of the crystallizer was reduced to T_{cr} (25.0°C) to allow the solution to become supersaturated. As soon as the crystallizer reached T_{cr} (indicated by the in situ thermocouple), the appropriate amount of seeds (given by Table 5.1) were added to the crystallizer solution and both pumps, from the feed tank to the crystallizer and from the crystallizer to the collection unit, were started. A sintered glass filter was submerged in the suspension in order to carry solid free solution to the polarimeter in order to measure enantiomeric excess during the process.

5.2.4 Experimental Design

The experimental plan was created using a screening design of experiments (DoE) approach in MODDE Pro 11 software (UMetrics) in order to construct Table 5.1. DoE is a useful method for reducing the experimental workload required to assess the effect of a number of parameters on a particular experimental response or responses.[10] Five parameters were chosen for investigation; initial supersaturation S (1.2, 1.4 or 1.6), residence time τ in the crystallizer (10, 20 or 30 min), seed loading L (2, 6 or 10 wt%), seed sieve fraction F (small = 180-250 μm, medium = 250-355 μm or large = 355-500 μm) and initial enantiomeric excess E_s of the feed solution (0, 60 or 100%). These parameters were varied to investigate their effects on the start-up time to steady state and on the robustness of the steady state. Because there are five input variables, a full factorial DoE was not carried out as this design would have yielded

255 experiments. Instead, a fractional factorial DoE of 19 experiments was used to highlight the main parameters affecting the start-up time and time to steady state. The run order of the experiments was randomized by the MODDE software.

Table 5.1. Experimental parameters investigated for continuous cooling crystallization experiments. All experiments were performed at T_{cr} = 25.0°C. Seed loading L is given by the percentage weight of total asparagine monohydrate dissolved per ml solvent in the feed solution. Seed size fraction F is characterized as small, medium and large for seed sizes of 180-250, 250-355 and 355-500 μm, respectively.

Experiment Number	S	τ [min]	L [wt%]	F	Feed E_s [%]	Start-up Time [τ]	Steady State Robustness
MP-1	1.4	20	6	medium	60	3	2
MP-2	1.4	20	6	medium	60	2.5	2
MP-3	1.4	20	6	medium	60	2.5	3.5
1	1.2	10	2	small	0	0*	0*
2	1.6	10	2	small	100	7	3
3	1.2	30	2	small	100	2	3.5
4	1.6	30	2	small	0	2	1
5	1.2	10	10	small	100	4	8
6	1.6	10	10	small	0	1	2
7	1.2	30	10	small	0	5	7
8	1.6	30	10	small	100	5	6
9	1.2	10	2	large	100	6	5
10	1.6	10	2	large	0	0*	0*
11	1.2	30	2	large	0	6	1
12	1.6	30	2	large	100	5	7
13	1.2	10	10	large	0	3.5	3
14	1.6	10	10	large	100	7	2
15	1.2	30	10	large	100	7	5
16	1.6	30	10	large	0	0*	0*

*A start-up time or steady state robustness value of 0 means that the process did not reach steady state i.e. control was lost during start-up.

5.2.5 Process Analysis

Optical rotation analysis was conducted using an AUTOPOL IV Polarimeter (Rudolph Research Analytical, UK) with a 100 mm optical rotation cell. Solid free solution was continuously removed from the crystallizer via sintered glass filter (ROBU Glasfilter, Germany, 250 x 13 mm) of pore size 10-20 μm (porosity 4), and pumped through the polarimeter cell via a Watson-Marlow (UK) 520 DU peristaltic pump at a flow rate of 45 ml/min. Each optical rotation measurement was measured at 30°C (T_c + 5 °C) and wavelength of 436 nm.

Gravimetric analysis was conducted to determine the total solution concentration. For this, a slurry sample was collected in a pre-weighed vial. The slurry was then filtered and a known amount of the filtrate was added to another pre-weighed vial and left to evaporate.

Chiral HPLC analysis was carried out using an Agilent UPLC instrument to determine the solid enantiomeric excess E_{cr}. Solid samples obtained from the filtered slurry were dissolved in water at a concentration of 1 - 2 mg/ml solvent. Solution samples were diluted to a concentration of between 0.5 and 1 mg/ml. A CHIROBIOTIC T column (Astec, 150 x 4.6 mm with 5 μm particle size) was used at 25.0°C with a 70/30 (v/v) methanol/water mobile phase (flow rate of 0.5 ml/min) with UV detection at 205 nm. The injection volume was 5 μl.

5.2.6 Data Analysis

5.2.6.1 Start-up and Steady State Determination

Start-up Time. Each experiment was monitored using an *in-situ* FBRM probe to monitor particle number, online polarimetry to monitor E_s (for experiment with an initial E_s of 0 or 60%) or solution concentration (for experiments with an initial E_s of 100%) and gravimetric analysis to determine solution concentration. In order for the whole process to be considered in metastable steady state, all three monitoring techniques must be in steady state.

For the start-up time and steady robustness determination, the decision tree in Figure 5.2 was used. Starting at (1), it was determined at the end of the experiment

whether control was lost. This was given by the trend of each monitoring technique; if the value was constant during the last residence time of each experiment the control was not lost. Any up or down trend during this period was considered an indication of loss of control. From (3) we then determine whether control was lost at time *t* during the process, at which point we go to (2). Or, if no control was gained at all during the process then the process is considered to still be in start-up.

If control was not lost by the end of the experiment, or we determine it was lost at time *t* during the process, then it is considered whether or not the system reached steady state (2). Steady state for each technique is reached when there is no significant change (<±5%) in the measurement value for 2 residence times. For the system to be in steady state the FBRM counts, optical rotation measurement and gravimetric solution concentration measurements must all be in steady state. If all three monitoring techniques are in steady state, then the start time of the steady state in determined and thus the start-up period of the process can be determined. For experiments that do not meet any of these criteria, control is considered to be lost during start-up/still be in start-up.

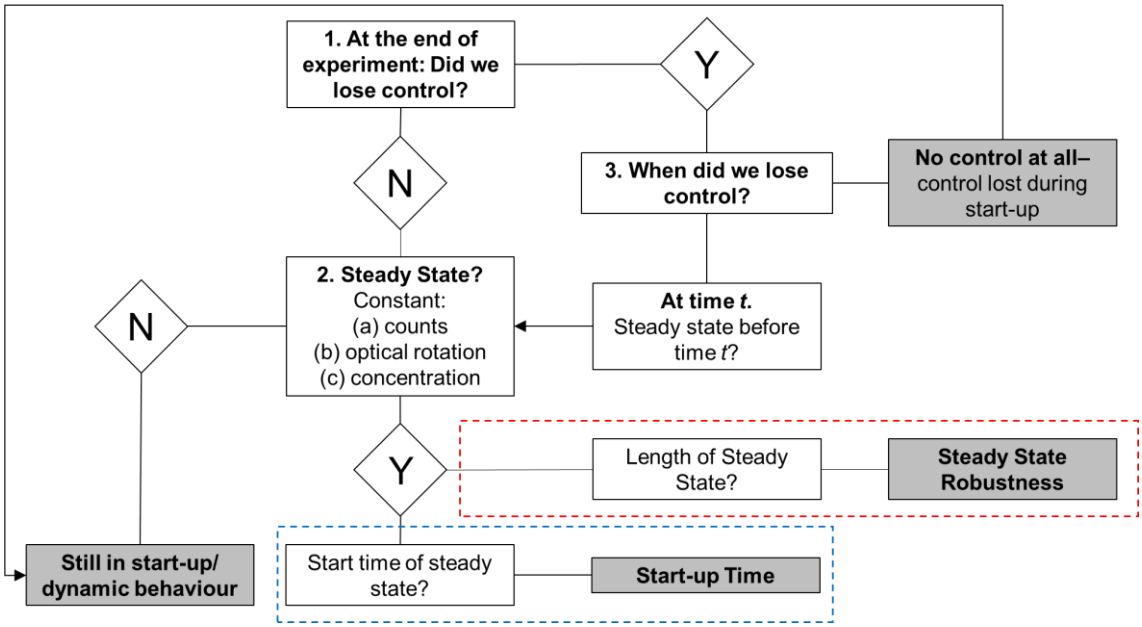

Figure 5.2. Decision tree of how start-up time and the steady state robustness is determined for each monitoring technique in each experiment in Table 1. The blue dashed enclosed section is the path followed for determining the start-up time to steady

state. The red dashed enclosed section is the path followed for determining steady state robustness.

Steady State Robustness. If the process reaches steady state, then the length of the steady state reaches (measured in τ) determines the robustness value of the process i.e. if the process is in steady state for 4 residence times then the robustness value of the process is 4. Once one of the three monitoring techniques falls out of steady state then the system is no longer in steady state. There are three possible scenarios that would cause the system to lose control and fall out of steady state:

(1) D-asn nucleation. This can only occur in experiments with an initial E_s of 0%, since in experiments with an initial E_s of 60% the process runs in the region of the phase diagram where D-asn cannot crystallize. Nucleation of D-asn is indicated by a reverse in the optical rotation trend measured by the polarimeter i.e. it tends towards 0° and a rise in the total number particle counts. A drop in the solution concentration measured by gravimetric analysis would also occur. Given these indications the nucleation of D-asn would be confirmed by HPLC analysis of the solid product collected.

(2) Crystal accumulation in the crystallizer. Accumulation in the crystallizer can occur if crystals are too large to be suspended and thus settled towards the bottom of the reactor. This would cause the total number of particle counts measured by the FBRM probe to increase since new particles would be produced due an increased amount of secondary nucleation whilst larger particles would not leave the crystallizer. The solution concentration would decrease further since more crystals (and therefore surface area) are present in the crystallizer available for growth. An increase in the optical rotation measured would also occur.

(3) Crystal wash-out. If there is not enough secondary nucleation generated, either by a low number of crystals (meaning there are less crystal-crystal and crystal-impeller collisions) or low supersaturation in the crystallizer (secondary nucleation via contact nucleation and fluid shear are highly supersaturation dependent) the seed crystals added to the system will eventually be removed in the product stream without generating enough new particles available for secondary nucleation. This would result in a decrease in particle counts (towards zero), and the solution concentration would

return to the initial feed concentration value. The optical rotation would therefore also return to its starting value.

All the criteria discussed I this section was applied to each monitoring technique for each experiment in Table 5.1.

5.2.6.2 DoE Analysis

Each of the start-up times and steady state robustness results was input into the DoE screening model in the MODDE software. The model was constructed by applying logarithmic transformations and fitting the transformed data using partial least squares (PLS). Models for both the start-up time and steady state robustness were generated using individual factors as well as factor-factor interactions. Insignificant terms i.e. terms whose presence or absence had very little or no effect on the outcome of the model, were removed from the model in order to improve the model statistics. The model generates effects plots highlighting the important parameters and parameter-parameter interaction that significantly affect the start-up time and steady state robustness of the process.

5.3 Results

5.3.1 Start-up and Steady State Determination

An example of how the start-up time to steady state is determined is shown in Figure 5.3, which illustrates the experimental results obtained from experiment MP-1 in Table 5.1. The FBRM (black solid line), optical rotation (red squares) and gravimetric concentration (blue squares) data is shown. At $\tau = 0$, the initial total concentration of asn in solution is 52.5 mg/ml solvent with an initial E_s of 60%. This corresponds to an initial optical rotation value of -0.257°. At start-up, 2.52 g (6 wt%) of enantiopure L-asn seeds of size 250-355 μm were added to the crystallizer. This caused the FBRM total counts trend to increase to around 200 counts. At the same time, the optical rotation value increases as L-asn is removed from solution by the seed crystals. Grow of the seed crystals also causes the total solution concentration to decrease. At around 10 minutes into the process (half a residence time), the total counts value measured by the FBRM starts to decrease until it reaches a steady state value of around 100 counts at 1.6 residence times. The solution concentration reaches steady

state at 2 residences times with a steady state value of around 48 mg/ml solvent. The optical rotation value finally reaches steady state at approximately 3 residence times with a steady state value of -0.222°. It is at this point that the whole system is now in steady state.

At steady state we have constant FBRM total counts, optical rotation and solution concentration values ±5%. The steady period in this experiment last for approximately 2 residence times. At 5 residence times, the total count value increases for the remainder of the experiment until it reaches a final value of around 600 counts.

As mentioned in Section 5.2.6.1, an increase in the particle counts could be due to either the unwanted nucleation of D-asn or accumulation of crystals in the crystallizer. In this experiment, the increase in counts is likely due to crystals not leaving the crystallizer in the outflow and thus accumulating in the crystallizer since (a) the optical rotation trend does not decrease and tend towards the starting value, which would occur on the nucleation of D-asn, (b) HPLC confirmed that only crystals of pure L-asn were produced after 100 min and (c) we are operating in the region of the phase diagram where D-asn cannot crystallize. Even though at steady state secondary nucleation already occurs in the crystallizer in order to replace crystals removed in the outflow, accumulation in the crystallizer would cause further secondary nucleation in the system which would increase the number of counts. There is a slight increase in the optical rotation value after 5 residence times, as well as a drop in the total solution concentration value, however the changes in these values are not significant enough to be considered a deviation from steady state i.e. they are within ±5% of their steady state values.

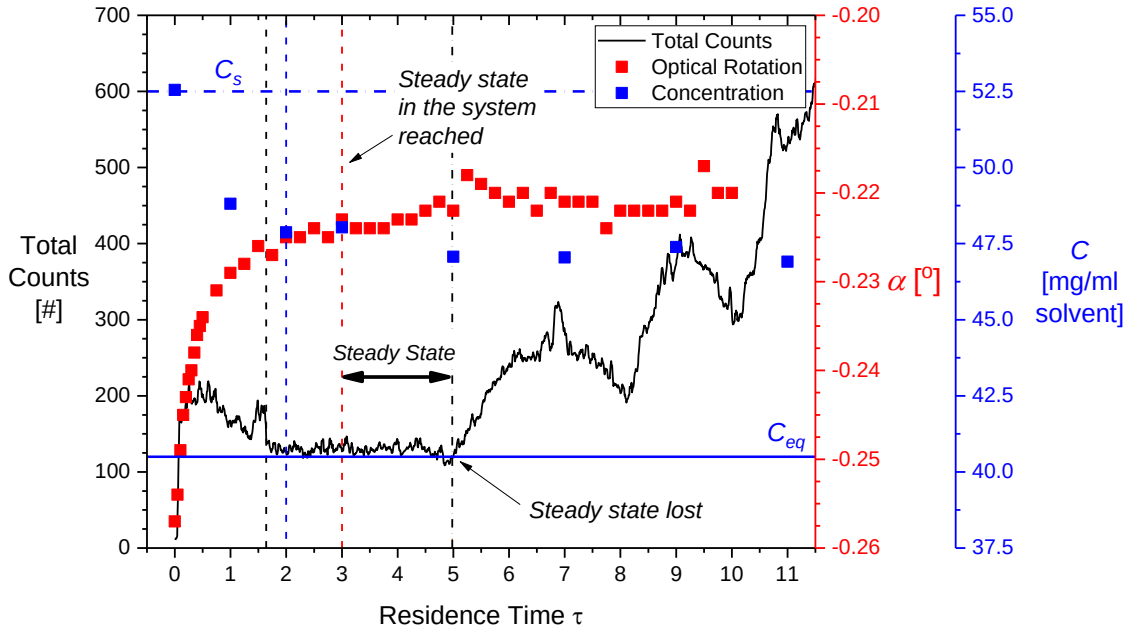

Figure 5.3. Experimental results from experiment MP-1 in Table 5.1, showing the FBRM total counts (-), optical rotation (■) and concentration (■) trends as a function of residence time τ. The point at which steady state is reached is shown for FBRM (---), optical rotation (---) and concentration (---). Once the optical rotation trend reaches steady state the system is in steady state for the period of time shown. At 5 τ steady state is lost (-·-) due to an increase in the total number of particle counts in the system. The saturation concentration C_s (-·-) and equilibrium concentration C_{eq} (-) are also shown.

5.3.2 Mid-point Experiments MP-1, MP-2 and MP-3

Figure 5.4 compares the results from experiments MP-1, MP-2 and MP-3. In Figure 5.4a, the FBRM total count trends are compared. The steady state regions for each experiment are highlighted in black (i) for experiment MP-1, red (ii) for MP-2 and blue (iii) for MP-3. The total count value for each experiment reaches steady state at similar time (around 1.5 residence times for experiments MP-1 and MP-2, and at around 2 residence times for MP-3). Additionally, the steady state counts value between the three experiments ranges by only approximately 75 counts. Similarly, the optical rotation trend of all three experiments reaches steady state within 3 residence times. The gravimetric solution concentration measurement trend for all three mid-point experiments reaches steady state in 2 residences times. This gave system start up

times of 3, 2.5 and 2.5 residence times for experiments MP-1, MP-2 and MP-3 respectively.

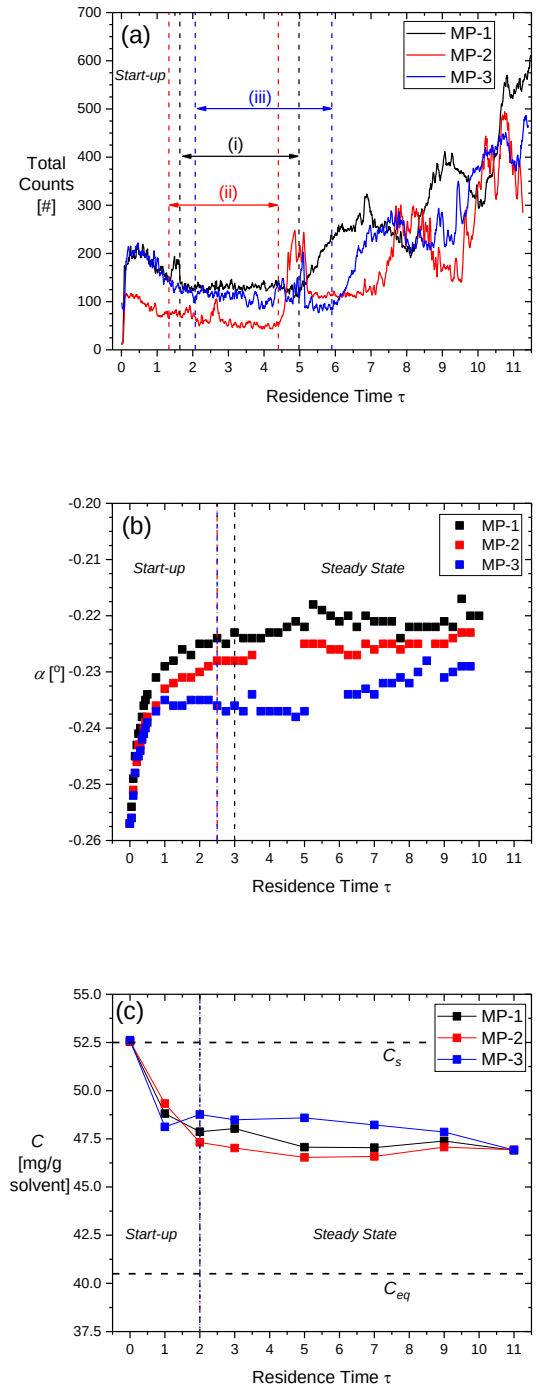

Figure 5.4. Comparison of (a) FBRM total counts trends, (b) optical rotation trends and (c) total solution concentration trends as a function of residence time τ for

experiments MP-1, MP-2 and MP-3 in Table 5.1. (a) FBRM total counts trends for experiment MP-1 (-), MP-2 (-) and MP-3 (-) showing the start-up times (dashed lines) and steady state regions: (i) MP-1, (ii) MP-2 and (iii) MP-3. (b) Optical rotation trends for experiments MP-1 (■), MP-2 (■) and MP-3 (■) showing start-up times (dashed lines) and steady state region. (c) Total solution concentration trends for experiments MP-1 (■), MP-2 (■) and MP-3 (■) showing the start-up times (dashed lines) and steady state region. The saturation concentration C_s (--) and equilibrium concentration C_{eq} (--) are also shown.

Both the optical rotation and solution concentration trends for the three mid-point experiments maintain steady state for the remainder of the process. However, similarly to experiment MP-1, in which stead state was lost at around 5 residence times due to an increase in the particle counts, experiments MP-2 and MP-3 also fell out of steady state due to particle count increase. Experiment MP-2 lost steady state at approximately 4.5 residence times and experiment MP-3 lost steady state at slightly under 6 residence times. This gives steady state robustness values of 2, 2 and 3.5 for MP-1, MP-2 and MP-3 respectively.

It is likely that the cause of the particle count increase in experiment MP-2 and MP-3 is also due to increased secondary nucleation within the crystallizer from the accumulation of crystals. However, since this occurred in all three experiments, at approximately the same time in the process, it shows that the process is reproducible since similar experiment results were obtained. Therefore, the mid-point values chosen for this work is well chosen.

5.3.3 Start-up and Steady State

5.3.3.1 DoE Results

Figure 5.5 illustrates the start-up time and steady state robustness determined for each experiment in Table 1. For example, experiment 7, which has initial conditions S = 1.2, τ = 30 min, seed loading = 10%, small seed size and an initial enantiomeric excess of 0%, had a start-up time of 5 residence times and steady state robustness value of 7. Ideally, an experiment would have a short start-up time and high

robustness value. However, from Figure 5.5, there is no recognizable correlation between start-up time and steady state robustness.

A summary of fit plot for both start-up time and steady state robustness is shown in Figure 5.6. This figure describes the statistics of the model and in turn whether the model is valid or not. R^2 is the goodness of fit of the model and measures how well the regression model fits the raw data. A value between 0 and 1 is obtained where 1 is a perfect model and 0 is no model at all. Q^2 is the goodness of prediction and give information on the usefulness of the model for predicting the outcome of future experiments. For a model to be considered good, both R^2 and Q^2 should be high (>0.5) and separated by no more than 0.3. The model validity is calculated once the repeat experiments have been completed and reflect whether the right type of model has been chosen. A value >0.25 indicates a valid model. Finally, the model reproducibility indicates how reproducible the model is. The larger the value the smaller the error between replicate experiments in relation to the variability across the remaining experiments in the design. A value <0.5 means that there is a large pure error and poor control over the experimental procedure.

The model for start-up shows satisfactory results for model fit (R^2) of 0.95, model predictability (Q^2) of 0.72, model validity (0.44) and model reproducibility (0.97). For steady state robustness, the model also shows a good fit of around 0.8 and good model validity (0.75) and reproducibility (0.84). The Q^2 value for this model is lower and within 0.3 of the R^2 value, meaning the model is still useful for predicting the outcomes of future experiments. This mean the models created for both start-up time and stead state robustness are valid models that can be useful for predicting the outcome of future experiments.

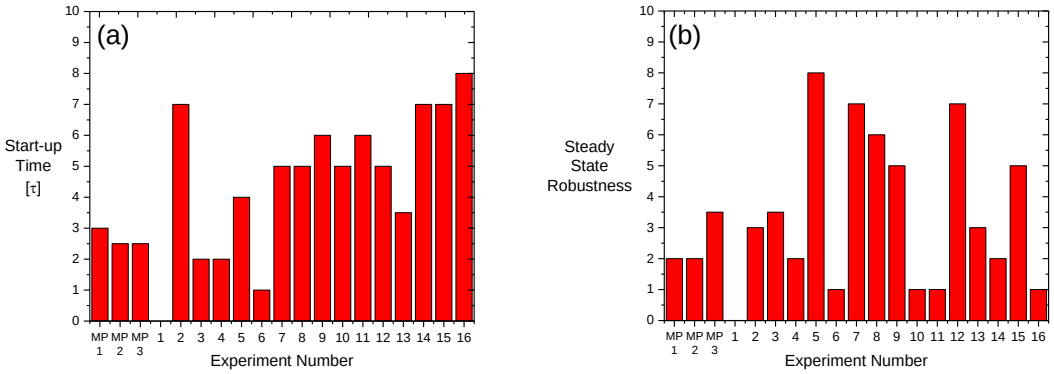

Figure 5.5. Start-up time to steady state (left) and steady state robustness (right) for each experiment in Table 5.1. Experiment 1 in Table 5.1 did not reach a steady state.

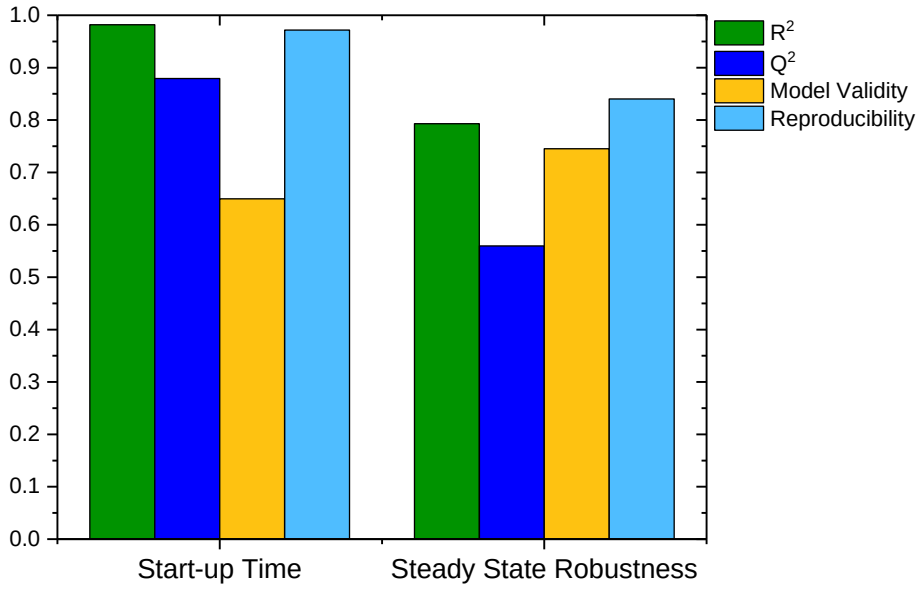

Figure 5.6. Summary of fit plots for start-up time (left) and steady state robustness (right). (■) R^2 value, (■) Q^2 value, (■) model validity and (■) model reproducibility. Both models are considered to be valid. The model for start-up time shows a high R^2 value of 0.98, Q^2 value of 0.87, model validity of 0.65 and model reproducibility of 0.97. For steady state robustness, the model also shows a good fit R^2 of around 0.8 and good model validity (0.75) and reproducibility (0.84). The Q^2 value for this model is lower and within 0.3 of the R^2 value, meaning the model is still useful for predicting the outcomes of future experiments.

5.3.3.2 Factors Affecting Start-up Time

An effects plot was created by MODDE to highlight the factors and/or factor-factor interactions which have the greatest effect on the start-up time to reach steady state in a continuous process. Figure 5.7 shows the results of the main effects on the start-up time to steady state. The plot shows the change in the start-up time to steady state when a particular factor is varied from its low level to its high level when all other factors are kept at their mid-point values e.g. changing the sieve fraction used from small (180-250 μm) to large (355-500 μm) while keeping supersaturation, residence time, seed loading and initial E_s at 1.4, 20 min, 6% and 60% respectively. A positive effect value indicates that changing that particular parameter from its low value to its high value will increase the start-up time to steady state. Vice versa a negative effect value will mean a reduction in the start-up time to steady state (which in this case is what we want). The magnitude of this increase depends on the relative effect a parameter has compared to other parameters. Where the plot shows that an interaction of effects has a significant change in the response, the effect of one of these factors depends on the level of the other.

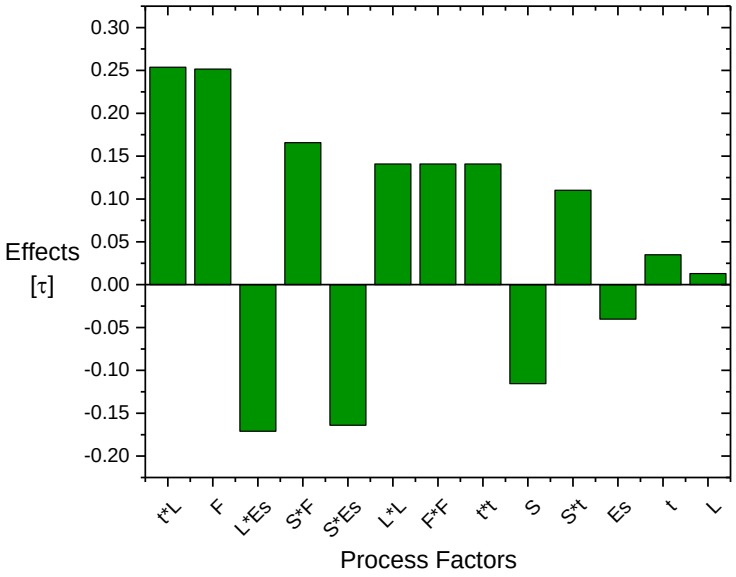

Figure 5.7. Start-up time effects plot showing the process factors and factor-factor combinations that have the most effect of the start-up time to steady state from largest to smallest (left to right). τ = residence time, L = seed loading (%), F = sieve fraction (μm), S = supersaturation (C/C^*) and E_s = initial enantiomeric excess in the feed

solution. Where two factors are shown e.g. t*L, this indicates an interaction of each factor with each other.

Figure 5.8 (a-e) shows the effect on start-up time as a function of the top five process factors indicated by Figure 5.7. The factor that has the greatest effect on the start-up time is the interaction effect between residence time and seed loading. Figure 5.8a shows the predicted change in the start-up time when using both a high and low seed loading value as a function of residence time when all other factors are set to their mid-point values. The results indicate that at a low residence time, a high seed loading (10 wt% in this case) should be used, however, at a high residence time, a low seed loading (2 wt%) should be used. For a given size of seed crystals, using a high seed loading means there is a larger surface area on which solute can grow. In contrast, a low seed loading would have a lower surface area. At low residence times, crystals in the crystallizer have less time to grow before being removed. Therefore, a higher seed loading (therefore a higher seed surface area) should be used in order to allow more growth of these crystals in the shorter space of time due to the increase in crystal surface area. Furthermore, with more crystals in the suspension when using a high seed loading, more crystal-impeller and crystal-crystal collisions can occur generating more secondary nuclei in the system to now act as new seeds for further growth. Since a high density of crystals can allow collisions to happen at a higher rate, the secondary nucleation rate equal to the rate of removal of crystals from the crystallizer can be reached in a shorter time than if a less seed material is used, and thus steady state is achieved sooner. In contrast, if a high seed loading is used at a higher residence time value, the secondary nucleation rate could potentially be higher than the rate of removal of crystals from the crystallizer. Therefore, by using a lower seed loading a higher residence time, fewer crystal-crystal collisions occur and thus the secondary nucleation rate is reduced. Furthermore, with a longer residence time these fewer crystals are given more time to grow in order to reach the required size for attrition to occur.

The seed sieve fraction used has the second largest effect on the start-up time to steady state. Similarly, the interacting effect of residence time and seed loading, by increasing the sieve fraction from a low value to a high value, the start-up time is

increased. This is visualized in Figure 5.8b, which shows the average start-up time and standard deviation for each sieve fraction for all experiments in Table 5.1. From the average values obtained a minimum average start-up time can be seen at 250-355 μm sieve fraction. At a higher sieve fraction, the crystal number and crystal surface area available for growth are smaller than for using a smaller sieve fraction (for a given seed loading). Therefore, like the previous description, the number of crystal-crystal collisions with the crystallizer will be smaller, and it will therefore take longer for the secondary nucleation rate to equal the rate of removal from the crystallizer (of course this will also depend on the seed loading and residence time used as well). The large variation for the small and large seed loadings is due to the effect of the other process parameters in of the experiments e.g. in experiment 2 in Table 5.1 (S = 1.6, τ = 10 min, L = 2 wt%, F = 180-250 μm and E_s = 100%) the start-up time takes 7 residence times, whereas in experiment 3 (S = 1.2, τ = 30 min, L = 2 wt%, F = 180-150 μm and E_s = 100%) the start-up time takes 2 residence times.

The interacting effect of supersaturation and seed sieve fraction also increases the start-up time changing from its low value to its high value. At a low supersaturation (S = 1.2), both low and high seed sieve fraction values show similar start-up times. However, on increasing supersaturation, there is a significant drop in the start-up time when using a low seed sieve fraction. This is likely due to the high surface area of the crystals at the lower fraction for a given seed loading. These smaller crystals are able to grow sufficiently quickly as to reach a secondary nucleation rate which equals that of the rate of removal from the crystallizer. At higher sieve fractions however, due to the larger size of the crystals, the amount secondary nucleation generated may initially be too large at these higher supersaturations and thus the start-up time is increased for larger sieve fractions as supersaturation is increased.

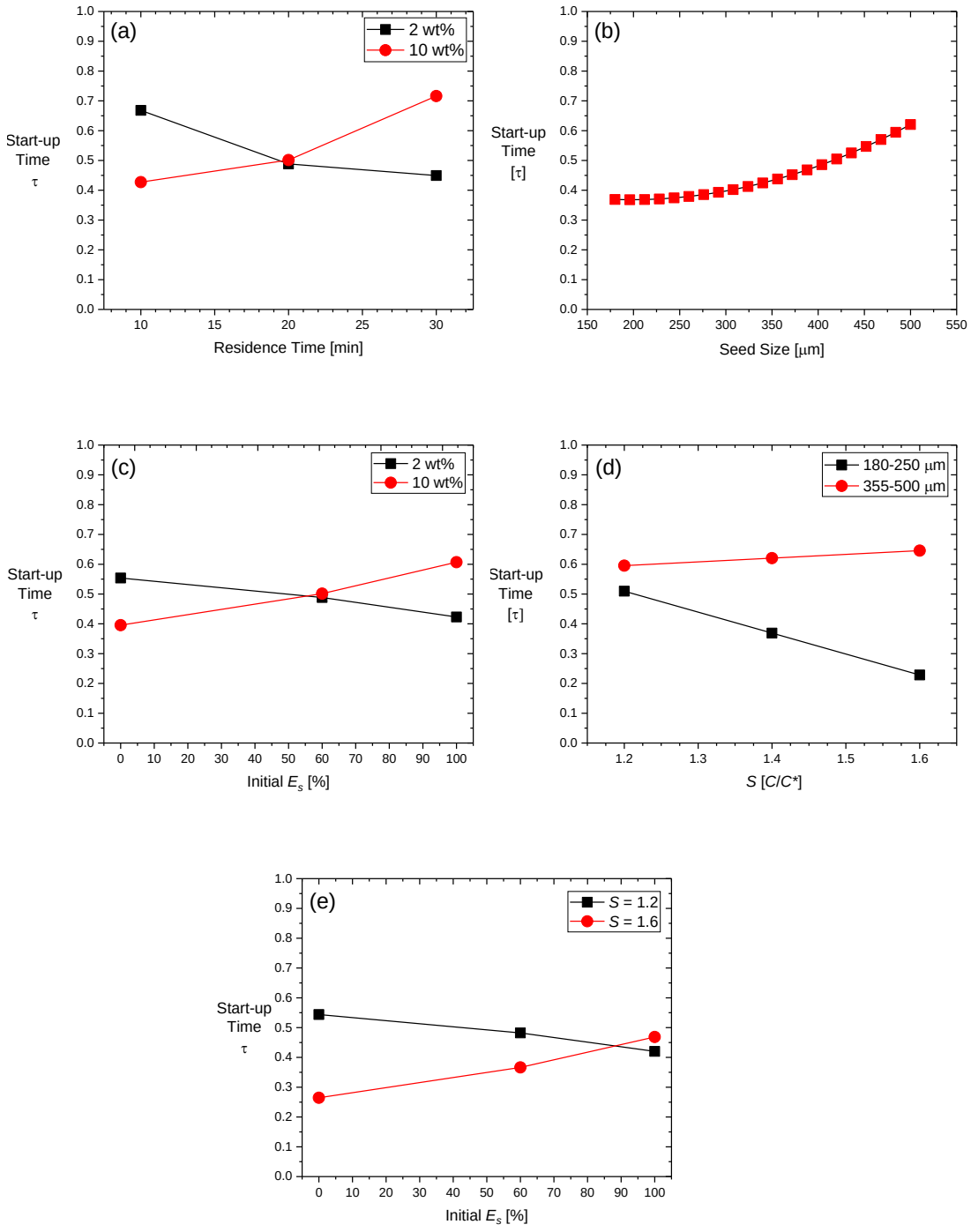

Figure 5.8. The effect on start-up time of the top five parameter interactions of Figure 5.7. (a) Interaction effect of residence time and seed loading (b) effect of seed sieve fraction (c) interaction effect of initial E_s and seed loading, (d) interaction effect of supersaturation and seed sieve fraction and (e) interaction effect of initial E_s and supersaturation.

The interacting effect of initial E_s in the feed solution and solid seed loading has the largest effect on reducing the start-up time changing from its low value to its high value (given by Figure 5.7). This can be explained by the relative growth rates of L-asn crystals in enantiopure and racemic solutions, whereby the growth rate is slower in a racemic solution than in an enantiopure solution.[11] Therefore, at lower concentrations of D-asn (or no D-asn at all), the growth rate of the L-asn seed crystals will be higher than it would be in a racemic solution, meaning that at lower seed loadings these crystals can still grow sufficiently large in order for the secondary nucleation rate to equal the removal rate of the crystals from the crystallizer. At high concentrations of D-asn, however, a high seed loading is required in order to increase the crystal surface area enough to account for the reduced growth rate of each crystal. In this way, crystals than therefore grow large enough to induce enough secondary nucleation quickly enough to reach steady state in a short period of time. By using a low seed loading at a high D-asn concentration (low E_s), crystals need longer to grow in the reactor, therefore longer residence times are required in order reduce the start-up time to steady state.

A 4-D contour plot is shown in Figure 5.9 which shows the predicted start-up time for various combinations of supersaturation, residence time, seed loading and seed sieve fraction at a constant initial E_s in the feed of 60%. Here, the effects described in Figure 5.7 can also be realized, with the most notable differences being seen between the seed loadings and seed sieve fractions used. The range of start-up times for each seed sieve fraction used can also be see across the various residence times and supersaturations.

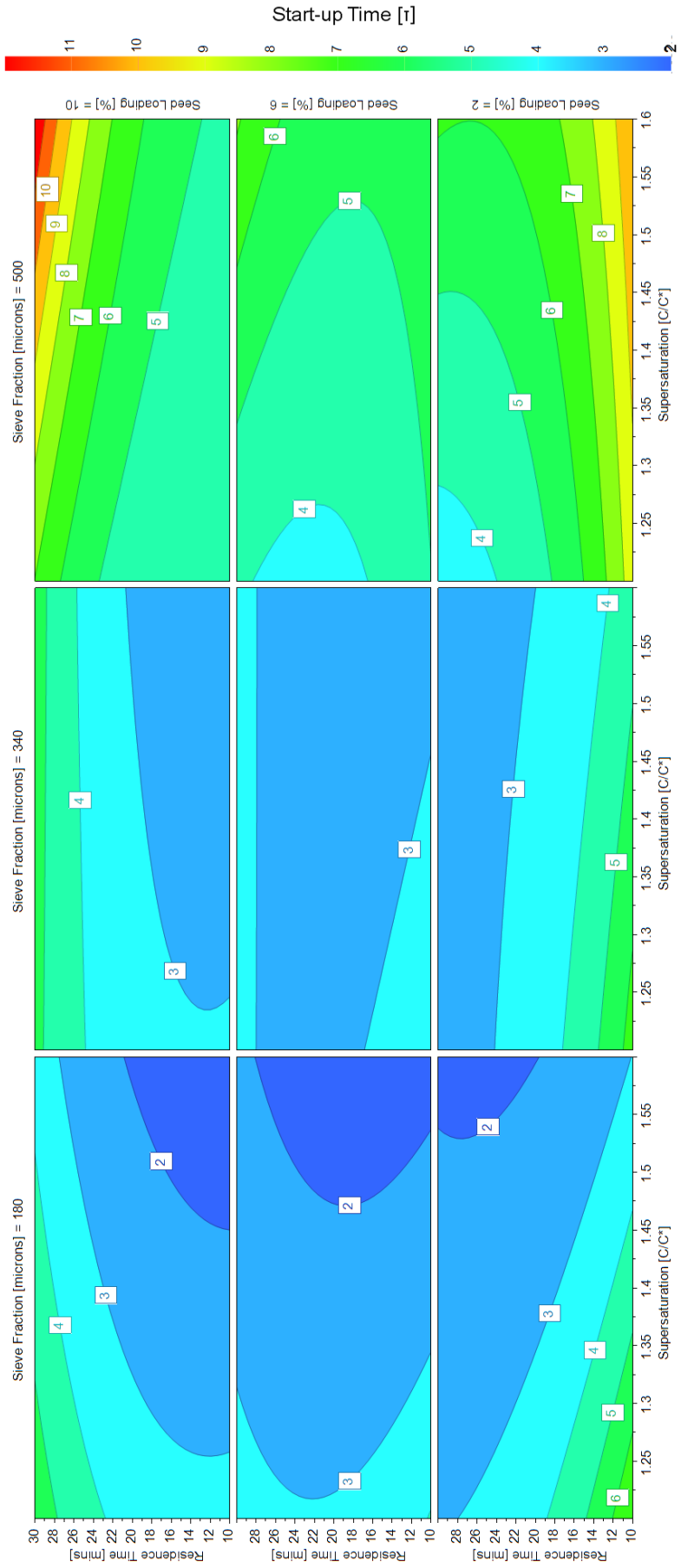

Figure 5.9. 4-D contour plot for start-up time to steady state model. The initial E_s is kept constant at 25%.

5.3.3.3 Fractors affecting Steady State Robustness

Only 4 of the 19 experiments maintained a steady state throughout the process (experiments 5, 7, 8, 12 and 15). Figure 5.10 shows the process factors and factor-factor interactions that had the biggest influence on the robustness of the steady state during the continuous crystallization processes investigated. The corresponding change in steady state robustness as a function of each of these process factors in shown in Figure 5.11(a-d). The error bars shown are confidence intervals of 95% for each effect. It is advised that confidence intervals which cross zero are removed from the model in order to improve statistics (as is the case with supersaturation and seed loading in Figure 5.10). However, in removing the individual factors alone, the interacting effect between these factors with other factors would also be removed by the model. For this reason, therefore, they are left in the model.

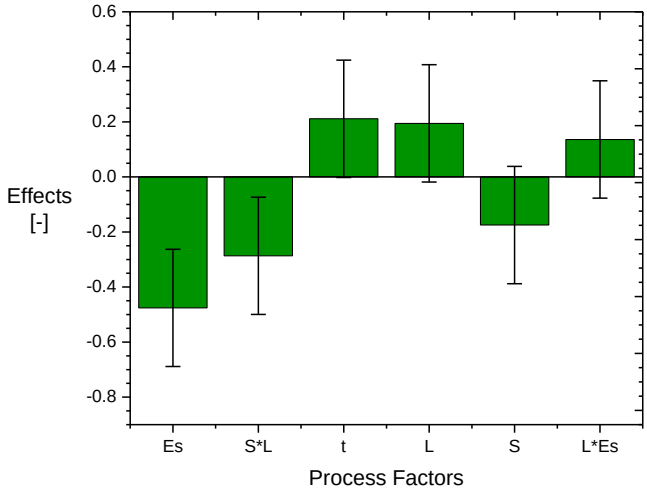

Figure 5.10. Steady state robustness effects plot showing the process factors that have the highest impact on the steady state of a continuous process from most to least effective (left to right) with a 95% confidence interval.

As expected from a continuous preferential crystallization, the presence of the counter enantiomer has the biggest effect on the stability of the steady state, since nucleation of the counter enantiomer is inevitable. The negative effect value in Figure 5.10 shows that when the D-asn value is changed from its low level concentration (0%) to its high level concentration (50%), that this has a negative effect on the steady state

robustness value i.e. steady state robustness will decrease. This is due to the unwanted primary nucleation of D-asn, which becomes increasingly more likely at both higher concentrations of D-asn and at higher supersaturations.

The most significant interaction effect between factors is that of supersaturation and seed loading (Figure 5.11c). Again, the reasons for this are most likely due to the high crystal numbers providing a large enough surface area for growth, such that crystals can grow large enough to induce enough secondary nucleation to maintain crystal numbers within the reactor and account for the simultaneous removal of crystals. Where this high seed loading has a negative effect is when the supersaturation is increased. The most likely reason for this is that due to the large supersaturation crystals grow much larger than they would at a lower supersaturation (for a given residence time) and it is possible that too much secondary nucleation occurs that the crystal number within the crystallizer simply continuous to increase of time due to the rate of formation of these secondary nucleation being higher than the removal rate of crystals in the outlet stream.

In contrast we see that increasing residence time has a positive effect on the steady state robustness of the process, which is also seen for the seed loading used. In Figure 5.11, the effect of residence time and seed loading on the robustness of the steady state in shown (Figure 5.11b and 11d, respectively). Both these factors show not only similar trends for changing the value of each factor, but also similar results in the robustness of the steady state they achieve. In the case of residence time, it could be said that by allowing crystals to spend more time in the crystallizer, not only will they grow more, but the number of crystal-crystal collisions is likely to be higher than for a lower residence time. Therefore, enough secondary nucleation is induced over the course of the process that a steady state can be maintained in terms of crystal counts (measured by FBRM) and concentration and therefore optical rotation (measuring a concentration difference between D-asn and L-asn in solution. Likewise, with seed loading, by having a higher number of seeds in the crystallizer, there are more crystal–crystal collisions and therefore secondary nucleation in the crystallizer can also be maintained.

The 4-D contour plot generated showing the predicted steady state stability for a combination of process factors (residence time, D-asn concentration in the feed

solution, sieve fraction and seed loading) at a constant sieve fraction of 250-355 μm (this was since seed sieve fraction was shown to have no effect on the steady state robustness by Figure 5.10) is shown in Figure 5.12. Here the various effects of each factor and factor-factor interactions can also be seen. The most notable difference in steady state robustness can be seen in increasing the concentration of D-asn in the feed solution, as already described by Figure 5.10, not only for each supersaturation but also for each seed loading value. The plot predicts that the most robust steady state is achieved at a low supersaturation, high seed loading and low concentration of D-asn in the feed solution.

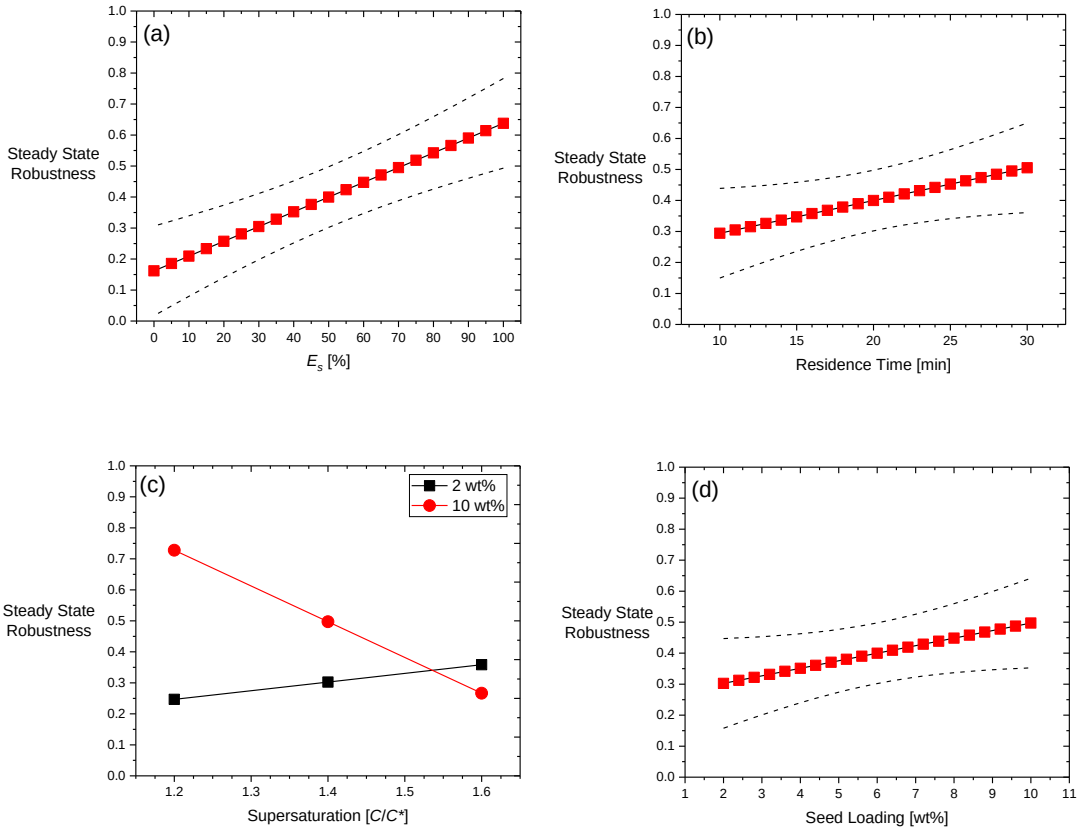

Figure 5.11. The effect on the steady state robustness of the top four process parameters as determined by Figure 8. (a) Effect of D-asn in the feed concentration, (b) effect of residence time, (c) interaction effect of supersaturation and seed loading and (d) effect of seed loading. Plots (a), (b) and (d) show the results with a 95% confidence interval (--).

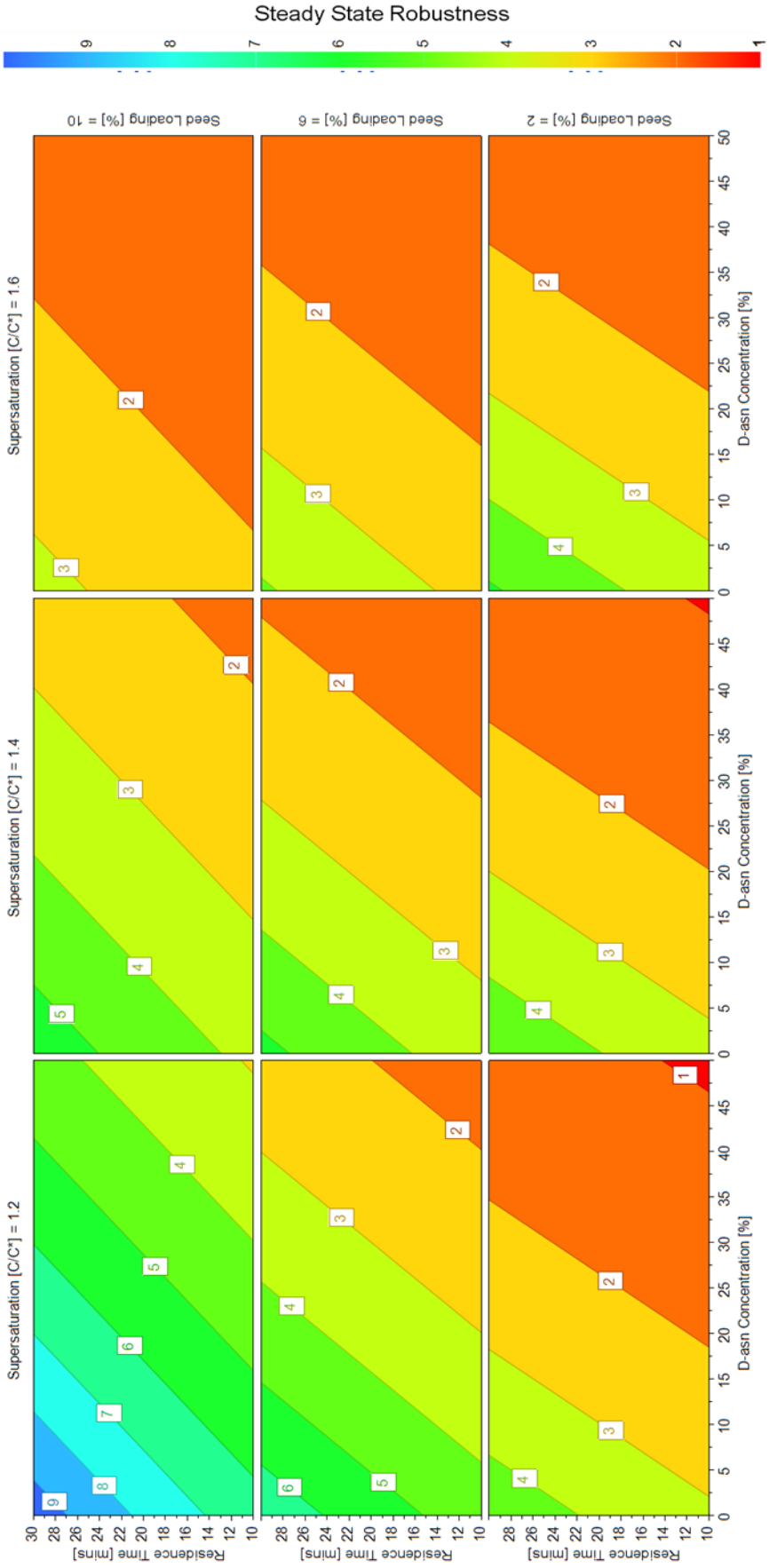

Figure 5.12. 4-D contour plot for steady state robustness model. The seed sieve fraction *F* kept constant at 250-355 µm.

5.4 Discussion

In order to achieve steady state in a continuous crystallization process, the rate of new nuclei generation (via secondary nucleation) must be equal to the rate of removal of crystals from the crystallizer. Thus, if the secondary nucleation rate is lower than the rate of removal, eventually wash-out of the crystals will occur. This occurred in experiment 1 in Table 5.1, where the experimental parameters were: S = 1.2, τ = 10 min, L = 2 wt%, F = 180-250 μm and an initial E_s = 0%. Since, in this experiment, the composition of the feed solution was racemic, the growth rate of the L-asn seed crystals was lower than compared to an enantiopure feed[11]. This factor, combined with a low seed loading of 2 wt%, meaning a low crystal surface area available for growth, and a low residence time, meaning crystals have less time to grow, meant that the secondary nucleation rate achieved was lower than the rate of removal of crystals from the crystallizer. In contrast, the mid-point experiments MP-1, MP-2 and MP-3 showed that accumulation of the crystals in the reactor caused an increase in the secondary nucleation rate such that it was greater than the rate of removal and hence the particle counts increased. Furthermore, previous literature[7,12] has also highlight the importance of the seed material used in relation to the start-up of a continuous process. Thus the results obtained in this work agree with previous findings since all the parameters that were found to have the biggest effect on the start-up time are parameters or parameter-parameter interactions involving characteristics of the seed material.

In a PC process, it is no surprise that the parameter with the greatest effect on the robustness of the steady state is the concentration of the counter enantiomer D-asn in the feed solution. As aforementioned, counter enantiomer nucleation is inevitable in any PC process. However, the likelihood of this unwanted nucleation increases at both higher concentrations of the counter enantiomer (if the process is run in the 3-phase region of the phase diagram) and supersaturation (since induction time for nucleation decreases with supersaturation). The plot in Figure 5.13 shows the solid enantiomeric excess E_{cr} results determined by HPLC for each of the experiments in Table 5.1 with an initial E_s of 0%. In all experiments with an initial supersaturation of S =1.6 (symbols with dashed lines in Figure 5.13), steady state was not reached due to early nucleation of the counter enantiomer. Even though over 12 residence times no nucleation of the counter enantiomer occurred i.e. E_{cr} remained at 100%, in experiments with an initial

racemic composition and supersaturation of S =1.2 (symbols with solid lines), given enough time, this would occur.

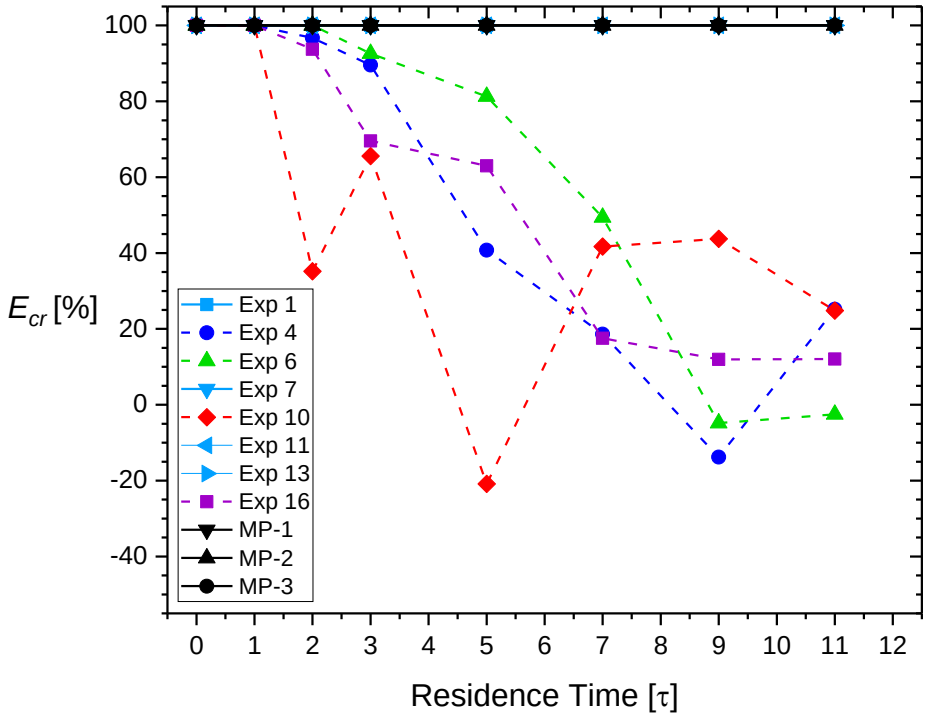

Figure 5.13. HPLC results showing solid enantiomeric excess E_{cr} as a function of residence time for experiments in Table 5.1. with an initial E_s of 0% and 60% and an initial supersaturation of S = 1.2: experiment 1 (■), 7 (▼), 11 (◀), and 13 (▶), and an initial supersaturation of S =1.6: experiments 4 (-●-), 6 (-▲-), 10 (-♦-) and 16 (-■-). Mid-point experiments MP-1 (▼), MP-2 (▲) and MP-3 (●) are also shown.

It is therefore important to strike a balance between the want for a short start-up time in order to save time and/or material and the need for a robust steady state. However, no correlation between the start-up time to steady state and the steady state that was achieved was found i.e. a short start-up time did not mean a robust or non-robust steady state or vice versa. This finding agrees with previous researchers who determined that the steady state achieved was independent of the start-up procedure used. Therefore, having a robust steady state at the expense of 1 or 2 extra residence times for start-up (during which any material produced can be recycled) is more

important than have a short start-up time of 1-2 residence times, especially if the steady state achieved cannot be controlled.

Once steady state is achieved, using control strategies such as automated direct nucleation control[6] or integrating a wet-mill[13] into the setup have been proven to maintain and control the steady state that it achieved. However, these strategies have not been used for PC process on chiral molecules. Since even in a continuous PC process nucleation of the counter enantiomer is inevitable, such control strategies only control particle size and shape, not product purity. For PC processes therefore, it would be useful to use such control strategies along with the resolution control approach also demonstrated by our group[14] in order to control all aspects of the continuous process. In general, the steady state that is achieved for a particular continuous process will depend on the requirements of the process i.e. whether yield, particle size and shape or product purity is the most important factor. For PC process, product purity is considered the most important particle attribute to control.

5.5 Conclusions

In this work, we have described the effect of continuous process parameters (initial supersaturation, residence time, seed size, seed loading and initial enantiomeric excess of the feed solution) on the start-up time and steady state robustness of a continuous preferential crystallization process. The results show that there is no correlation between the start-up time of a continuous preferential crystallization process and the robustness of its steady state. It is clear that factor-factor interactions play a more significant role in the start-up time of the process rather than any of the individual factors alone. The combination effect of residence time and seed loading had the biggest effect on the start-up time. However, this interaction effect caused the start-up time to increase. The combination effect of seed loading an initial solution enantiomeric excess had the largest effect in reducing the start-up time. In contrast, individual factors only affected the robustness of the steady state achieved in the process, with the concentration of D-asn have the biggest effect on reducing the robustness of the steady state achieved due to its unwanted primary nucleation. Not only that, but it is clear than the amount of secondary nuclei generated (by way of supersaturation, seed size, seed loading and residence time) is an incredibly important

crystallization parameter to consider in such a process, since the properties of the seed material can influence the process. The model obtained was a screening model, and so the most important factors determined should be investigated further in a full-factorial DoE and optimized the reduce the start-up time and achieved the most robust steady state in order to work towards a fully optimized process.

5.6 References

(1) Baxendale, I. R.; Braatz, R. D.; Hodnett, B. K.; Jensen, K. F.; Johnson, M. D.; Sharratt, P.; Sherlock, J.-P.; Florence, A. J. Achieving Continuous Manufacturing: Technologies and Approaches for Synthesis, Workup, and Isolation of Drug Substance May 20–21, 2014 Continuous Manufacturing Symposium. *Journal of Pharmaceutical Sciences*. 2015, pp 781–791. https://doi.org/10.1002/jps.24252.

(2) Alvarez, A. J.; Singh, A.; Myerson, A. S. Crystallization of Cyclosporine in a Multistage Continuous MSMPR Crystallizer. *Cryst. Growth Des.* **2011**, *11* (10), 4392–4400. https://doi.org/10.1021/cg200546g.

(3) Vervaet, C.; Remon, J. P. Continuous Granulation in the Pharmaceutical Industry. *Chem. Eng. Sci.* **2005**, *60* (14), 3949–3957. https://doi.org/10.1016/j.ces.2005.02.028.

(4) Plumb, K. Continuous Processing in the Pharmaceutical Industry: Changing the Mind Set. *Chem. Eng. Res. Des.* **2005**, *83* (6), 730–738. https://doi.org/10.1205/cherd.04359.

(5) Yang, Y.; Nagy, Z. K. Combined Cooling and Antisolvent Crystallization in Continuous Mixed Suspension, Mixed Product Removal Cascade Crystallizers: Steady-State and Startup Optimization. *Ind. Eng. Chem. Res.* **2015**, *54* (21), 5673–5682. https://doi.org/10.1021/ie5034254.

(6) Yang, Y.; Song, L.; Nagy, Z. K. Automated Direct Nucleation Control in Continuous Mixed Suspension Mixed Product Removal Cooling Crystallization. *Cryst. Growth Des.* **2015**, *15* (12), 5839–5848. https://doi.org/10.1021/acs.cgd.5b01219.

(7) Hou, G.; Power, G.; Barrett, M.; Glennon, B.; Morris, G.; Zhao, Y. Development and Characterization of a Single Stage Mixed-Suspension,

Mixed-Product-Removal Crystallization Process with a Novel Transfer Unit. *Cryst. Growth Des.* **2014**, *14* (4), 1782–1793. https://doi.org/10.1021/cg401904a.

(8) Su, Q.; Nagy, Z. K.; Rielly, C. D. Pharmaceutical Crystallisation Processes from Batch to Continuous Operation Using MSMPR Stages: Modelling, Design, and Control. *Chem. Eng. Process. Process Intensif.* **2015**, *89*, 41–53. https://doi.org/10.1016/j.cep.2015.01.001.

(9) Yang, Y.; Song, L.; Zhang, Y.; Nagy, Z. K. Application of Wet Milling-Based Automated Direct Nucleation Control in Continuous Cooling Crystallization Processes. *Ind. Eng. Chem. Res.* **2016**, *55* (17), 4987–4996. https://doi.org/10.1021/acs.iecr.5b04956.

(10) Eriksson, L.; Johansson, E.; Kettaneh-Wold, N.; Wikstrom, C.; Wold, S. *Design of Experiments: Principles and Applications*, Third.; Umetrics AB: Umea, 2008.

(11) Kongsamai, P.; Maneedaeng, A.; Flood, C.; ter Horst, J. H.; Flood, A. E. Effect of Additives on the Preferential Crystallization of L-Asparagine Monohydrate. *Eur. Phys. J. Spec. Top.* **2017**, *226* (5), 823–835. https://doi.org/10.1140/epjst/e2016-60257-3.

(12) Powell, K. A. Improving Continuous Crystallisation Using Process Analytical Technologies : Design of a Novel Periodic Flow Process, Loughborough University, 2017.

(13) Yang, Y.; Song, L.; Gao, T.; Nagy, Z. K. Integrated Upstream and Downstream Application of Wet Milling with Continuous Mixed Suspension Mixed Product Removal Crystallization. *Cryst. Growth Des.* **2015**, *15* (12), 5879–5885. https://doi.org/10.1021/acs.cgd.5b01290.

(14) Dunn, A. S.; Svoboda, V.; Sefcik, J.; ter Horst, J. H. Resolution Control in a Continuous Preferential Crystallization Process, *Org. Process Res. Dev*,**2019**, 23 (9), 2031-2041.

Chapter 6

6 Resolution Control in a Continuous Preferential Crystallization Process

Andrew S. Dunn, Vaclav Svoboda, Jan Sefcik, Joop H. ter Horst

Preferential crystallization is a technique used to separate enantiomers, usually performed in batch mode. For a continuously operated preferential crystallization process from a supersaturated racemic solution, however, nucleation and growth of the unwanted counter enantiomer eventually becomes inevitable and a controlling measure should be taken. Using polarimetry as an effective monitoring tool to detect the crystallization of the unwanted enantiomer, a novel strategy is presented to eliminate the unwanted enantiomer crystals in a continuous cooling preferential crystallization process. The strategy involves switching from the racemic feed solution to an enantiopure feed solution upon detecting the counter enantiomer crystals. This allows selective dissolution of the counter enantiomer crystals while the preferred enantiomer crystals continue to crystallize. Once the crystals of the undesired counter enantiomer have dissolved by decreasing the counter enantiomer solution concentration sufficiently below its solubility, the feed is switched back to the racemic solution. Through the use of this model-free controlling action the process does not have to be terminated, but, instead, this method rectifies the situation to the initial metastable steady state by using a portion of the produced enantiomer product. The process can therefore operate at higher supersaturations compared to existing processes, for longer periods of time since the control action does not rely on the dissolution kinetics of the system but rather on the thermodynamics of the phase diagram. We show that this new approach is an effective and scalable control strategy for achieving enantiopure product in a continuous preferential crystallization process.

6.1 Introduction

If a molecule has a non-superimposable mirror image it is termed chiral.[1] The importance of chiral molecules in the pharmaceutical industry became clear during the 1960's when Thalidomide was used as a treatment for morning sickness during pregnancy.[2] Another example is ibuprofen, which is administered in racemic form, however, only the S-enantiomer is reported to have a therapeutic effect.[3] Drug regulatory agencies have now enforced that both enantiomers of an active pharmaceutical ingredient (API) must be tested and that, if necessary, only the active enantiomer should be marketed.[4] It is therefore important to be able to separate enantiomers efficiently and effectively.

Crystallization-based resolution techniques such as Viedma Ripening[5–8] and preferential crystallization[7–13] (PC) are very efficient due to the highly enantioselective crystalline phase. In a PC process, by seeding a racemic or enantiomerically enriched solution with the preferred pure enantiomer crystals, control is obtained over the crystallizing enantiomer. This process can be applied for resolution only if the racemic mixture of enantiomers in the solution forms a conglomerate system in the solid phase,[6] i.e. a racemic mixture of enantiopure crystals.[1] A racemic solution of the amino acid asparagine in water, for instance, forms a conglomerate of asparagine monohydrate crystals.[16]

However, PC processes can only run for a limited period of time as the nucleation of the counter enantiomer in the supersaturated solution becomes increasingly likely with process time.[17,18] There are control strategies using coupled batch PC processes that significantly reduce the risk of unwanted primary nucleation of the counter enantiomer by decreasing its supersaturation through exchange of solution between coupled crystallizers.[19,20] Continuous processes have many advantages over batch processes, including higher throughput[18] and greater reproducibility,[21] as well as reduced costs[22] and a reduction in the number of process steps.[23,24] The pharmaceutical industry is therefore becoming increasingly interested in introducing continuous crystallization in its manufacturing.[25–27] A continuous PC process in a continuously stirred crystallizer with solution feed and suspension outflow operates in a metastable steady state in which only the preferred enantiomer is crystallized while the counter enantiomer remains dissolved in the supersaturated

solution.[28,29] Thus, the counter enantiomer crystals will eventually crystallize and contaminate the product from the continuous PC.

Here, we aim to define a novel control strategy to eliminate the counter enantiomer crystals upon their detection in a continuous PC process. The conglomerate system of DL-asparagine monohydrate (DL-asn) in water was used as a model compound. Since polarimetry has been shown previously to be a useful monitoring tool for PC processes,[11,13,29,30] first, a monitoring technique based on this was verified using PC in batch. For enantiopure systems, polarimetry can give concentration information and for enantiomerically enriched systems, it can give an accurate determination of the enantiomeric excess in the solution and therefore, through a mass balance, the enantiomeric excess in the crystalline phase.[31] Then, an attempt was carried out to try and dissolve any particles of D-asn that spontaneously nucleated by raising the temperature within the vessel of a batch PC. Finally, a continuous PC process was carried out using an effective control strategy based on temporarily switching the feed stream from a racemic solution to an enantiopure solution in order to undersaturate D-asn, leading to complete dissolution of this form in the crystallizer.

6.2 Experimental

6.2.1 Materials and Methods

DL-asparagine monohydrate (DL-asn) and L-asparagine monohydrate (L-asn) were purchased from Sigma-Aldrich (Germany). Seed crystals of L-asn were prepared through subsequent sieving to obtain a sieve fraction of 180-250 μm. Deionised water, purified by Milli-Q gradient system from Milipore SAS (France), was used as a solvent.

Optical rotation analysis was conducted using an AUTOPOL IV Polarimeter (Rudolph Research Analytical, UK) with a 100 mm optical rotation cell. Solid free solution was continuously removed from the crystallizer via a sintered glass filter (ROBU Glasfilter, Germany, 250 x 13 mm) of pore size 10-20 μm (porosity 4), and pumped through the polarimeter cell via a Watson-Marlow (UK) 520 DU peristaltic pump at a flow rate of 45 ml/min. Using these conditions, the solution from the reactor takes 20 seconds to reach the polarimeter to be measured. Optical rotation measurements were recorded every 10 seconds and each measurement was obtained

at 30°C and a wavelength of 436 nm. The path length of the polarimeter cell was 100 mm. Points which deviated significantly from the observed trend e.g. due to bubbles in the sample line, were removed from the data. The nucleation of D-asn caused fluctuations in optical rotation as some crystals of D-asn most likely blocked the sintered filter. To remedy the blockage, the filter was replaced with a clean one. This meant no optical rotation reading was available for approximately two minutes during the change.

Gravimetric analysis was conducted to determine total solution concentration. For this, a slurry sample was filtered and a known amount of the filtrate was added to a pre-weighed vial and left to evaporate. The ratio of remaining mass and evaporated solvent volume is the overall concentration of chiral compound.

Chiral HPLC analysis was carried out using an Agilent HPLC instrument to determine enantiomeric excess of the solution and recovered solid product. Solid samples obtained from the filtered slurry were dissolved in water at a concentration of 1 mg/ml solvent. A CHIROBIOTIC T column (Astec, 150 x 4.6 mm with 5 μm particle size) was used at 25.0°C with a 70/30 methanol/water (v/v) mobile phase (flow rate of 0.5 ml/min) with UV detection at 205 nm. The injection volume was 5 μl.

6.2.2 Solubility and MSWZ Measurements

Solubility measurements were carried out using the Crystal16 (Technobis, Netherlands). L-asn samples of increasing concentration from 5 – 85 mg/ml H_2O in increments of 5 mg/ml were made up in 1 ml Crystal16 vials. The temperature profile was set to run from 5 to 55°C at a heating rate of 0.3°C/min and held at 55°C for 30 minutes. The temperature was then reduced again to 5°C at a cooling rate of -0.3°C/min and held there for 30 minutes. The cycle was repeated 3 times. The stirring rate was set to 700 rpm. The Crystal16 uses turbidity to measure the clear point (the temperature point at which no more crystals are present in solution) and the cloud point (the temperature at which the first appearance of crystals in suspension). The difference between the clear and cloud point temperature gives the metastable zone width (MSZW). For vials which crystallized during the 30 min hold at 5°C the cloud point was discarded.

6.2.3 Batch Seeded PC

6.2.3.1 Experimental Setup

The experimental setup, shown in Figure 6.1, consisted of a jacketed stirred tank reactor (STR) (Radleys, UK) with a working volume of 500 ml. The temperature in the vessel was controlled by a PT-100 connected to a Lauda Eco630 (Germany) heater-chiller. Solid free solution was continuously pumped from the vessel via the sintered glass filter through the polarimeter and recycled back via a peristaltic pump (P_1). The filter was prone to blocking, particularly during primary nucleation events. However, quickly changing the filter proved the simplest and most effective workaround. The polarimeter was connected to a computer to log optical rotation measurements. This computer was also connected to the heater-chiller in order to monitor and control the temperature within the vessel.

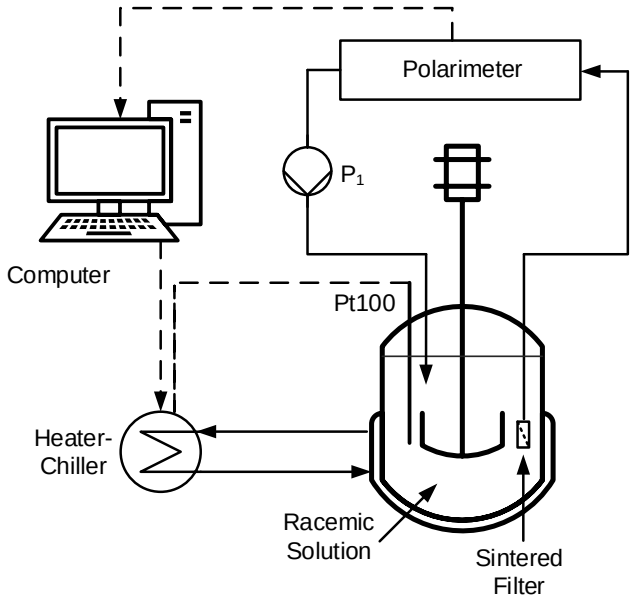

Figure 6.1. Batch crystallization setup for temperature control strategy. The enantiomeric excess E in solution is measured continuously via the polarimeter loop. The optical rotation measured is logged by the computer which also controls the set-point temperature of the heater chiller.

6.2.3.2 Experimental Procedure

DL-asn was added to water in the vessel such that the overall composition of 78 mg/ml solvent was obtained. The vessel was heated to 10°C above the saturation

temperature T_{sat} = 32.0°C until all solid was dissolved and a clear solution was obtained. Once a clear solution was obtained, the set point temperature was changed to the crystallization temperature T_{cr} = 25.0°C, generating a supersaturation ratio of S = 1.3. As soon as T_{cr} was reached, 0.6 g L-asn seeds were added to the 500 ml of solution in the vessel to grow under isothermal conditions.

On the detection of D-asn crystal formation given by a decrease in optical rotation value in time the set point temperature T_{sp} was increased to 13°C above the saturation temperature of both enantiomers i.e. 45.0°C to rapidly increase temperature within the vessel. Just before T_s was reached, T_{sp} was decreased back to T_{cr}. When D-asn crystallizes, the solution composition tends towards a racemic composition, decreasing the total asn concentration and hence the optical rotation value decreases towards 0° Therefore, a decrease in the optical rotation value can be used as a detection for D-asn crystal formation.

6.2.4 Concentration Control Approach for Continuous PC

6.2.4.1 Experimental Setup

For the concentration control approach, a continuous setup was used as depicted in Figure 6.2. The crystallization vessel used was as described in section 6.2.3.1, but as a mixed suspension mixed product removal (MSMPR) vessel with the polarimeter connected in the same way. This time, however, the crystallizer had a working volume of 250 ml. Two feed vessels were used; a 5 L racemic feed vessel solution and a 1 L enantiopure feed vessel. Only one of these vessels continuously fed saturated solution to the crystallizer at any one time whilst product slurry was continuously removed from the crystallizer. The temperature in the racemic feed vessel was controlled by Lauda Alpha heater-chiller and the temperature in the enantiopure feed vessel was controlled by a Lauda Eco630 heater-chiller. The flow from each feed vessel was delivered by a Watson-Marlow (UK) 520 DU peristaltic pump. The product slurry was continuously removed by a Masterflex (USA) L/S peristaltic pump.

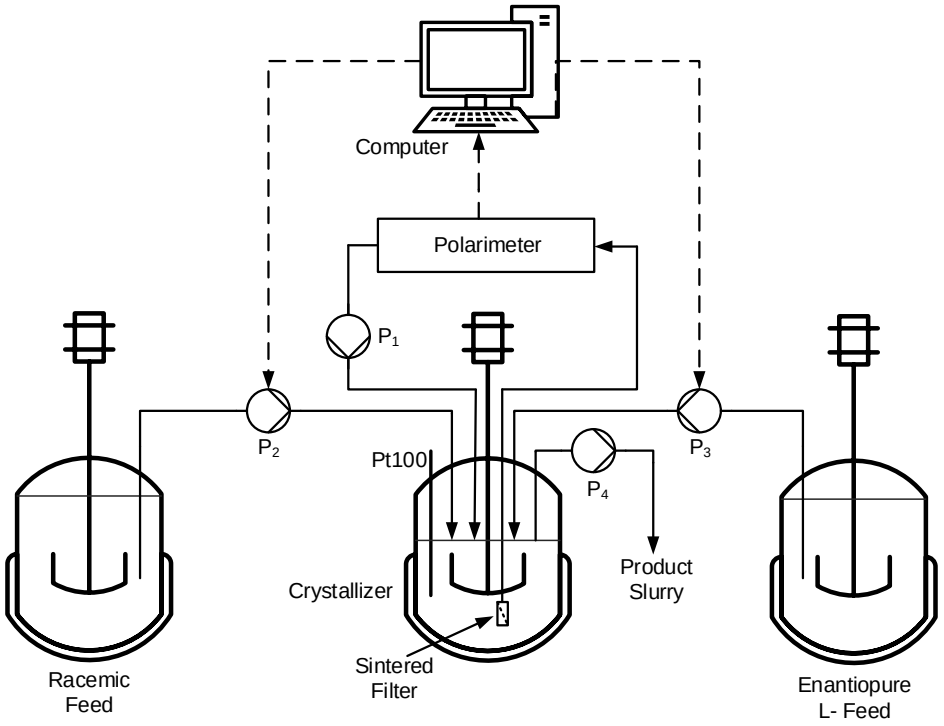

Figure 6.2. Continuous crystallization setup for concentration control strategy. A second enantiopure feed tank is used for process control; only one feed tank is active at any one time. The feed tank that is active depends on the optical rotation trend, which is continuously measured by the polarimeter.

6.2.4.2 Experimental Procedure

The racemic feed vessel was charged with a solution of DL-asn at a concentration of 87 mg/ml solvent (T_s = 35.0°C). Enantiopure solution of L-asn was added to the 1 L vessel such that the concentration of L-asn in this solution was the same as the concentration of L-asn in the racemic solution i.e. 43.5 mg/ml solvent. Once the crystallizer cooled to T_{cr} = 25.0°C giving a supersaturation ratio of S = 1.45, the polarimeter loop pump P_1 was started giving an initial optical rotation value of 0.000. Soon after, 2 g L-asn seeds were added and P_2 and P_4 were started. Inlet pumps from each feed vessel (P_2, P_3) were calibrated to deliver a flow rate of 4.17 g/min giving a residence time of 60 minutes in the crystallizer (the pump from the enantiopure feed P_3 was on standby until nucleation of D-asn occurred). The outlet of the crystallizer was level controlled by pump P_4. Steady state in the system was determined when the optical rotation value obtained remained constant (to within ±0.003°).

On the appearance of D-asn crystals, indicated by a decrease in optical rotation value from the steady state value determined by the polarimeter, pump P_2 was stopped and P_3 was started. The target concentration for D-asn is predetermined based on the ternary phase diagram (see Figure 6), however a target supersaturation ratio of S_D = 0.9 was used in order to ensure all D-asn dissolved while the supersaturation ratio for L- was maintained. The time period *t* the feed solution is switched for, assuming perfect mixing, is given by

$$Accumulation = Input - Output \tag{6.1}$$

$$\frac{dM_D}{dt} = in_D - out_D \tag{6.2}$$

Concentration of D-asn in the feed is zero, therefore:

$$\frac{dM_D}{dt} = -out_D = -C_D\dot{m} \tag{6.3}$$

$$\frac{dC_D}{dt} = -\frac{C_D}{\tau} \tag{6.4}$$

$$\int_0^t dt = -\tau \int_{C_0}^{C_f} \frac{dC_D}{C_D} \tag{6.5}$$

$$t = -\tau \ln\left(\frac{C_f}{C_0}\right) \tag{6.6}$$

$$t = \tau \ln\left(\frac{C_0}{C_f}\right) \tag{6.7}$$

Where M_D is the mass of D-asn in the vessel, C_D is the mass fraction of D-asn in the vessel, $\dot{m}$ is the flow rate, τ is the residence time in the crystallizer, C_0 is the starting concentration of D-asn in the crystallizer and C_t is the target final concentration of D-asn. After time *t*, the final concentration was reached, the enantiopure feed solution P_3

was stopped and the racemic feed solution P_2 was restarted. Slurry samples and subsequent solid and liquid samples were taken at various points during the process (see section 6.3.3) for concentration and enantiomeric excess determination.

6.3 Results

6.3.1 Solubility and MSZW

The solubility and metastable zone width (MSZW) of asparagine monohydrate are shown in Figure 6.3. Each experimental point shown is the average clear (solid squares) or cloud (square rings) point over three measurements of a single sample and the variation in the clear and cloud points obtained was not larger than the symbol. At a temperature of 25°C the solubility of DL-asparagine monohydrate is 60.0 mg of DL-asn per ml of water while that of L-asparagine monohydrate is 29.9 mg/ml. Since the solubility of L-asn is half that of DL-asn it shows that for this conglomerate system the solubility of L-asn is not significantly affected by an equal amount of D-asn at 25.0°C.[14] This measured solubility compares well to literature values.[14,32,33] Furthermore, the measured MSZW of L-asn is substantial, approximately 18°C between clear and cloud points, although it varies by approximately 2°C across different concentrations.

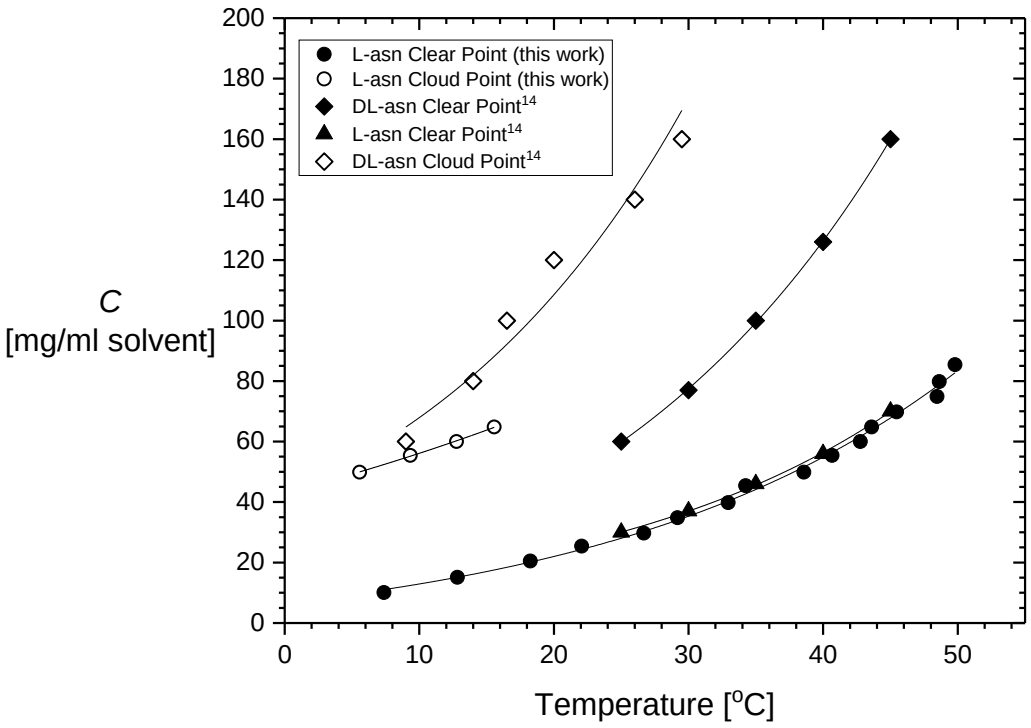

Figure 6.3. Experimental and reference solubility of L-asn and DL-asn. (●) experimental L-asn solubility curve determined in this work, (○) experimental L-asn cloud point determined in this work, (♦) solubility of DL-asn monohydrate, (▲) enantiopure solubility of L-asn and (◊) racemic cloud point of DL-asn monohydrate, determined by Kongsamai et al.[14] All concentrations of asparagine are based on the monohydrate solid form.

6.3.2 Batch Seeded PC

It is possible to preferentially crystallize L-asn monohydrate under well controlled conditions,[13,14] for instance through a batch-wise seeded preferential crystallization (PC) of L-asn from a racemic solution of 78.0 mg/ml of DL-asn monohydrate in water. Such a solution is saturated at a temperature of 32.0 °C. We performed such a PC by initially cooling the solution to 25.0°C to create supersaturation in the racemic solution. This supersaturation is equal towards the L-asn and D-asn solid phases because concentration and solubility of L-asn and D-asn are equal. By adding L-asn seeds the supersaturation for L-asn decreases due to L-asn crystal growth while D-asn remains in solution as long as no primary nucleation occurs. Therefore, the solution concentration of L-asn decreases while that of D-asn remains constant. The solution concentration difference between D- and L-asn is monitored by a polarimeter measuring the optical rotation.

In Figure 6.4a, the optical rotation increases from 0° in the initially racemic solution to 0.034° in 10 hours. The increasingly positive optical rotation of the solution indicates that the solution becoming more enriched in D-asn and the concentration difference between the enantiomers increases. This is due to L-asn growing from seed crystals, as L-asn is removed from solution. The rate of increase of the optical rotation decreases due to the decreasing supersaturation for L-asn growth so that the growth rate decreases and the solute concentration of L-asn decreases with a lower rate in time.

However, still a large supersaturation for D-asn remains in the solution and at some point in time D-asn crystals nucleate and grow. This is indicated by a decrease in the optical rotation, corresponding to a decrease in the concentration difference between the two enantiomers in solution. Figure 6.4b shows that this optical rotation decrease happens shortly after 10 hours.

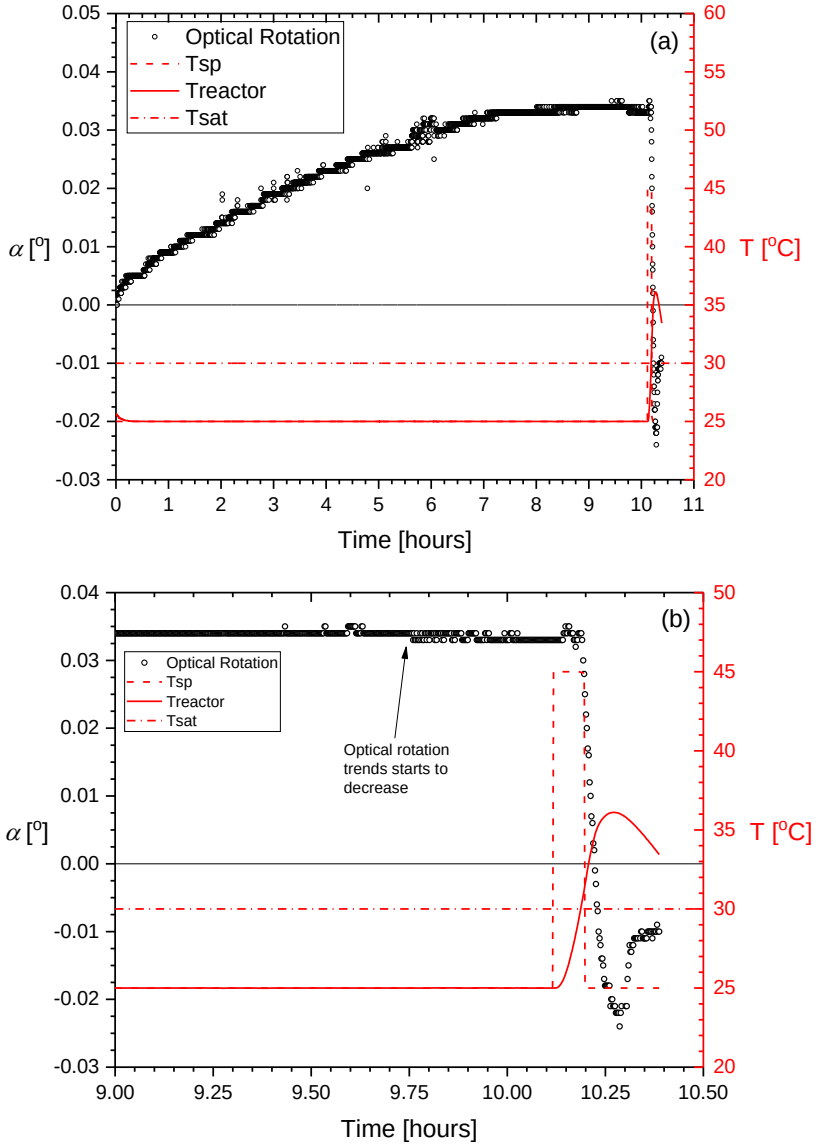

Figure 6.4. Optical rotation (●) and reactor temperature profiles; saturation temperature T_{sat} (-·-), set point temperature T_{sp} (---) and actual crystallizer temperature $T_{reactor}$ (-), during (a) the first 10 hours of the batch PC process and (b) the attempted dissolution of nucleated counter enantiomer crystals by increasing suspension temperature. The process had an initial supersaturation of S =1.3. The horizontal line at 0° indicates the optical rotation value of a racemic mixture of enantiomers in solution.

Upon nucleation, the presence of D-asn can only be detected once its growth rate has reached levels such that the solution concentration difference between D-asn

and L-asn is decreasing – resulting in a decrease in optical rotation. For this decrease to occur in a batch-wise preferential crystallization, the mass based total growth rate of the D-asn crystalline phase has to be significantly larger than that of L-asn. If there is only a small amount of D-asn crystals present, for instance right after nucleation of the first crystals, the mass based total growth rate of D-asn can be smaller than that of L-asn and the optical rotation might still rise. There thus is a time lag between the nucleation of the unwanted enantiomer crystals and the subsequent detection. This makes it difficult, using a polarimeter, to establish the exact time when D-asn nucleates in such batch wise seeded preferential crystallizations. However, Figure 4a show that in this case the drop in optical rotation is substantial in a short time and, therefore, we concluded that the unwanted nucleation in this experiment was shortly before this drop.

An attempt to alleviate the presence of the relatively small D-asn crystal by preferentially dissolving them by heating the suspension failed. In this experiment, all the particles inside the vessel, including the seed crystals of L-asn that were added to the racemic solution, dissolved due to the difficulty in exactly controlling suspension temperature which is shown in the optical rotation value dropping below zero.

The productivity of the batch process was calculated based on a batch end time $t_{(end)}$ of 5.5 hours to be 0.0185 g/g hr based on:

$$P(t_{end}) = \frac{m_p^{(L)} - m_s^{(L)}}{m_i^{(L)} \times t_{end}} \tag{6.8}$$

Where $m_p^{(L)}$ is the mass of L-asn produced at t_{end}, $m_s^{(L)}$ is the mass of L-asn seed crystals added at the start of the process and $m_i^{(L)}$ is the initial mass of L-asn in solution. A t_{end} time of 5.5 hours was chosen since we are confident that the counter enantiomer D-asn had not crystallized at this point. The yield of the process was calculated to be 44% based on:

$$Y\,(t_{end}) = \frac{m_c^{(L)}}{m_t^{(L)}} \times 100\% \tag{6.9}$$

Where $m_c^{(L)}$ is the actual mass of L-asn crystallized out at t_{end} and $m_t^{(L)}$ is the theoretical mass of L-asn that would be crystallized out if the process reached equilibrium for L-asn.

An approach to alleviate D-asn crystals could be to simply increase the temperature to the saturation temperature T_s of the system. Since there will be an excess of L-asn present due to the seeds added, all D-asn and L-asn would dissolve except for these seeds. However, this means that the system is simply being reset rather than being controlled. Since usually a small amount of seeds with a small average size is used, dissolution of the counter enantiomer crystals while remaining with the preferred enantiomer seed crystals has only a very small, difficult to control, temperature region (<1°C). The approach could be improved by changing the way of heating; microwave heaters have been shown to be an effective way to rapidly heat a lab scale process/reaction and have been shown to have greater control over conventional heating methods.[34–37] Multiple heater-chillers with different set temperatures could also be used to improve rapid heating and cooling of the suspension.

6.3.3 Concentration Control Approach for Continuous PC

The optical rotation results from a continuous preferential crystallization experiment with concentration control are shown in Figure 6.5a. In Figure 6.5b, we show the corresponding liquid phase trajectory during the continuous PC process focusing on the area of the ternary phase diagram around the eutectic point. The start-up of the process takes place in the first 80 minutes (1.33 residence times). In the start-up region (Figure 6.5a, region a_1) the optical rotation is initially at 0° due to the presence of a supersaturated racemic solution in the crystallizer. Point A in Figure 6.5b shows the racemic feed composition (87.7 mg/ml solvent) entering the crystallizer. After seed crystals of L-asn are added, the optical rotation increases as the seed crystals grow and due to secondary nucleation, new seed crystals are created, removing L-asn solute from solution. Growth of the added L-asn seeds is represented by a change in liquid composition from point A to point B in Figure 6.5b and the optical rotation levels off, upon approaching steady state b_1 in Figure 6.5a.

In steady state region b_1 the continuous feed, growth and secondary nucleation and suspension removal allow a steady state to develop with a solution concentration C_L = 38.57 mg L-asn/ml solvent and C_D = 43.5 mg D-asn/ml solvent (Figure 6.5b),

determined by gravimetric and subsequent HPLC analysis. This corresponds to a constant optical rotation value of around 0.035° in the steady state regions b_1, b_2, b_3 in Figure 6.5a. If the system reached equilibrium i.e. all possible L-asn crystallized from solution, an optical rotation value of 0.080° would have been obtained.

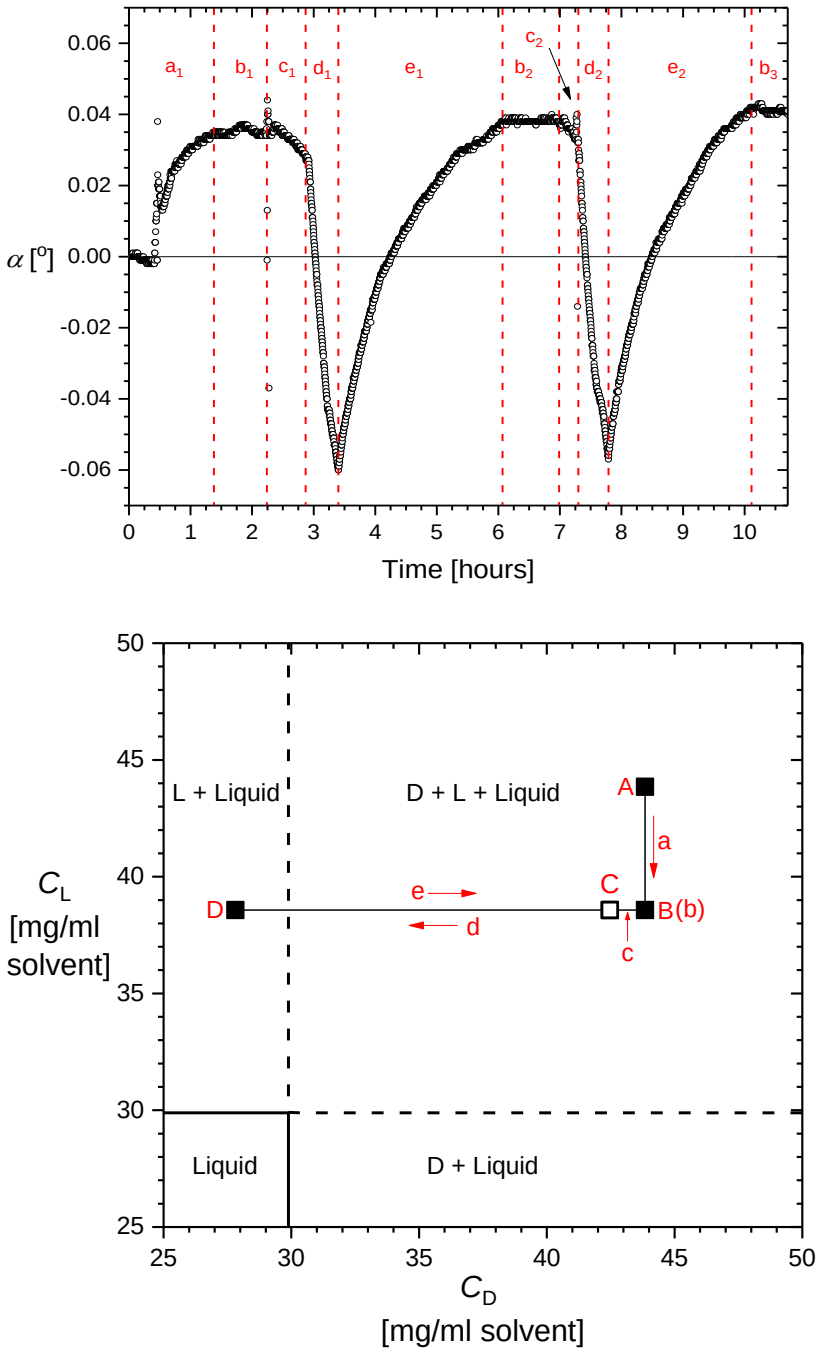

Figure 6.5. (a) Optical rotation (○) results for the continuous PC of L-asn utilising concentration control at a supersaturation ratio S = 1.45. a_1 = start-up, $b_{1/2/3}$ = steady

state, $c_{1/2}$ = nucleation and detection of D-asn crystals, $d_{1/2}$ = application of switch to enantiopure feed to dissolve D-asn crystals and $e_{1/2}$ = switch back to racemic feed and return to steady state. Red dashed lines show the boundaries for each part of the process. The line across the centre at 0° indicates the optical rotation value of a racemic mixture of enantiomers in solution. (b) Ternary phase diagram of D- and L-asn in water at 25.0°C. The two solid segments of the lines show phase boundaries between solid and solid-liquid regions while the dashed lines represent the boundary between two different solid-liquid phase regions. The point at which the two lines intersect represents the eutectic point. A, B, C and D are the operating points: A = racemic feed concentration (87.7 mg/ml solvent, T_s=35.0°C), B = steady state concentration (L-asn concentration 38.57 mg/ml solvent), C = concentration at time of feed switch, after detection of presence of D-asn, D = concentration after controlling action to dissolve unwanted D-asn (D-asn 27.81 mg/ml solvent). a, b, c, d and e are the process stages: a = start-up, b = steady state, c = nucleation and growth of D-asn, d = application of switch to enantiopure feed and e = switch back to racemic feed.

However, this steady state is metastable due to the prevailing supersaturation for the counter enantiomer crystals and, like the batch PC process, they will eventually crystallize. The optical rotation during steady state in the continuous PC process is constant, therefore the formation of unwanted counter enantiomer crystals is easily observed in a deviation from the steady state optical rotation with much less delay. The change in steady state value chosen to be more than 0.004°. In the continuous case, the change in optical rotation trajectory does not depend on the relative growth rates of L-asn and D-asn once L-asn has reached steady state. We merely need a detectable decrease in steady state optical rotation, which is determined by the capabilities of the instrument. This decrease in optical rotation is detected at the beginning of region c_1. On the nucleation and growth of D-asn the concentration of D-asn in the solution decreases and we see a decrease in optical rotation (Figure 6.5a, region c_1). In Figure 6.5b, this corresponds to a change in solution trajectory from point B towards point C (giving a change in optical rotation value from 0.035 to 0.028°). In practice, of course, such a large change in optical rotation before applying the control would not occur, and region c in Figure 6.5a would be as small as possible. However,

we allowed some time before applying the control so that the deviation from steady state was obvious.

At the start of region d_1, to dissolve all formed D-asn crystals while keeping the feed concentration of L-asn constant, the racemic feed is switched off and an enantiopure feed is switched on for a predetermined duration calculated by Eq. (6.7). In this case, in order to reach a target undersaturated concentration of 27.0 mg D-asn/ml solvent, the feed was switched for 28 minutes and 36 seconds. By doing this, the concentration of D-asn in the crystallizer solution is reduced so that it becomes undersaturated and any D-asn crystals in the suspension preferentially dissolve. This transition to an undersaturated region with respect to D-asn is shown in the phase diagram by region d_1 (Figure 6.5), finally arriving in point D in Figure 6.5b. As only L-asn solution is fed to the crystallizer during this period, D-asn concentration in the vessel is being diluted, resulting in a drop in optical rotation visible in region d_1 (Figure 6.5a). Since this reduction of D-asn concentration results in an excess of L-asn with respect to D-asn in solution, the optical rotation value eventually becomes negative. There is a subtle change in the slope observed towards the end of region d_1 and d_2, which could be explained by D-asn reaching undersaturated conditions at which D-asn crystals dissolve rather than grow.

The growth of L-asn is inhibited by the presence of D-asn solute. During periods of lower concentration of D-asn, growth of L-asn therefore may be slightly faster[14] and the crystallizer may operate slightly closer to equilibrium with respect to L-asn. Therefore, there might be a small deviation from steady state with respect to L-asn concentration in solution in regions $d_{1,2}$ in Figure 6.5a. However, due to the large concentration of D-asn this deviation is not substantial and does not affect the control strategy negatively.

Once the target concentration of D-asn has been reached, all solid D-asn is dissolved since the feed is switched for a period of time that ensures the target concentration of D-asn is well in the undersaturated region and the crystals have sufficient time to dissolve. The feed is then switched from the enantiopure feed back to the racemic feed. As D-asn in solution is added again to the vessel (along with L-asn), the optical rotation increases and approaches steady state b_2. The return to a steady state with respect to optical rotation was relatively long due to the asymptotic nature of reaching the same concentration of D-asn in solution in the crystallizer as is

in the feed. More importantly, the suspension consists only of L-asn crystals and therefore an enantiopure product is obtained in this region as well. The cycle then repeats showing one more nucleation event in c_2 and a correction region d_2 demonstrating the robustness and reproducibility of the control strategy within the same process run.

Figure 6.6 shows the enantiomeric excess results from the HPLC analysis carried out on the solid product. The solid phase consisted of only L-asn during steady state regions b_1 and b_2. The solid contained as much as 12% D-asn in regions c_1 and c_2 after counter enantiomer nucleation but before the control action. An increasing amount of D-asn was present in the sample collected in region c_1, consistent with the substantially decreasing optical rotation value of the solution in that region. All D-asn has been dissolved by the end of d_1 and d_2, and that product enantiopurity returns to 100% after the implementation of the control strategy verifying its effectiveness.

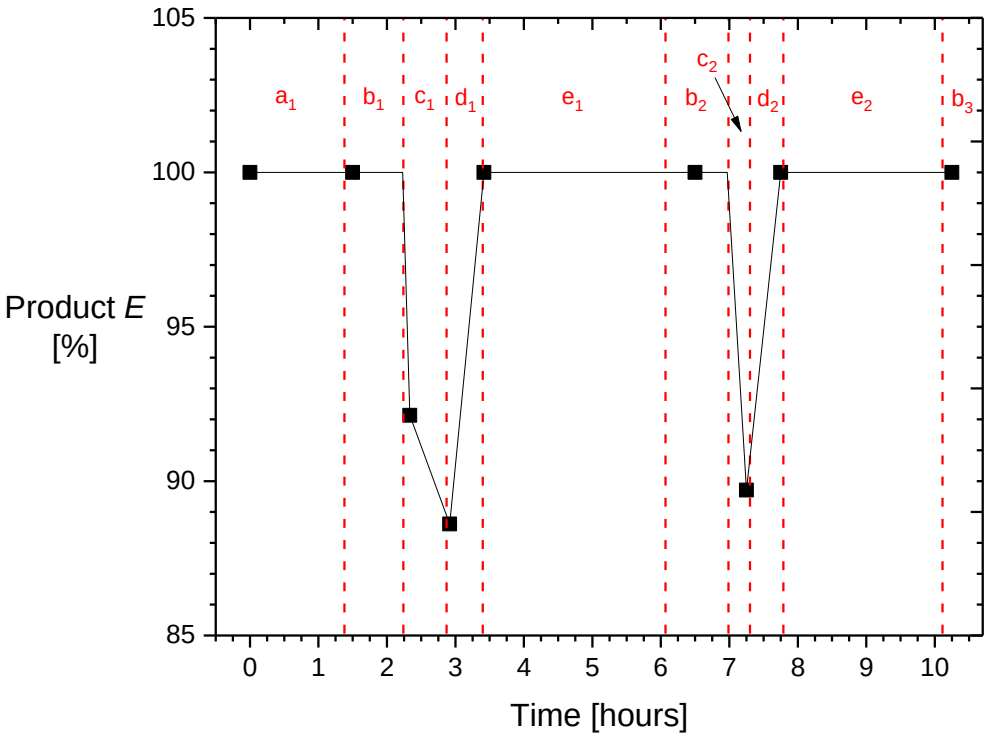

Figure 6.6 Solid product enantiomeric excess (■) results from chiral HPLC analysis on the product collected at each sample point for continuous crystallization experiment at supersaturation ratio S = 1.45. The sample at time = 0 is the enantiopurity of the seed crystals used in the continuous preferential crystallization. The red dashed lines show the boundaries of each period in the process as shown in Figure 6.5. The results

show that enantiopure product is obtained after application of the control. The black solid line is a guide to the eye.

Compared to a standard batch-wise preferential crystallization, being able to detect and correct for the formation of the undesired enantiomer allows for the process to potentially operate at higher concentration and thus higher productivity. The magnitude of this increase depends on the rise in productivity compared to higher demand for enantiopure feed due to increase in nucleation frequency of the undesired enantiomer. To illustrate this, we conducted two further continuous experiments, both at the same crystallization temperature (25.0°C) but one was run at a higher feed concentration (S = 1.60), and one at a lower feed concentration (S = 1.20). The optical rotation profiles of these experiments are shown in Figure 6.7a and 6.7b, respectively. In the experiment of S = 1.60 the steady state period was much shorter (approximately 0.2 hours) than in the previous experiment of S = 1.45 (approximately 0.85 hours), meaning that use of the control action would be more frequent. However, in the experiment of the lower supersaturation S = 1.20 (Figure 6.7b), the steady state period lasted around 10 hours before nucleation of the counter enantiomer occurred, meaning that use of the control action would be used much less frequently and thus less enantiopure feed is required for correction. Unfortunately, some accumulation of larger crystals occurred in this experiment, as indicated on Figure 6.7b. This was due to large crystals circulating in the lower half of the reactor. Since these crystals did not leave the crystallization vessel, they continued to grow while secondary nucleation rate decreased. Thus, more and more L-asn was removed from solution, giving an increasing excess of D-asn in solution causing the optical rotation to increase. The agitation speed was increased, however, in order to suspend these crystals more and allow them to leave the reactor as well as to stimulate secondary nucleation. As a result the optical rotation value returned to steady state. The measured optical rotation fluctuated between 9 and 11 hours due to bubbles in the sample line. A solid sample was taken during this time to confirm enantiopure product was still being produced (see ESI).

The solution trajectory for each continuous PC experiment is shown in the corresponding ternary phase diagram in Figure 6.8, in which the solution trajectory of S = 1.45 explained in Figure 6.5b is compared to S = 1.20 and S = 1.60 (the inset shows

an enlarged region for S = 1.20). As the supersaturation decreases, the steady state concentration of the process is closer to a racemic composition. Furthermore, the difference between the steady state value and the target D-asn concentration is smaller as the initial supersaturation decreases, meaning that less pure material is required for implementation of the control strategy.

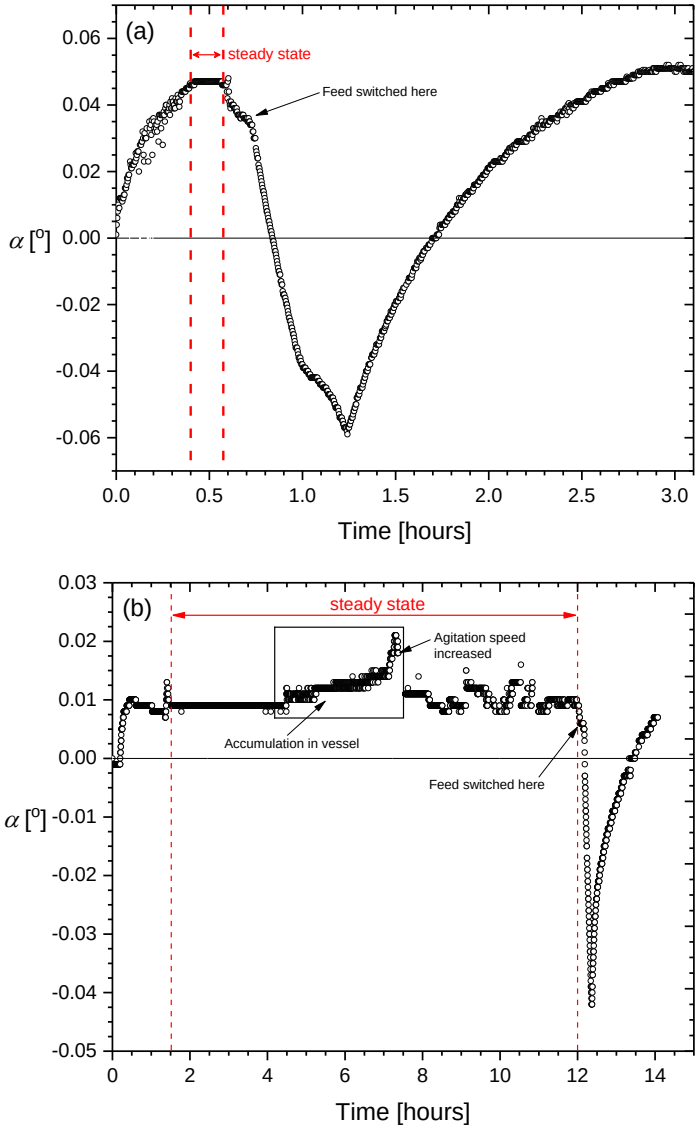

Figure 6.7. Optical rotation (●) results from continuous crystallization experiments carried out with an initial supersaturation ratio of (a) S = 1.60 and (b) S = 1.20 showing the steady state region of each process. The line across the centre at 0° indicates the optical rotation value of a racemic mixture of enantiomers in solution.

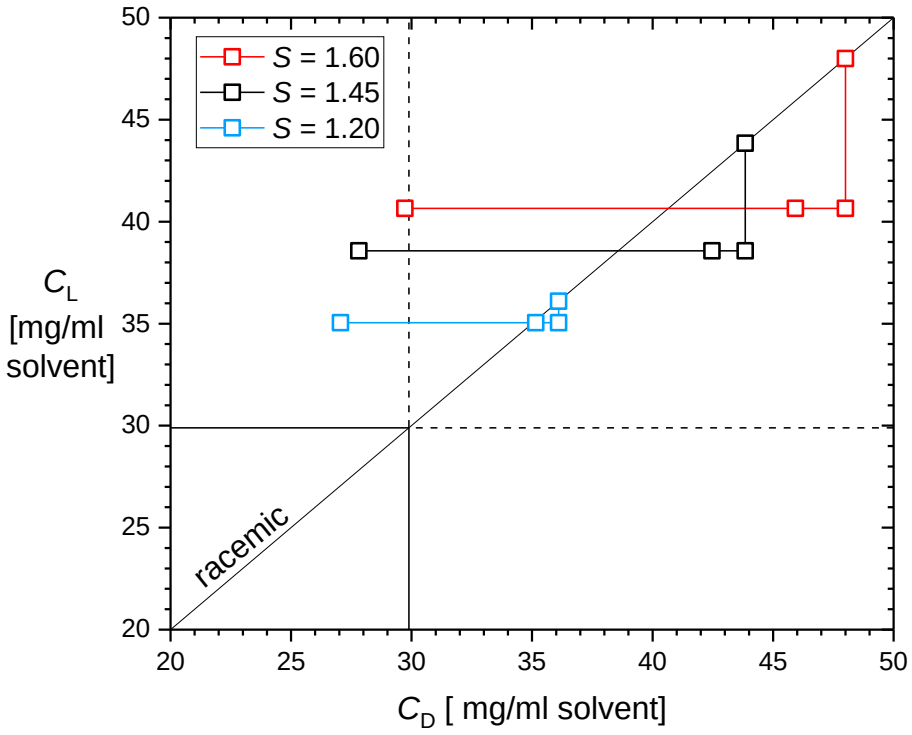

Figure 6.8. Ternary phase diagram showing the solution trajectories for the control strategy at different supersaturations ratios, (□) S = 1.60, (□) S = 1.45 and (□) S = 1.20.

6.4 Discussion

The economic feasibility of such a process control approach depends on the amount of desired enantiomer invested in the enantiopure feed during the control action compared to the pure enantiomer recovered as total crystalline product. These in turn depend on the production rate of the desired enantiomer and the nucleation frequency of the counter enantiomer crystals. A high nucleation frequency of the undesired enantiomer means that the steady state cannot be maintained for substantial times and many controlling actions are needed. The nucleation frequency will decrease with decreasing steady state supersaturation of the undesired enantiomer. The production rate of the preferred enantiomer is enhanced by high secondary nucleation and growth rates which increase with increasing supersaturation of the preferred enantiomer. Thus, there is a balance between the high supersaturation towards the preferred enantiomer and the low supersaturation towards the unwanted enantiomer.

The controlling action of switching the feed from racemic to enantiopure is effective in dissolving the counter enantiomer. During the process, since L-asn continues to be produced, pure product can be collected except for relatively short

periods when crystalline D-asn is present in the crystallizer, for instance in regions c_1, d_1, c_2 and d_2 in Figure 6.6. During regions $c_{1,2}$, the suspension leaving the crystallizer can, after dissolution, be recycled back into the racemic feed to avoid product loss since the overall outgoing suspension stream has the same composition as the feed. However, in regions $d_{1,2}$ in Figure 6.5, when switched to an enantiopure feed of L-asn, the overall outgoing suspension stream composition is becoming more enriched with L-asn over time due to a decrease in the overall D-asn concentration. Therefore, after recycling the suspension leaving the crystallizer during regions $d_{1,2}$ the feed solution will contain a slightly lower concentration of D-asn compared to L-asn. This would cause the supersaturation and therefore nucleation frequency of D-asn to decrease and thus the process would become more stable. Product can be collected again once the feed is switched back to the racemic feed (Figure 6.5, regions $e_{1,2}$).

6.4.1 Productivity and Yield

Table 6.1 summarizes the productivity and yield results obtained for each supersaturation run. Yield and productivity calculations were carried out based on one control cycle consisting of the regions steady state b, counter enantiomer detection c, control action d and return to steady state e in Figure 6.5. The productivity $P^+(t_{cycle})$ of L-asn production for one cycle of the process can be determined using Eq. 6.10:

$$P_L^+ (t_{cycle}) = \frac{m_p^{(L)}}{V_r \cdot t_{cycle}} \tag{6.10}$$

Where m_p is the mass of L-asn crystal product in the product outlet stream in grams in one control cycle (the product obtained in regions b and e), V_r is the operating volume of the reactor in L and t_{cycle} is cycle time in minutes from the start of region b to the end of region e. This cycle time for the experiment with S = 1.45 is 4.94 hours as can be determined from **Figure 6.5**a. In contrast the use $P^-(t_{cycle})$ of L-asn per cycle per unit volume in the control action is determined by:

$$P_L^- (t_{cycle}) = \frac{m_c^{(L)}}{V_r \cdot t_{cycle}} \tag{6.11}$$

Where m_c is the mass of L-asn in the pure solution during the control in grams in one control cycle (the amount of product used in region d). The net productivity $P_L(t_{cycle})$ of one control cycle of the process is therefore determined by:

$$P_L\,(t_{cycle}) \;=\; P_L^{+} - P_L^{-} \tag{6.12}$$

The net percentage yield of L-asn obtained from each experiment can be calculated by Eq. 6.13.

$$Y_L\,(t_{cycle}) = \left(\frac{m_p^{(L)} - m_c^{(L)}}{m_t^{(L)}}\right) \times\; 100\% \tag{6.13}$$

where m_t is the theoretical mass of L-asn that can be crystallized out in one full cycle if the system reaches equilibrium.

Table 6.1. Summary of the production rate, L-asn used, productivity and yield obtained for supersaturations, S = 1.20, 1.45 and 1.60. For each experiment the residence time, τ, was 60 minutes and the seed mass added at start-up was 2 g. $m_p^{(L)}$ = mass L-asn produced in g, $m_c^{(L)}$ = mass L-asn used during correction in g, $Y_L(t_{cycle})$ = net percentage yield of L-asn produced for one cycle of the process, $P^+(t_{cycle})$ = productivity of L-asn produced for one cycle of the process in g/(L hr), $P^-(t_{cycle})$ = productivity of L-asn used for the correction during the process in g/(L hr) and Net productivity $P(t_{cycle}) = P^+ - P^-$ in g/(L hr).

S [-]	$m_p^{(L)}$ [g]	$m_c^{(L)}$ [g]	t_{cycle} [hours]	$Y_L(t_{cycle})$ [%]	$P^+(t_{cycle})$ [g/(L hr)]	$P^-(t_{cycle})$ [g/(L hr)]	$P(t_{cycle})$ [g/(L hr)]
1.20	3.007	1.817	12.48	19.4	0.96	0.58	0.38
1.45	4.825	4.804	4.94	0.15	3.91	3.89	0.017
1.60	3.044	6.299	2.48	-18.0	4.90	10.15	-5.24

The productivity values P^+ and P^- can be plotted as a function of supersaturation ratio, as shown in Figure 6.9. The P^+ value is shown to have a close to linear correlation with supersaturation; as supersaturation increases the P^+ value increases. The P^- value however increases exponentially as a function of

supersaturation increase. As long as $P^+ > P^-$ the process will have a net positive productivity value. This is achieved for $S = 1.20$ where a net productivity of 0.38 g/(L hr) was achieved. Around 40% of the product had to be used for the control action. Since there is remaining supersaturation in the outgoing supersaturation at this supersaturation finally a yield of 19.4% was achieved.

The relative difference between these P^+ and P^- values (which ultimately dictates the net productivity of the process) can be changed by increasing the growth rate of the preferred enantiomer (therefore increasing P^+) and decreasing the nucleation rate of the unwanted enantiomer (decreasing P^-). Such a change can be achieved by enriching the feed with the preferred enantiomer. This could be done by recycling a part of the product into the feed. One way of doing so is to recycle the remaining solution from region d in Figure 6.5a containing decreased D-asn concentrations back into the feed. Decreasing the P^- value could also be achieved by using additives to inhibit growth of the unwanted enantiomer. Several such additives were found such as D-aspartic acid and D-glutamic acid.[14]

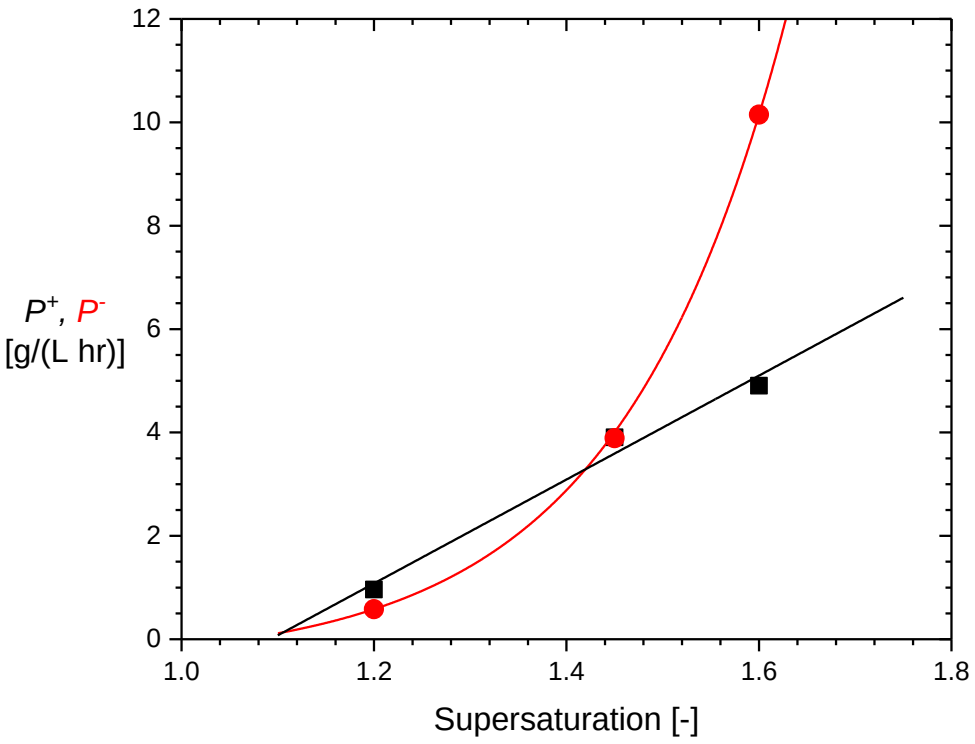

Figure 6.9. Correlation between the mass of L-asn produced per unit volume per cycle time, P^+ (■), and the mass of L-asn used during the correction (region d in Figure 6.5)

per unit volume per cycle time, P^- (●), as a function of supersaturation ratio, S. For a net positive productivity value, $P(t_{cycle})$, $P^+ > P^-$. Lines are a guide to the eye.

As expected, a supersaturation ratio of 1.60 gives the most inefficient process when using the control strategy. As shown in Table 6.1, a net yield of -18.0% is obtained, and so use of the control strategy is inefficient. A small positive net yield of 0.15% is obtained at a supersaturation ratio of 1.45. A good positive net yield of 19.4% is obtained for the supersaturation ratio of 1.20. The process can still be further optimized by determining the supersaturation which gives the maximum net yield for the process, as this work is only a demonstration of the control strategy. However, the presented results do not account for recycling of any solution, which in practice would most certainly be applied so as not to waste valuable product.

6.5 Process Improvement

The efficiency and yield of the process can be improved by recycling the mother liquor produced during the process. A schematic of a potential process setup with such a recycle loop is shown in Figure 6.10. Since, however, the mother liquor in the outlet stream during regions b and e in Figure 6.5 has an excess of D-asn in the solution, a further crystallization step must be carried out in order to obtain a solution of racemic composition again. A portion of enantiopure product (denoted by X in Figure 6.10) can be used along with solvent to make enantiopure feed solution for the control strategy. During regions c and d in Figure 6.5, the solid (contaminated with D-asn crystals) and mother liquor solution can be recycled back directly to the feed solution (blue dashed line in Figure 10). During this period, as discussed in Section 6.4, the solution will become more enriched with L-asn over time thus reducing the nucleation frequency of D-asn. For such a process to be economically feasible, the less expensive enantiomer should be crystallized in the first crystallization vessel, since part of the produced solid will be used for the enantiopure feed. Furthermore, utilizing the control strategy in a coupled batch or continuous setup similar to one used by Galan et al.[29] could also improve the overall process efficiency. In such a setup, the supersaturation of counter enantiomer is reduced since it has been previously crystallized in a coupled vessel before entering the crystallizer seeded with the preferred enantiomer. Therefore, steady state periods of preferred enantiomer

production would be extended meaning fewer uses of the controlling action and in turn higher net yields could be obtained.

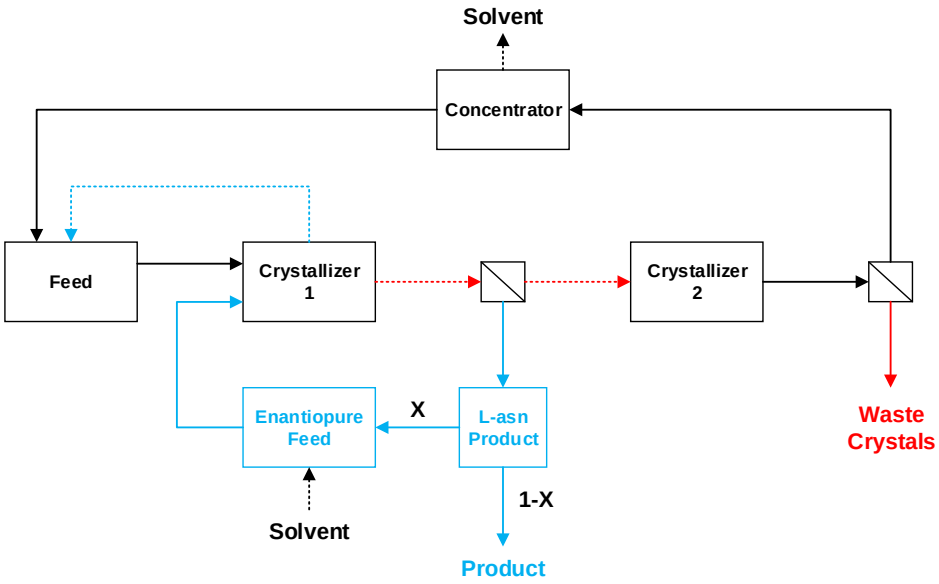

Figure 6.10. Schematic of potential setup for improving the efficiency of the control strategy. By utilizing a second crystallization vessel, the counter enantiomer can be crystallized to return the solution to a racemic composition which can then be recycled into the feed vessel via a concentrating vessel so that waste can be reduced. (-) racemic solution, (--) pure solvent, (-) pure L-asn solid or solution, (--) enriched L-asn suspension recycled during region d in Figure 5, (-) pure D-asn solid and (--) enriched D-asn solution.

6.6 Conclusions

We have demonstrated control over a continuous preferential cooling crystallization process using a new approach. In this approach, we utilized an additional feed tank containing enantiopure solution to undersaturate the undesired counter enantiomer crystals when they appear in a continuous process. The continuous approach is easy to scale due to the control strategy relying on movement through regions of the phase diagram by adjusting composition rather than kinetics of dissolution. The control strategy has also demonstrated reproducibility over several cycles and runs, correcting for the nucleation of the undesired enantiomer. The benefit of this strategy comes from being able to operate an MSMPR at higher supersaturation

compared to an uncontrolled process. Using a single stage MSMPR is most likely not the most efficient application of this strategy, however, it also allows for new process arrangements such as combination with a coupled batch setup or MSMPR cascade for improved productivity. The control strategy should be optimized for the chosen system to find the supersaturation which generates the maximum yield, since this will depend on the growth and nucleation kinetics of the system of interest.

6.7 References

(1) Jacques, J.; Collet, A. *Enantiomers, Racemates and Resolutions*; John Wiley & Sons Ltd, 1981.

(2) Köllges, T.; Vetter, T. Model-Based Analysis of Continuous Crystallization/Reaction Processes Separating Conglomerate Forming Enantiomers. *Cryst. Growth Des.* **2017**, *17* (1), 233–247. https://doi.org/10.1021/acs.cgd.6b01487.

(3) Chhabra, N.; Aseri, M. L.; Padmanabhan, D. A Review of Drug Isomerism and Its Significance. *Int. J. Appl. basic Med. Res.* **2013**, *3* (1), 16–18. https://doi.org/10.4103/2229-516X.112233.

(4) Maier, N. M.; Franco, P.; Lindner, W. Separation of Enantiomers: Needs, Challenges, Perspectives. *J. Chromatogr. A* **2001**, *906* (1–2), 3–33. https://doi.org/10.1016/S0021-9673(00)00532-X.

(5) Viedma, C. Chiral Symmetry Breaking During Crystallization: Complete Chiral Purity Induced by Nonlinear Autocatalysis and Recycling. *Phys. Rev. Lett.* **2005**, *94* (6), 065504. https://doi.org/10.1103/PhysRevLett.94.065504.

(6) Spix, L.; van Enckevort, W. J. P.; van der Wal, L. J. M.; Meekes, H.; Vlieg, E. Resolution of Asparagine in a Coupled Batch Grinding Process: Experiments and Modelling. *CrystEngComm* **2016**, *18* (48), 9252–9259. https://doi.org/10.1039/C6CE02043G.

(7) Xiouras, C.; Ter Horst, J. H.; Van Gerven, T.; Stefanidis, G. D. Coupling Viedma Ripening with Racemic Crystal Transformations: Mechanism of Deracemization. *Cryst. Growth Des.* **2017**, acs.cgd.7b00908. https://doi.org/10.1021/acs.cgd.7b00908.

(8) Sögütoglu, L.-C.; Steendam, R. R. E.; Meekes, H.; Vlieg, E.; Rutjes, F. P. J. T. Viedma Ripening: A Reliable Crystallisation Method to Reach Single Chirality.

Chem. Soc. Rev. **2015**, *44* (19), 6723–6732. https://doi.org/10.1039/C5CS00196J.

(9) Fogassy, E.; Nógrádi, M.; Kozma, D.; Egri, G.; Pálovics, E.; Kiss, V. Optical Resolution Methods. *Org. Biomol. Chem.* **2006**, *4* (16), 3011–3030. https://doi.org/10.1039/B603058K.

(10) Mane, S. Racemic Drug Resolution: A Comprehensive Guide. *Anal. Methods* **2016**, *8* (42), 7567–7586. https://doi.org/10.1039/C6AY02015A.

(11) Lorenz, H.; Seidel-Morgenstern, A. Processes to Separate Enantiomers. *Angewandte Chemie - International Edition*. January 27, 2014, pp 1218–1250. https://doi.org/10.1002/anie.201302823.

(12) Coquerel, G. Novel Optical Resolution Technologies; Sakai, K., Hirayama, N., Tamura, R., Eds.; Springer Berlin Heidelberg, 2006; pp 1–51. https://doi.org/10.1007/128_2006_077.

(13) Petruševska-Seebach, K.; Seidel-Morgenstern, A.; Elsner, M. P. Preferential Crystallization of L-Asparagine in Water. *Cryst. Growth Des.* **2011**, *11* (6), 2149–2163. https://doi.org/10.1021/cg101408e.

(14) Kongsamai, P.; Maneedaeng, A.; Flood, C.; ter Horst, J. H.; Flood, A. E. Effect of Additives on the Preferential Crystallization of L-Asparagine Monohydrate. *Eur. Phys. J. Spec. Top.* **2017**, *226* (5), 823–835. https://doi.org/10.1140/epjst/e2016-60257-3.

(15) Steendam, R. R. E.; ter Horst, J. H. Continuous Total Spontaneous Resolution. *Cryst. Growth Des.* **2017**, *8*, 4428–4436. https://doi.org/10.1021/acs.cgd.7b00761.

(16) Srisanga, S.; ter Horst, J. H. Racemic Compound, Conglomerate, or Solid Solution: Phase Diagram Screening of Chiral Compounds. *Cryst. Growth Des.* **2010**, *10* (4), 1808–1812. https://doi.org/10.1021/cg901483v.

(17) Elsner, M. P.; Menéndez, D. F.; Muslera, E. A.; Seidel-Morgenstern, A. Experimental Study and Simplified Mathematical Description of Preferential Crystallization. *Chirality* **2005**, *17* (S1), S183–S195. https://doi.org/10.1002/chir.20135.

(18) Rougeot, C.; Hein, J. E. Application of Continuous Preferential Crystallization to Efficiently Access Enantiopure Chemicals. *Org. Process Res. Dev.* **2015**, *19* (12), 1809–1819. https://doi.org/10.1021/acs.oprd.5b00141.

(19) Levilain, G.; Coquerel, G. Pitfalls and Rewards of Preferential Crystallization. *CrystEngComm* **2010**, *12* (7), 1983. https://doi.org/10.1039/c001895c.

(20) Lorenz, H.; Perlberg, A.; Sapoundjiev, D.; Elsner, M. P.; Seidel-Morgenstern, A. Crystallization of Enantiomers. *Chem. Eng. Process. Process Intensif.* **2006**, *45* (10), 863–873. https://doi.org/10.1016/j.cep.2005.11.013.

(21) Li, J.; Lai, T. C.; Trout, B. L.; Myerson, A. S. Continuous Crystallization of Cyclosporine: Effect of Operating Conditions on Yield and Purity. *Cryst. Growth Des.* **2017**, acs.cgd.6b01212. https://doi.org/10.1021/acs.cgd.6b01212.

(22) Alvarez, A. J.; Singh, A.; Myerson, A. S. Crystallization of Cyclosporine in a Multistage Continuous MSMPR Crystallizer. *Cryst. Growth Des.* **2011**, *11* (10), 4392–4400. https://doi.org/10.1021/cg200546g.

(23) Baxendale, I. R.; Braatz, R. D.; Hodnett, B. K.; Jensen, K. F.; Johnson, M. D.; Sharratt, P.; Sherlock, J.-P.; Florence, A. J. Achieving Continuous Manufacturing: Technologies and Approaches for Synthesis, Workup, and Isolation of Drug Substance May 20–21, 2014 Continuous Manufacturing Symposium. *Journal of Pharmaceutical Sciences*. 2015, pp 781–791. https://doi.org/10.1002/jps.24252.

(24) Mascia, S.; Heider, P. L.; Zhang, H.; Lakerveld, R.; Benyahia, B.; Barton, P. I.; Braatz, R. D.; Cooney, C. L.; Evans, J. M. B.; Jamison, T. F.; et al. End-to-End Continuous Manufacturing of Pharmaceuticals: Integrated Synthesis, Purification, and Final Dosage Formation. *Angew. Chem. Int. Ed. Engl.* **2013**, *52* (47), 12359–12363. https://doi.org/10.1002/anie.201305429.

(25) Plumb, K. Continuous Processing in the Pharmaceutical Industry: Changing the Mind Set. *Chem. Eng. Res. Des.* **2005**, *83* (6), 730–738. https://doi.org/10.1205/cherd.04359.

(26) Myerson, A. S.; Krumme, M.; Nasr, M.; Thomas, H.; Braatz, R. D. Control Systems Engineering in Continuous Pharmaceutical Manufacturing May 20-21, 2014 Continuous Manufacturing Symposium. *J. Pharm. Sci.* **2015**, *104* (3), 832–839. https://doi.org/10.1002/jps.24311.

(27) Wang, J.; Li, F.; Lakerveld, R. Process Intensification for Pharmaceutical Crystallization. *Chem. Eng. Process. - Process Intensif.* **2018**, *127*, 111–126. https://doi.org/10.1016/J.CEP.2018.03.018.

(28) Chaaban, J. H.; Dam-Johansen, K.; Skovby, T.; Kiil, S. Separation of

Enantiomers by Continuous Preferential Crystallization: Experimental Realization Using a Coupled Crystallizer Configuration. *Org. Process Res. Dev.* **2013**, *17* (8), 1010–1020. https://doi.org/10.1021/op400087g.

(29) Galan, K.; Eicke, M. J.; Elsner, M. P.; Lorenz, H.; Seidel-Morgenstern, A. Continuous Preferential Crystallization of Chiral Molecules in Single and Coupled Mixed-Suspension Mixed-Product-Removal Crystallizers. *Cryst. Growth Des.* **2015**, *15* (4), 1808–1818. https://doi.org/10.1021/cg501854g.

(30) Alvarez Rodrigo, A.; Lorenz, H.; Seidel-Morgenstern, A. Online Monitoring of Preferential Crystallization of Enantiomers. *Chirality* **2004**, No. 16, 499–508.

(31) Bruice, P. Y. How Specific Rotation Is Measured. In *Organic Chemistry*; Pearson, 2011; pp 208–210.

(32) Dalton, J. B.; Schmidt, C. L. A. The Solubilities of Certain Amino Acids and Realted Compounds in Water, the Densities of Their Solutions at Twenty-Fice Degrees, and the Calculated Heats of Solution and Poartial Molal Volumes. II. *J. Biol. Chem.* **1935**, *3* (109), 241–248.

(33) Temmel, E.; Gänsch, J.; Lorenz, H.; Seidel-Morgenstern, A. Measurement and Evaluation of the Crystallization Kinetics of l -Asparagine Monohydrate in the Ternary l -/ d -Asparagine/Water System. *Cryst. Growth Des.* **2018**, *18* (12), 7504–7517. https://doi.org/10.1021/acs.cgd.8b01322.

(34) Cameli, F.; Xiouras, C.; Stefanidis, G. D. Intensified Deracemization *via* Rapid Microwave-Assisted Temperature Cycling. *CrystEngComm* **2018**, *20* (21), 2897–2901. https://doi.org/10.1039/C8CE00575C.

(35) Gogate, P. R. Intensification of Chemical Processing Applications Using Ultrasonic and Microwave Irradiations. *Curr. Opin. Chem. Eng.* **2017**, *17*, 9–14. https://doi.org/10.1016/J.COCHE.2017.05.003.

(36) Kacker, R.; Radoiu, M.; Kramer, H. J. M. Novel Design Integrating a Microwave Applicator into a Crystallizer for Rapid Temperature Cycling. A Direct Nucleation Control Study. *Cryst. Growth Des.* **2017**, *17* (7), 3766–3774. https://doi.org/10.1021/acs.cgd.7b00368.

(37) Kacker, R.; Salvador, P. M.; Sturm, G. S. J.; Stefanidis, G. D.; Lakerveld, R.; Nagy, Z. K.; Kramer, H. J. M. Microwave Assisted Direct Nucleation Control for Batch Crystallization: Crystal Size Control with Reduced Batch Time. *Cryst. Growth Des.* **2016**, *16* (1), 440–446.

https://doi.org/10.1021/acs.cgd.5b01444.

Chapter 7

7 Conclusions and Future Work

The main aim of this thesis was to control the preferential crystallization of a conglomerate forming compound in both batch and continuous preferential crystallization processes in order to improve product enantiopurity as well as process yield and productivity compared to a conventional batch-wise preferential crystallization process. A variety of novel strategies and modifications to existing setups were demonstrated in order to show control of preferential crystallization, in both batch and continuous preferential crystallization processes.

In chapter 3, a novel strategy for the separation of enantiomers in a batch preferential crystallization process was demonstrated in order to address the issue of inevitable unwanted primary nucleation of the counter enantiomer. This strategy involves seeding a supersaturated racemic solution with pure crystals of both enantiomers. Using dynamic cooling profiles determined by a population balance model optimization, a bias in the crystal size distribution of each enantiomer was created so that pure crystals of each enantiomer could be subsequently separated mechanically using a sieving procedure. As such, unwanted primary nucleation of the counter enantiomer was avoided. However, some secondary nucleation occurs in the system, creating crystals smaller than the input seed size of each enantiomer.

In chapter 4, a coupled preferential crystallization process was demonstrated in an internally coupled single moving-fluid oscillatory baffled crystallizer (OBC). A mesh filter was inserted between connecting sections of the OBC to allow solution to transfer between sections whilst pure crystals of each enantiomer were kept separate. This process has been shown to operate at higher supersaturations than previously investigated in literature. Furthermore, this setup negates the need for additional tanks, pumps or tubing (compared to a coupled preferential crystallization process in two stirred tank reactors) due to its direct exchange of solution in a single piece of equipment. However, at high seed loadings secondary nucleation via attrition occurs creating small crystals smaller than the filter pore size, causing contamination of pure product in the opposite section of the setup.

Before product of consistent specification is produced during steady state in a continuous process, the system must go through a start-up period. During this time, product of inconsistent specification is produced, and valuable time is wasted. In chapter 5, therefore, the effect of continuous process parameters on the start-up time and steady state robustness for a continuous preferential crystallization process was determined. Although the results show no correlation between the start-up time and robustness of the steady state, it was found that parameter-parameter interactions play a more significant role in the start-up time than independent parameters (the interacting effect of residence time and solid seed loading had the greatest effect on the start-up time whereby it could be reduced by using a higher seed loading for a shorter residence time. In contrast, individual parameters had a more significant effect of the steady state robustness. The initial concentration of the counter enantiomer D-asn had the greatest effect on the robustness of the steady state since the likelihood of its unwanted nucleation increases with increasing concentration.

Finally, in chapter 6, a novel control strategy was demonstrated in order to gain control over a continuous preferential crystallization process when the counter enantiomer inevitably nucleated. In this strategy, an additional feed tank was utilized containing enantiopure solution to undersaturate the unwanted counter enantiomer crystals when they appear. The strategy was shown to be robust over several cycles and was effective at initial supersaturation of S = 1.2, 1.4 and 1.6. The need to stop and restart the process was therefore avoided and after application of the control strategy, production of enantiopure material was able to continue.

The work carried out in this thesis has developed new ideas for preferential crystallization processes and has such has opened new avenues for investigation. Through further development of these methods and strategies, preferential crystallization processes can continue to be built on and improved in order to consistently achieve production of high quality enantiopure material without the risk or fear of counter enantiomer contamination to the process.

7.1 Future Work

Chapter 3. Enabling Mechanical Separation of Enantiomers through Batch Controlled Concomitant Crystallization. In order to further optimize the predicted power of the population balance model generated in this work, nucleation terms (both

primary and secondary) should be added. Experimentally, pre-treatment (e.g. washing) of the seed material would ensure that any fines that exist on the surface of the seeds would be removed. This way secondary nucleation via initial breeding can be ruled out as a mechanism within the system. Additionally, using a control strategy such as supersaturation control (SSC) would ensure the operation trajectory during the process remains constant. Added to this, determining the secondary nucleation limit for the phase diagram would ensure secondary nucleation via contact nucleation and/or fluid shear could be ruled out.

Chapter 4. Coupled Batch-wise Preferential Crystallization a Single Moving-Fluid Oscillatory Baffled Crystallizer. In this chapter the concept of using a filter between connecting sections of the OBC allowing movement of solution and separation of crystals was demonstrated. However, for future work on this type of process, it will be important to investigate several process factors so that it can be as efficient as possible. Firstly, the critical mixing intensity for asparagine monohydrate should be investigated as a function of supersaturation and seed loading, as was done by Cruz et al. In doing so, secondary nucleation via attrition and/or fluid shear can be avoided. Next, different filter pore size should be investigated since the pressure drop across the filter will increase as the filter pore size decreases for a given mixing intensity. In an optimized process the smallest pore size possible should be used (to minimize contamination of pure material due to the passing of very small particles across the filter) whilst not causing a pressure drop large enough to affect mixing on the other side of the OBC. Finally, in this work, the preferential crystallizations were carried out under isothermal conditions. Therefore, by applying cooling profiles, even through the use of SSC strategies, secondary nucleation can be minimized and the risk of unwanted primary nucleation at high initial supersaturations can be avoided. Combining all the suggestions mentioned would yield a fully optimized coupled-batch preferential crystallization process in such an OBC setup.

Chapter 5. Start-up and Steady State of a Continuous Preferential Crystallization in a Continuous Stirred Tank Reactor. The fractional factorial (screening) DoE approached used in this chapter identified the main process factors that affect the start-up and steady state of a continuous preferential crystallization process. Moving

forward, these important factors could be used in a full factorial DoE, whilst insignificant factors can be kept constant. This would allow for the full optimization of a continuous preferential crystallization process using the initial process parameters.

Chapter 6. Resolution Control in a Continuous Preferential Crystallization. The efficiency of the control strategy presented depends the amount of desired enantiomer invested in the enantiopure feed compared to the pure enantiomer recovered as crystalline product. This in turn will depend on the nucleation and growth kinetics of the compound of interest. Modelling of the strategy would therefore aid in the determination of the optimum supersaturation at which the process should run such that the net productivity P is at its maximum. This would ensure minimum usage of pure material for the enantiopure feed whilst also producing the maximum amount of product available. Furthermore, applying recycle loops during periods where counter enantiomer crystals are present would reduce waste and improve the productivity of the process.